Spring 2008

Secondary organic aerosol formation of relevance to the marine boundary layer

Xuyi Cai
University of New Hampshire, Durham

SECONDARY ORGANIC AEROSOL FORMATION OF RELEVANCE TO THE MARINE BOUNDARY LAYER

BY

XUYI CAI

BS, Chengdu College of Geology, 1986

MA, Duke University, 2002

Doctor of Engineering, China University of Geosciences

(Beijing), 1993

DISSERTATION

Submitted to the University of New Hampshire

In Partial Fulfillment of

the Requirements for the Degree of

Doctor of Philosophy

In

Earth and Environmental Sciences

May, 2008

This dissertation has been examined and approved.

Dissertation Director, Robert J. Griffin
Associate Professor of Atmospheric Chemistry

Jack E. Dibb
Research Associate Professor of Atmospheric Chemistry

Howard R. Mayne
Professor of Chemistry

Barkley C. Sive
Research Associate Professor of Atmospheric Chemistry

Robert W. Talbot
Research Professor of Atmospheric Chemistry

27 FEB 2008
Date

ACKNOWLEDGMENTS

My advisor Dr. Robert Griffin has guided me through all stages of my studies at the University of New Hampshire; I would like to thank him for all the opportunities he has opened for me and for his patience and encouragement. Committee members Dr. Jack Dibb, Dr. Howard Mayne, Dr. Barkley Sive, and Dr. Robert Talbot, have provided valuable discussion and input at all stages of this project. I thank all of you for your guidance and insight!

I would like to thank Jianjun Chen, Luke Ziemba, Kabindra Shakya and other aerosol group members for their help and friendship.

TABLE OF CONTENTS

LIST OF TABLES

LIST OF FIGURES

ABSTRACT

SECONDARY ORGANIC AEROSOL FORMATION OF RELEVANCE TO THE MARINE BOUNDARY LAYER

Xuyi Cai

University of New Hampshire, May, 2008

The chlorine atom (Cl) is a potential oxidant of volatile organic compounds (VOCs) in the atmosphere and is hypothesized to lead to secondary organic aerosol (SOA) formation in coastal areas. The purpose of this dissertation is to test this hypothesis and quantify the SOA formation potentials of some representative biogenic and anthropogenic hydrocarbons when oxidized by Cl in laboratory chamber experiments. The chosen model compounds for biogenic and anthropogenic hydrocarbons in this study are three monoterpenes (α-pinene, β-pinene, and d-limonene) and two aromatics (*m*-xylene and toluene), respectively. Results indicate that the oxidation of these monoterpenes and aromatics generates significant amounts of aerosol. The SOA yields of α–pinene, β-pinene, and d-limonene obtained in this study are comparable to those when they are oxidized by ozone, by nitrate radical, and in photooxidation scenarios. For aerosol mass up to 30.0 μg m^{-3}, their yields reach approximately 0.20, 0.20, and 0.30, respectively. The SOA yields for *m*-xylene and toluene are found to be in the range of 0.035 to 0.12 for aerosol concentrations up to 19 μg m^{-3}. For d-limonene and toluene, data indicate two yield curves that depend on the initial concentration ratios of Cl precursor to hydrocarbon

hydrocarbon. Zero-dimensional calculations based on these yields show that SOA formation from the five model compounds when oxidized by Cl in the marine boundary layer could be a significant source of SOA in the early morning.

In addition, the mechanistic reaction pathways for Cl oxidation of α-pinene, β-pinene, d-limonene, and toluene with Cl have been developed within the framework of the Caltech Atmospheric Chemistry Mechanisms (CACM). Output from the developed mechanisms is combined with an absorptive partitioning model to predict precursor decay curves and time-dependent SOA concentrations in experiments. Model calculations are able to match (in general within general ± 50%) final measured SOA concentrations. Species predicted to dominate SOA composition include carboxylic acids and organic peroxides.

Finally, the influence of surface tension on the formation of SOA is investigated using a size-dependent absorptive partitioning model that accounts for the influence of surface tension on the gas/particle partitioning of semi-volatile organic compounds (the Kelvin effect). Results from numerical simulations indicate that if non-polar organic species constitute a significant fraction of pre-existing aerosol (PA), the Kelvin effect on SOA formation may be negligible. However, if PA is dominated by polar organic compounds, the Kelvin effect on SOA formation is significant when the PA initial diameter is smaller than approximately 100 nm (decreasing SOA formation from specific compounds by as much as a factor of 2.5). If the PA is an aqueous aerosol, the Kelvin effect on SOA formation is most important (decreasing SOA formation from specific compounds by as much as a factor of 10).

CHAPTER I

INTRODCUTION

Secondary organic aerosol (SOA) is formed when products generated from the gas- or liquid-phase oxidation of volatile organic compounds (VOCs) condense onto pre-existing particles, homogeneously nucleate to form new particles, or remain in the condensed phase after cloud evaporation [*Pankow*, 1994a; *Pankow*, 1994b; *Saxena and Hildemann*, 1996; *Blando and Turpin*, 2000]. In contrast, primary organic aerosols (POA) are emitted directly to the atmosphere from various sources [*Rogge et al.*, 1993; *Schauer et al.*, 1996]. SOA and POA can be biogenic or anthropogenic in origin. POA and SOA together constitute organic aerosol (OA), which is a ubiquitous constituent of atmospheric particulate matter [*Murphy et al.*, 1998]. No reliable analytical method is available currently to distinguish completely between SOA and POA in observed OA.

SOA is estimated to account for a significant portion of the OA burden in the troposphere on regional and global scales. It has been estimated that a range of 20 to 80% of observed OA in the South Coast Air Basin (SoCAB) of California is secondary in nature, depending on factors such as specific location, time of day, meteorological conditions, and method of calculation [*Turpin and Huntzicker,* 1995; *Schauer et al.,* 1996]. The modeling results of *Chung and Seinfeld* [2002] indicate that SOA generally constitutes 10 to 20% of the total OA at the Earth's surface. Many additional studies

show that SOA contributes substantially to the tropospheric OA burden under various geographical and meteorological conditions [*Griffin et al.*, 1999a; *Andersson-Skold and Simpson,* 2001; *Schell et al.,* 2001; *Griffin et al.*, 2002a; *Pun et al.*, 2003; *Tsigaridis and Kanakidou*, 2003; *Lack et al.*, 2004; *Liousse et al.*, 2005].

Aerosol particles affect climate significantly [*Twomey et al.*, 1978; *Charlson et al.*, 1992], cause visibility degradation [*Mazurek et al.*, 1997], and are associated with human disease and mortality [*Dockery et al.*, 1993]. Fine aerosols (with diameters smaller than 2.5 μm) have sizes close to wavelengths of light in the visible and have longer lifetimes in the atmosphere than do coarse particles. Therefore, it is believed that fine particles are responsible for virtually all of the important climate, visibility, and human health effects associated with particulate matter. OA accounts for 20-90% of the total fine aerosol mass depending on geographic location [*Artaxo et al.*, 1988; *Talbot et al.*, 1988; *Artaxo et al.,* 1990; *Talbot et al.*, 1990; *Saxena and Hildemann*, 1996; *Andreae and Crutzen*, 1997; *Roberts et al.*, 2001; *Putaud et al.*, 2004]. The significant contribution of SOA to the OA tropospheric burden highlights the important role that SOA likely plays in direct and indirect climate forcing and other environmental effects.

Many studies conducted in the past decade provide insight into the chemical reactions and thermodynamic processes that lead to SOA formation. Chamber studies have focused on SOA yield, gas-phase products, aerosol component speciation, chemical reaction pathways, and product phase partitioning. Heterogeneous reactions between gas- and condensed phase species such as oligomerization and cloud processing have been found to contribute to SOA formation [*Jang et al.*, 2002; *Warneck*, 2003; *Ervens et al.*, 2004a; *Ervens et al.*, 2004b; *Gao et al.*, 2004; *Iinuma et al.*, 2004; *Kalberer et al.*,

2004; *Jang et al.*, 2005; *Lim et al.*, 2005]. The effects on SOA formation of environmental factors such as temperature, relative humidity, and nitrogen oxide (NO_x) level have also been studied [*Sheehan and Bowman*, 2001; *Cocker et al.*, 2001a; *Cocker et al.*, 2001b; *Hurley et al.*, 2001; *Johnson et al.*, 2004; *Johnson et al.*, 2005; *Martin-Reviejo and Wirtz*, 2005; *Presto et al.*, 2005; *Song et al.*, 2005; *Ng et al.*, 2007].

A factor often ignored in previous studies that may affect significantly the SOA formation under certain conditions is surface tension. SOA in the ambient atmosphere is generally found to reside in submicron particles [*Pickle et al.*, 1990; *Mylonas et al.*, 1991; *Wainman et al.*, 2000; *Geller et al.*, 2002; *Yao et al.*, 2002; *de Gouw et al.*, 2005; *Takegawa et al.*, 2006]. In chamber studies of SOA formation, submicron particles are commonly used as the condensation seeds [*Odum et al.*, 1996]. Evidence suggests that SOA may form directly from homogeneous nucleation of semi-volatile oxidation products under ambient conditions [*Marti et al.*, 1997; *Kerminen*, 1999; *Leaitch* et al., 1999; *Kavouras and Stephanou*, 2002; *Anttila and Kerminen*, 2003; *Held et al.*, 2004; *Lunden et al.*, 2006; *Russell et al.*, 2007]. Therefore, in both ambient and laboratory cases, surface tension may play a significant role in the formation and the size distribution of SOA through the Kelvin effect that describes the size-dependent influence of particle curvature on the vapor pressures of components in the particle phase [*Köhler*, 1936]. The effect of surface tension on partitioning is examined in Part II of this dissertation.

SOA concentrations measured under ambient conditions compared to those predicted by absorptive partitioning models tend to be much larger [*de Gouw et al.*, 2005; *Heald et al.*, 2005; *Volkamer et al.*, 2006; *Johnson et al.*, 2006]. New SOA sources (precursors, oxidants, or processes) need to be identified to reconcile this inconsistency.

The chlorine atom (Cl) forms in coastal and marine environments, near industrial sources, and in close proximity to swimming pools. In marine boundary layer, it has been suggested that atomic chlorine (Cl) may be generated by sea salt aerosol reactions with OH or/and NO_y [*Spicer et al.,* 1998*; Knipping et al.*, 2000, *Rossi*, 2003; *Finlayson-Pitts*, 2003; *von Glasow and Crutzen*, 2003]. Photolysis of Cl_2 then leads to Cl. Many studies have been conducted to estimate tropospheric Cl concentrations to evaluate its importance as a tropospheric oxidant of VOCs in the troposphere. The estimated Cl atom concentrations vary from 10^2 to 10^5 molecule cm^{-3} depending on time of day and geographic locations [*Spicer et al.*, 1998; *Wingenter et al.*, 1999; *Wingenter et al.*, 2005; *Pszenny et al.,* 2007].

Chlorine atom is partly responsible for ozone (O_3) depletion events observed during sunrise in the Arctic [*Kieser et a*l., 1993; *Jobson et al.*, 1994; *Ariya et al.*, 1998; *Ariya et al.*, 1999]. Recent studies have also demonstrated the significant potential for Cl to act as an organic oxidant in coastal and industrialized areas [*Ganske et al.,* 1992*; Keene et al.,* 1996*; Spicer et al.,* 1998; *Canosa-Mas et al.,* 1999*; Finlayson-Pitts et al.*, 1999; *Tanaka et al.,* 2003]. At dawn, Cl-initiated oxidation of VOCs is estimated to be comparable with that initiated by OH [*Canosa-Mas et al.,* 1999; *Finlayson-Pitts et al.*, 1999]. Inclusion of Cl-VOC reactions in a three-dimensional air quality model for the SoCAB indicates increases of up to 10 ppb in O_3 mixing ratios in coastal locations when the release of Cl_2 from sea salt aerosol is parameterized [*Knipping and Dabdub*, 2003].

Because Cl-initiated oxidation of VOCs likely affects O_3 formation in marine and industrialized locations, it is naturally hypothesized that such reactions may also enhance significantly the formation of SOA in similar areas. Outside of the study of *Karlsson et*

al. [2001], in which SOA formation from the Cl-initiated oxidation of toluene was studied, little work has been done to examine this phenomenon. Laboratory studies involving Cl-initiated oxidation of some typical biogenic and anthropogenic VOCs are described in Parts III and IV of this dissertation.

Empirical and mechanistic approaches are employed in current numerical simulation of SOA formation [*Kanakidou et al.*, 2005]. In one empirical approach, the two-product model is used to simulate equilibrium SOA concentration; this assumes that all the oxidation products of a VOC can be lumped into two hypothetical products and that the SOA is generated only from the condensation of these two products. The SOA yield can be evaluated based on the two apparent stoichiometric coefficients and the two apparent equilibrium partitioning coefficients, which are obtained empirically by calibrating the two-product model with observed yield data from chamber experiments. The two-product model can easily be extended easily to simulate a multiple VOC system [*Griffin et al.*, 1999a; *Griffin et al.*, 1999b]. The mechanistic approach, in which detailed reaction mechanisms are combined with an equilibrium absorptive partitioning model, has been used to simulate SOA formation in chamber and field experiments [*Barthelmie and Pryor*, 1999; *Kamens et al.*, 1999; *Kamens and Jaoui*, 2001; *Griffin et al.*, 2002a; *Griffin et al.*, 2002b; *Colville and Griffin*, 2004a; *Colville and Griffin*, 2004b; *Jenkin*, 2004; *Chen and Griffin*, 2005; *Johnson et al.*, 2006]. In most of these modeling studies, SOA mass growth is reproduced reasonably when estimated vapor pressures are lowered by 2 orders of magnitude. And field observed SOA formation is also simulated qualitatively using this approach. Generally speaking, modeling SOA formation is still in its early stage. The results from the laboratory experiments described in Parts III and IV

have lead to the development of a mechanistic computational model to simulate SOA formation from Cl-VOC reactions. This model is described in Part V of this dissertation. In Part VI, this dissertation provides overall conclusions and suggestions for future work.

CHAPTER II

THE SIZE-DEPENDENT INFLUENCE OF SURFACE TENSION ON THE ABSORPTIVE PARTITIONING OF SEMI-VOLATILE ORGANIC COMPOUNDS

Introduction

The lifetime of fine particulate matter (PM), its contribution to visibility degradation, and its respirability depend on its size distribution. Secondary organic aerosol (SOA) is the fraction of PM that is formed via gas-particle partitioning of the semi-or non-volatile products of the oxidation of volatile organic compounds. Available measurements indicate that ambient SOA most likely resides in submicron particles (Pickle *et al.*, 1990; Mylonas *et al.*, 1991; Venkataraman and Friedlander, 1994; Kleeman *et al.*, 2000; Wainman *et al.*, 2000; Geller *et al.*, 2002; Yao *et al.*, 2002). In chamber studies of SOA formation, submicron particles are commonly used as the condensation seeds (e.g., Odum *et al.*, 1996). Leaitch *et al.* (1999) and Kavouras and Stephanou (2002) implicate SOA formation pathways in new particle generation in forested atmospheres. Therefore, it is speculated that under appropriate conditions, in both ambient and laboratory cases, surface tension may play a significant role in the formation and the size distribution of SOA through the Kelvin effect that describes the size-dependent influence of particle curvature on the vapor pressures of components in the phase (Köhler, 1936). To date, there are only a few measurements of cloud droplet

surface tension (*e.g.*, Hitzenberger particle *et al.*, 2002). To the knowledge of the authors, no measurements of ambient organic aerosol surface tension have been reported. Partly due to the lack of an estimation technique for the surface tension of particles containing a myriad of chemical species, the activation properties of such aerosols have not been established (VanReken *et al.*, 2003). The effect of surface tension on SOA formation and its size distribution has not been examined previously. Pandis *et al.* (1993) developed one of the first models to predict the ambient SOA size distribution; however, they did not consider the thermodynamic details associated with particle size. In the classic thermodynamic theory of gas-particle partitioning developed by Pankow (1994), the effect of aerosol size on the formation of SOA is implicitly not considered. In the more recent analysis of the steady-state aerosol size distribution achieved in a continuous-flow chamber in the presence of particle growth by gas-particle conversion and particle removal by wall deposition, Seinfeld *et al.* (2003) also did not include a correction for the Kelvin effect. Recent simulations of SOA formation in an urban airshed based on the theory of Pankow (1994) also did not consider the Kelvin effect (Griffin *et al.*, 2002). In this paper, a size-dependent absorptive partitioning model for the formation of SOA that includes a theoretical framework to estimate the surface tension at equilibrium is developed.

Theory

Size-dependent SOA Formation in the Presence of Uniform-Size Pre-existing Aerosol

If the molar volumes of semi-volatile organic compounds (SVOCs) in the condensed phase are much smaller than the corresponding ones in the gas phase, the effect of aerosol curvature on the chemical potential of a specific SVOC *i* in the aerosol phase is described by (Lupis, 1983):

$$\mu_{i,g} = \mu_{i,om} + \overline{V}_i \frac{2\sigma}{r}; \qquad i = 1, N_{SOA}; \qquad N = N_{SOA} + N_{PA} \tag{1}$$

where $\sigma = \sigma(X_1, X_2, ..., X_N)$ (atm m) is the surface tension in the aerosol surface phase, which is a function of the mole fractions (X_1, X_2, ... X_N) of pre-existing aerosol (PA) and SOA components in the aerosol phase, r (m) is the radius of the aerosol, $\overline{V_i}$ (m^3 mol^{-1}) is the liquid molar volume of aerosol component i, $\mu_{i,g}$ (m^3 atm mol^{-1}) is its gas-phase chemical potential, $\mu_{i,om}$ (m^3 atm mol^{-1}) is its aerosol-phase chemical potential, and N_{SOA} and N_{PA} are the total number of SOA components and PA components, respectively. For simplicity in the modeling scenarios presented here, PA components are assumed to be non-volatile species with aerosol-phase concentrations that are unaffected by the partitioning of the SVOCs.

The chemical potential of species *i* in each phase is described by:

$$\mu_{i,g} = \mu_0 + RT \ln P_i \tag{2a}$$

$$\mu_{i,om} = \mu_0 + RT\ln\left(X_i\gamma_i P^0_{L,i}\right) \tag{2b}$$

where μ_0 (m^3 atm mol^{-1}) is the reference-state chemical potential, R is the ideal gas constant (here $8.2\times10^{-5} m^3$ atm $mol^{-1}K^{-1}$), T is the temperature (K), P_i (atm) is the partial pressure of species i, $P^0_{L,i}$ (atm) is its vapor pressure in the pure liquid state at temperature T, X_i is its mole fraction in the aerosol phase, and γ_i represents its activity coefficient in the aerosol phase. Combining equations (1) and (2) results in an expression for the partial pressure of species i:

$$P_i = X_i\gamma_i P^0_{L,i}\exp\left(\frac{2\overline{V}_i\sigma}{RTr}\right) \tag{3}$$

Combining equation (2) with the ideal gas law, as in Pankow (1994), results in a size-dependent governing equation for the equilibrium mole fraction of species i in the condensed phase:

$$X_i = \frac{G_i RT}{10^6 MW_i\gamma_i P^0_{L,i}}\exp\left(-\frac{2\overline{V}_i\sigma}{RTr}\right) \tag{4}$$

where MW_i is its molecular weight (g mol^{-1}), and G_i is its concentration in the gas phase (μg m^{-3} air).

The partitioning constant for a specific SVOC, $K_{i,om}$ (m^3 air μg^{-1}), that describes the mass distribution of species i between the gas and condensed phases is given by (Pankow, 1994):

$$K_{i,om} = \frac{A_{i,om}/M_0}{G_i} \tag{5}$$

where M_0 ($\mu g\ m^{-3}$ air) is the total mass concentration of aerosol (in this case SOA, primary organic aerosol (POA), and water) available to act as an absorptive medium and $A_{i,om}$ ($\mu g\ m^{-3}$air) is the mass concentration of SVOC species i in the aerosol phase.

Substitution of equation (4) into equation (5) and conversion from mass to mole fraction results in:

$$K_{i,om} = \frac{10^{-6} RT}{\gamma_i P^0_{L,i} \sum_{j=1}^{N} X_j MW_j} \exp\left(-\frac{2\overline{V}_i \sigma}{RTr}\right) \qquad i = 1, N_{SOA} \tag{6}$$

Combination of equations (5) and (6) yields:

$$\frac{A_{i,om}}{M_0} = \frac{10^{-6} G_i RT}{\gamma_i P^0_{L,i} \sum_{j=1}^{N} X_j MW_j} \exp\left(-\frac{2\overline{V}_i \sigma}{RTr}\right) \qquad i = 1, N_{SOA} \tag{7}$$

Assuming that the volume of the mixture in the aerosol phase is the sum of the volumes of the partitioned SVOCs and the pre-existing components, the size of the aerosol after SOA formation is determined by:

$$\frac{4}{3}\pi N_0\left[r^3 - r_0^3\right] = 10^{-6}\sum_{i=1}^{N_{SOA}}\frac{X_i\overline{V}_i M_0}{\sum_{j=1}^{N}X_j MW_j} \tag{8}$$

where r and r_0 (m) are the particle radii after and before SOA formation, respectively, and N_0 is the number concentration of PA particles (m^{-3}). The total mass concentration of organic aerosol is determined by:

$$M_0 = M_T\sum_{i=1}^{N}X_i MW_i \tag{9a}$$

$$M_T = \frac{\sum_{k=1}^{N_{PA}}(PAm_k / PAMW_k)}{\sum_{k=1}^{N_{PA}}PAX_k} \tag{9b}$$

where M_T (μmol m^{-3}air) is the total molar concentration of aerosol after partitioning of the SVOCs, PAm_k is the mass concentration (μg m^{-3} air) of PA component k, $PAMW_k$ (g mol^{-1}) is its molecular weight, and PAX_k is its mole fraction in the aerosol phase. Note that if $\overline{V_i}$ is written as the ratio of molecular weight and density, ρ_i (g m^{-3}), combination of equations (8) and (9) leads to:

$$\frac{4}{3}\pi N_0\left[r^3 - r_0^3\right] = 10^{-6}\sum_{i=1}^{N_{SOA}}\frac{X_i MW_i\sum_{k=1}^{N_{PA}}(PAm_k / PAMW_k)}{\rho_i\sum_{k=1}^{N_{PA}}PAX_k} \quad (10)$$

The mass balance equation for SOA in K multiple size bins is:

$$T_i = G_i + \sum_{K=1}^{BN} A_{i,om}^K = G_i + \sum_{K=1}^{BN}\frac{X_{K,i}M_{K,0}MW_i}{\sum_{j=1}^{N}X_{K,j}MW_j};\ i = 1,\ N_{SOA} \quad (11)$$

where BN is the total number of size bins and T_i (μg m^{-3} air) is the total ambient mass concentration of SVOC component i.

Estimation of Surface Tension

It has been found that the so called 'surface phase' of a multiple-component organic mixture usually differs in composition from that of the bulk phase and that the component or components with the lower pure component values of surface tension preferentially concentrate in the surface phase (Poling *et al.*,2000). The governing equations for the surface tension of the surface phase of a multi-component mixture are (Poling *et al.*, 2000):

$$\sigma_m = \sigma_i + \frac{RT}{S_i}\ln\frac{X_i^\sigma\gamma_i^\sigma}{X_i\gamma_i} \quad (i = 1, N) \quad (12)$$

$$\sum_i X_i^\sigma = 1 \tag{13}$$

where σ_m (here, dyn cm^{-1}) is the surface tension of the surface phase in a multi-component mixture, σ_i (dyn cm^{-1}) is the surface tension of pure component i, S_i (cm^2 mol^{-1}) is its molar surface area, X^σ_i is its mole fraction in the surface phase, and γ^σ_i is its activity coefficient in the surface phase. R has a value of 8.314×10^7 dyn cm mol^{-1} K^{-1} in equation (12). Simultaneous solution of equations (12) and (13) yields the mole fractions for each component in the aerosol surface phase and the aerosol surface tension. The activity coefficients of components in the bulk and surface phases are determined by the routine Universal Quasi-chemical Functional-Group Activity Coefficients (UNIFAC) (Fredenslund *et al.*, 1977, Larsen *et al.*, 1987). The molar surface area of species i is estimated by the method of Tyn and Calus (Poling *et al.*, 2000):

$$S_i = 1.021\times10^8 V_{c,i}^{6/15} V_{b,i}^{4/15} \tag{14}$$

where $V_{c,i}$ (cm^3) is the critical volume for component i and $V_{b,i}$ (cm^3) is its volume at its normal boiling point. $V_{b,i}$ is determined by the empirical relationship $V_{b,i} = 0.285 V_{c,i}^{1.048}$. $V_{c,i}$ is estimated by a group contribution method (Poling *et al.*, 2000).

For strong hydrogen-bonding organics, the method of Sastri and Rao is used to estimate individual surface tensions in the pure liquid state. This empirical relationship for a specific organic compound in the aerosol phase is given by (Poling *et al.*, 2000):

$$\sigma_i = K_i P_{c,i}^{x_i} T_{b,i}^{y_i} T_{c,i}^{z_i} \left[\frac{1-T_{r,i}}{1-T_{br,i}}\right]^{m_i}; \quad T_{r,i} = T/T_{c,i}; \quad T_{br,i} = T_{b,i}/T_{c,i} \tag{15}$$

where $T_{b,i}$ (K) is the normal boiling point of species i, $T_{c,i}$ (K) is its critical temperature, and $P_{c,i}$ (bar) is its critical pressure. Empirical parameters K_i, x_i, y_i, z_i, and m_i are listed in Table 1 for different SVOC classes. For organics that have significantly weaker hydrogen bonding, the method of Brock and Bird is employed to estimate the pure liquid state surface tension (Poling *et al.*, 2000):

$$\sigma_i = P_{c,i}^{2/3} T_{c,i}^{1/3} Q_i \left(1-T_{r,i}\right)^{11/9} \tag{16a}$$

$$Q_i = 0.1196\left[1+\frac{T_{br,i}\ln(P_{c,i}/1.01325)}{1-T_{br,i}}\right]-0.279 \tag{16b}$$

The $T_{b,i}$, $T_{c,i}$, and $P_{c,i}$ values for organic compounds required in the Sastri-Rao and Brock-Bird methods are estimated by a group contribution method similar to that used in UNIFAC (Poling *et al.*, 2000). It is claimed that both the Sastri-Rao method and the Brock-Bird method have an error less than 5% (Poling *et al.*, 2000)

In each iteration step (described in the subsequent section on numerical implementation), a new set of estimated values for the mole fractions of components in the bulk aerosol phase is generated. The new estimates of the mole fractions of components in the bulk aerosol phase are used to correct the aerosol surface tension for each iteration step. The unknowns in equations (12) and (13) are the mole fractions for different components in the surface phase of the aerosol particle and the aerosol surface tension. The Newton-Raphson Method (Burden and Faires, 1989) is employed to solve

simultaneously equations (12) and (13). The bulk mole fractions for various components are used as the initial estimate for the surface phase mole fractions for different components. The initial estimate for the surface tension is taken as the arithmetic average of the pure liquid state surface tensions for the individual components.

The bulk activity coefficients of SVOC species are calculated by the common routine UNIFAC as described by Fredenslund *et al.* (1977). This version of UNIFAC has proven to be particularly useful for making reasonable estimates for activity coefficients in non-ideal mixtures for which data are sparse or totally absent (Poling *et al.*, 2000). In this study, the group volume parameters, group surface area parameters, and group interaction parameters required in UNIFAC are adopted from Walas (1985) and Gmehling *et al.* (1993). However, when evaluating aerosol surface tension, activity coefficients are computed by the Larsen version of UNIFAC (Larsen *et al.*, 1987) because this version of UNIFAC is the only one that can be used to predict successfully the surface tensions for both pure organic mixtures and aqueous mixtures (Suarez *et al.*, 1989). The modified UNIFAC model by Larsen differs from the original UNIFAC model in the computation of the residual part of activity coefficients and the group interaction parameters. The group interaction parameters in the Larsen version of UNIFAC are also temperature dependent. All other required parameters in both models are the same.

Numerical Simulation

Input Parameters and Case Design

Numerical simulations are conducted to investigate the size-dependent formation of SOA and the effect of surface tension based on the above theoretical framework. As in our previous work (Cai and Griffin, 2003), six semi-volatile organic oxidation products are chosen as SOA components: (1) pinic acid, a semi-volatile oxidation product of the biogenic hydrocarbons α- and β-pinene (Yu *et al.*, 1999a, 1999b); (2) 3-methyl-2,5 furandione; (3) 4-methyl-2-nitrophenol; (4) dihydro-2,5-furandione; (5) *m*-toluic acid (Components 2 through 5 are examples of oxidation products of aromatic organic pollutants (Forstner *et al.*, 1997).); and (6) methane sulfonic acid, which is the oxidation product of dimethylsulfide (Andreae and Crutzen, 1997). Eight organic PA components are assumed based on available observations (Duce *et al.*, 1983; Rogge *et al.*, 1993; Didyk *et al.*, 2000). These are (1) *n*-nonacosane, (2) succinic acid, (3) naphthalene-2,6-diacid, (4) benzo(ghi)perylene, (5) octadecanoic acid, (6) phthalic acid, (7) 17(α)H-21(β)H-hopane, and (8) cyclic/branched material. Ambient liquid water is also considered as an absorptive medium for the six SOA components in this study. The molecular structures of SOA and PA components, as well as their molecular properties, are described in our previous work (Cai and Griffin, 2003). Table 2 lists the assumed total mass concentrations of all six SOA components, eight POA components, and ambient liquid water content (LWC).

The temperature dependence of the vapor pressures of the partitioning species is estimated by their boiling points and vaporization entropy (Schwarzenbach *et al.*, 1993; Myrdal and Yalkowsky, 1997; Sheehan and Bowman, 2001). The expression of

Kistiakowsky with the Fishtine correction is used to estimate vaporization entropy for the partitioning species (Schwarzenbach *et al.*, 1993). If measured boiling points are unavailable, the methods of Sugden and McGowan based on chemical structure are employed to estimate the boiling points (Rechsteiner, 1990). Unknown pK_a values are estimated by the Hammett correlation (Schwarzenbach *et al.,* 1993) or assigned by analogy (Morrison and Boyd, 1987).

Three cases at 298K are studied: the polar-only PA case, the mixed PA case, and the water aerosol case. In the polar-only PA case, the PA consists of POA compounds 2 through 7, all of which have polar character (i.e., they contain functional or aromatic groups or have an asymmetric structure). In the mixed PA case, the PA includes all eight POA compounds. Water is the only absorptive medium in the water aerosol case. In each of these three cases, the SVOC components are the same. The particle number concentrations of POA and the ambient water aerosol are determined by a mass-volume relationship based on their assumed r_0. Simulations are performed to examine the Kevin effect on SOA formation by simulating SOA formation over a range of PA initial diameters (10 nm, 20 nm, 40 nm, 100 nm, and 200 nm). The existence of the aerosol surface phase is not taken into account in the evaluation of the partitioning equilibrium. No significant error should result from this assumption because the total mass of the bulk aerosol phase is very large compared to the total mass of the aerosol surface phase.

Treatment of Aqueous Aerosol

In the current work, an approach based on Raoult's law with activity correction is used to describe the secondary organic compound air-water partitioning. In this simplified case, water aerosol is assumed to contain no inorganic species. While this

limits the applicability of the results presented here, it is sufficient for a first-order estimate because it is often assumed that the surface tension of aerosol particles that consist of aqueous solutions is equivalent to that of water (Seinfeld and Pandis, 1998). A charge balance is considered to determine *p*H, which is used to compute the concentration of the ionic forms of each dissociative SVOC in the aqueous aerosol. The Davis formula (Stumm and Morgan, 1996) is used to correct for ionic strength in this case. Greater detail on the mathematical model used here to describe air-water partitioning can be found in Cai and Griffin (2003).

Numerical Implementation.

Equation (7) combined with equations (10) through (13) are solved numerically to evaluate the SOA concentration and final diameter at equilibrium. The iteration procedures are to: (1) provide an array of initial estimates of G_i; (2) estimate X_i; (3) compute activity coefficients of each SVOC in the bulk aerosol phase; (4) calculate the aerosol diameter after SOA formation by equation (10); (5) solve equations (12) and (13) simultaneously to evaluate aerosol surface tension; (6) solve equation (7) to compute the SOA concentration; and (7) check the mass balance (equation (11)) to generate a new set of G_i. Procedures (2) through (7) are repeated until each equation has a tolerable error of 1.0E-10.

Simplification of Numerical Calculations.

The computational scheme presented in section 3.3 is very computationally expensive and therefore is not amenable for implementation into three-dimensional air quality models. To save computational burden, it is possible to first calculate SOA concentrations without considering the Kelvin effect and then apply the Kelvin correction

based on the results. In equation (7), it is shown that the SOA distribution subject to the Kelvin effect is equivalent to a SOA distribution with a modified SVOC pure liquid state vapor pressure ($NEWP^0_{L,i}$) as follows:

$$NEWP^0_{L,i} = P^0_{L,i} \exp\left(\frac{2\overline{V_i}\sigma}{RTr}\right) \tag{17}$$

meaning that $A_{i,om}$, M_o, and G_i all differ between the case in which the Kelvin effect is considered and that in which the Kelvin effect is ignored. It is easy to derive from equation (7) and the theory of Pankow (1994) that:

$$\frac{A_{i,om}}{A'_{i,om}} = \frac{M_0 G_{i,g}}{M'_0 G'_{i,g}} \exp\left(-\frac{2\overline{V_i}\sigma}{RTr}\right) \tag{18}$$

where the apostrophe represents the case without considering the Kelvin effect. According to a mass balance for a given T_i, if $M_0 < M_0$', then we have G_i' $< G_i$. If the Kelvin effect is not too strong, the assumption that $M_0 G_i \sim M_0$'G_i' leads to:

$$A_{i,om} / A'_{i,om} = \exp\left(-2\overline{V_i}\sigma / RTr\right) \tag{19}$$

This approximation can be used to compute SOA concentrations under the influence of the Kelvin effect from the SOA concentrations without considering the Kelvin effect, or vice versa, and greatly reduce computational burden.

Results and Discussion

SOA Kelvin Factor

Figure 1 indicates the effect of PA initial diameter on the Kelvin factors of different SVOC species. The Kelvin factor is defined as the exponential part of equation (7). Due to the limited availability of SVOC species, particles do not grow to a size much larger than their initial size. Thus, SOA Kelvin factors are determined by the species molecular properties and the PA initial size. In the polar-only PA case, the aerosol surface tension is greater than that in the mixed PA case. Therefore, the Kelvin factors for pinic acid, dihydro-2,5-furandione and *m*-toluic acid in polar-only PA are lower than those in mixed PA. This means that when PA includes some non-polar organic compounds, its surface tension decreases and SOA formation increases due to the importance of the Kelvin effect decreasing. It is found that in both polar-only PA and mixed PA cases, the Kelvin factors for different SOA species decrease in the order of dihydro-2,5-furandione, *m*-toluic acid, and pinic acid. This is explained simply by their molecular weights (and therefore molar volumes), which increase in the same order. The same distribution pattern of the Kelvin factors of different SOA species is also found in water aerosol (Figure 2). The Kelvin factors of different SOA species in water aerosol are generally smaller than those in organic PA because water has larger surface tension than most organic compounds due to its very strong polarity. This indicates that the Kelvin effect is more likely to decrease SOA formation in aqueous aerosols relative to organic PM. The other important feature to note in Figures 1 and 2 is that the Kelvin factor for all species approaches 1.0 as PA initial diameter increases above 200 nm,

regardless of PA chemical characteristics. As would be expected, the effect of surface tension is greatest at the smallest particle sizes.

Total SOA Concentration

Figures 3 and 4 compare the total SOA concentration considering the Kelvin effect with the total SOA concentration without considering the Kelvin effect in the polar-only PA, mixed PA, and water aerosol cases. If an apparent Kelvin factor is defined as the ratio of the total SOA concentration in PA with the Kelvin effect to the total SOA concentration in the same PA without the Kelvin effect, Figures 3 and 4 indicate that this apparent Kelvin factor is between the maximum and minimum Kelvin factors for the six individual SVOC species under the same conditions but closer to the minimum one (Figures 1 and 2). Generally speaking, when the PA initial size is less than 100 nm, the Kelvin effect on total SOA concentration becomes significant and is controlled primarily by the polarity of the partitioning species and the absorbing medium. The Kelvin effect on total SOA concentration in the polar-only PA case is greater (i.e., a smaller Kelvin factor) than that in mixed PA case. The case of water aerosol is predicted to have the largest Kelvin effect on absorbed SOA concentrations.

Griffin *et al.* (2003) indicate that a ten-fold increase in the mass concentration of a relatively non-polar component in the PA causes about a 14% decrease of the total organic-phase SOA concentration. In that analysis, the Kelvin effect is ignored, but the total concentrations and species used are very similar to those in this work. The previous result is explained by the fact that a ten-fold increase in the mass concentration of the relatively non-polar PA component results in an absorbing medium that is dominated by non-polar components. This shift leads to an increase in activity and a subsequent

decrease in partitioning. However, Figure 3 in the current study shows that when the Kelvin effect is ignored, the addition of 4.16 μg m^{-3} of non-polar PA components (i.e., POA1 and POA8) causes a very small increase in the total SOA concentration. This is reconciled by the fact that the absorbing medium is still dominated by polar PA components after a combined 4.16 μg m^{-3} increase in the concentrations of the non-polar PA components. Therefore, in this case, the increase of the concentration of the absorbing medium outweighs the influence of the increase in activity.

In the case considering the Kelvin effect, the total concentration of SOA is influenced by the non-polarity of the PA components in two ways. On one hand, the non-polarity of PA components reduces the aerosol surface tension and the Kelvin effect, thereby increasing the total SOA concentration. (See Figure 3.) On the other hand, the non-polarity of PA may decrease the total SOA concentration due to activity considerations (Griffin *et al.*, 2003). When the mixed PA is dominated by polar PA components, the total SOA concentration in the mixed PA case is predicted to be higher than that in the case of polar-only PA (Figure 3). However, if the mixed PA were to be dominated by non-polar components, and the initial PA diameter were large (for example, larger than 200 nm), the total SOA concentration in the mixed PA case would be smaller than that in polar-only PA case. Conversely, the total SOA concentration in the mixed PA case is higher than that in the polar-only PA case when the initial PA diameter is small (for example, less than 50 nm).

The total SOA concentrations without considering the Kelvin effect, T'_{SOA} (μg m^{-3}), in Figures 3 and 4 are approximated via the method described in section 3.4:

$$T'_{SOA} = \sum_{i=1}^{N_{SOA}} A_{i,om} \exp\left(\frac{2\overline{V_i}\sigma}{RTr}\right) \quad (20)$$

This approximation is very good and agrees very well with the results from the code without considering the surface tension correction when the total SOA concentration is small (Figure 3). It is not as good when the total SOA concentration is high or when the Kelvin effect is very significant, as in Figure 4 when the water aerosol initial diameter is very small. This is why T'_{SOA} slightly increases with decreasing aerosol initial diameter when the initial diameter of the water aerosol is smaller than 50 nm.

Surface Tension

Three additional simulation runs are performed to obtain the relationships between the aerosol surface tension and the total SOA concentration in PAs for the three cases (i.e., the polar-only PA, mixed PA, and water aerosol cases). This is achieved by changing the total SOA concentrations in different PAs discretely and solving equations (12) and (13) simultaneously. In these simulations, the total SOA concentrations are increased gradually from zero to the previously predicted equilibrium SOA concentrations for each of the three cases (sections 4.1 and 4.2). The proportionality of each SVOC species concentration in PA is kept the same as that in the predicted equilibrium SOA distributions for each of the three cases. In the polar-only case (Figure 5), all PA and SOA components are polar and have similar surface tensions in the pure liquid state (Table 3). Thus, in the aerosol surface phase for the polar-only case, the surface tension does not vary strongly (note the scale). The slight change of surface tension is caused by the decrease of the mole fraction of the compound with the

minimum pure state surface tension with the addition of SVOC species. The compound with the minimum pure state surface tension in this case is POA7 (the hopane compound). In the mixed case (Figure 6), the non-polar compounds with the minimum pure liquid state surface tensions, POA1 and POA8 (the long-chain alkane and the highly cyclic and branched compound), preferentially dominate the composition in the aerosol surface phase, leading to aerosol surface tension becoming quite low. With the addition of SVOC species with higher pure liquid state surface tensions, the mole fraction of non-polar compounds in the aerosol surface phase slowly decreases, leading to a slow increase in aerosol surface tension.

Because the pure liquid state surface tensions for most of the SVOC species are lower than the surface tension of pure water, SVOC species tends to accumulate in the aerosol surface phase and lead to a decrease of aerosol surface tension (Figure 7). This agrees well with observations and other theoretical modeling studies (Facchini *et al.* 1999; Facchini *et al.*, 2000; Charlson *et al.*, 2001; Hitzenberger *et al.,* 2002). Nenes *et al.* (2002) found that the decrease of the surface tension of aqueous aerosol caused by organic compound partitioning may affect the number of cloud condensation nuclei as much as 50% of the Twomey effect for marine aerosols and even larger than the Twomey effect for urban aerosols. With regard to the prediction of the effect of organic compounds on the aerosol surface tension, the theoretical framework employed in current study is more advantageous than the empirical relationship used by Facchini *et al.* (1999). The methodology used here considers specifically a myriad of different organic compounds. The earlier empirical relationship considers only the total concentration of organic compounds in the aerosol and does not distinguish between different organic

compounds and their different combinations in the aerosol phase. Therefore, it is suggested that a surface tension estimation technique such as that presented here be used in future studies understanding the effect of organic species on cloud condensation nuclei formation if information on the speciation of the organic material is available.

Conclusions

Simulation results in this study indicate that the Kelvin effect on SOA formation depends on both the SVOC species and the polarity of the PA. If the PA contains a large fraction of non-polar organic species, aerosol surface tension becomes very small, and the Kelvin effect is small and may be negligible. If PA is dominated by polar organic compounds, the Kelvin effect on SOA formation is significant when PA initial diameter is smaller than approximately 100nm. The Kelvin effect is larger (i.e., smaller Kelvin factors) for SVOCs with larger molecular weights. Because SVOCs with larger molecular weights usually have lower vapor pressure, the Kelvin effect is greater for those SVOCs that are more likely to partition to the aerosol phase.

The size distribution of secondary carbonyl groups measured by Pickle *et al.* (1990) indicates maximal diameters in the 0.12 - 0.26 μm and 0.5 - 1.0 μm size ranges. The secondary organonitrate aerosol size distributions measured by Mylonas *et al.* (1991) were typically bimodal with maximal diameters in the 0.05 - 0.075 μm and 0.12 - 0.26 μm size ranges. Ambient polycyclic aromatic hydrocarbon and elemental carbon size distributions in the Los Angeles basin are also found to be bimodal with diameter peaks in the 0.05 - 0.12 μm and 0.5 - 1.0 μm size ranges (Venkataraman *et al.*, 1994). The particle mass distributions from all mobile sources tested by Kleeman *et al.* (2000) were

found to have a single mode that peaked at approximately 0.1 - 0.2 μm particle diameter. The smog chamber experiment studies on SOA formation in indoor air conducted by Wainman *et al.* (2000) indicate that measurable particle formation and growth occurred almost exclusively in the 0.1 - 0.2 μm and 0.2 - 0.3 μm diameter size fractions in all of their experiments. Yao *et al.* (2002) reported that the condensation mode of oxalate was usually observed at 0.177 - 0.32 μm (diameter size range) in a sampling site in downtown Hong Kong. The mass distribution of ultrafine organic carbon particles found in Downey and Riverside, Southern California, was concentrated in the 32 - 56 nm and 100 - 180 nm diameter size ranges (Geller *et al.,* 2002). Field measurements and modeling studies verified SOA formation via a nucleation pathway (Marti *et al.*, 1997; Kerminen, 1999; Leaitch *et al.*, 1999; Kavouras and Stephanou, 2002; Anttila and Kerminen, 2003). These observations and modeling studies in conjunction with the theoretical simulations presented here suggest that future modeling of ambient or indoor SOA formation may need to consider the Kelvin effect due to particle diameters often being less than 200 nm. In laboratory cases, where aerosol seed size is centered around approximately 100nm, the Kelvin effect on derived partitioning coefficients may also need to be considered.

Table 2.1. Values of constants for the Sastri-Rao method to estimate individual surface tensions (Poling *et al.,* 2000).

	K	*x*	*y*	*z*	*M*
Alcohols	2.280	0.25	0.175	0.00	0.80
Acids	0.125	0.50	-1.50	1.85	1.22
Others	0.158	0.50	-1.50	1.82	1.22

Table 2.2. Assumed total concentrations of SVOCs, PA components, and LWC for the case studies of size-dependent gas-particle partitioning. Species numbers refer to the order in which they are referenced in the text.

SVOC Species	Concentration ($\mu g\ m^{-3}$)	POA Species	Concentration ($\mu g\ m^{-3}$)	LWC	Concentration ($\mu g\ m^{-3}$)
1	10	1	0.83	LWC	50
2	35	2	0.83		
3	10	3	0.83		
4	20	4	3.33		
5	10	5	4.98		
6	1	6	1.66		
		7	0.83		
		8	3.33		

Table 2.3. Estimated pure liquid state surface tensions of SVOCs and PA components at 298K. For comparison, the pure liquid state surface tension of water at 298K is 72 dyn cm^{-1} (Seinfeld and Pandis, 1998). Species numbers refer to the order in which they are referenced in the text.

SVOC Species	Surface Tension (dyn cm^{-1})	PA Components	Surface Tension (dyn cm^{-1})
1	34.22	1	0.60
2	36.68	2	34.81
3	91.66	3	44.36
4	34.47	4	40.89
5	37.20	5	31.60
6	48.68	6	40.54
		7	28.81
		8	0.44

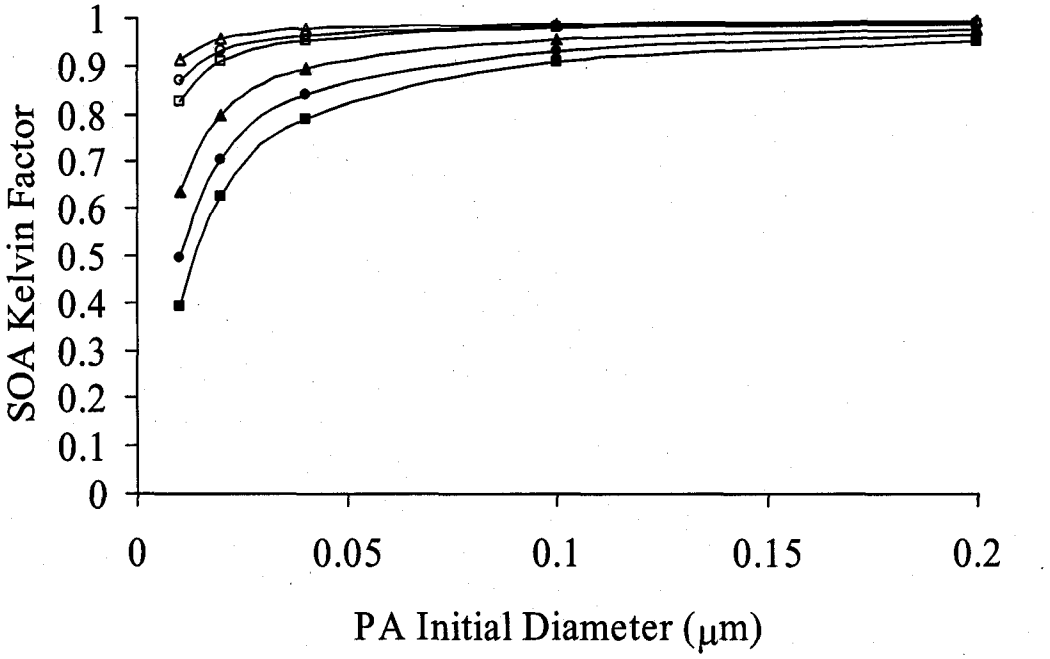

Figure 2.1. SOA Kelvin factors for dihydro-2,5-furandione (triangles), *m*-toluic acid (circles), and pinic acid (squares) as a function of POA initial diameter in the polar-only PA (filled) and mixed PA (open) cases.

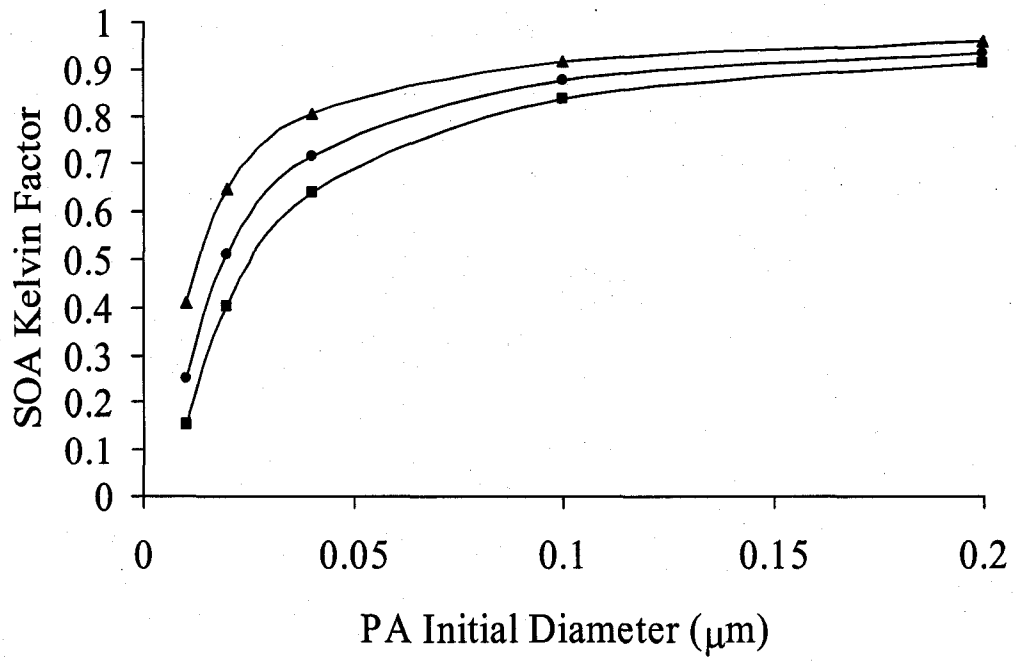

Figure 2.2. SOA Kelvin factors for dihydro-2,5-furandione (triangles), *m*-toluic acid (circles), and pinic acid (squares) as a function of water aerosol initial diameter.

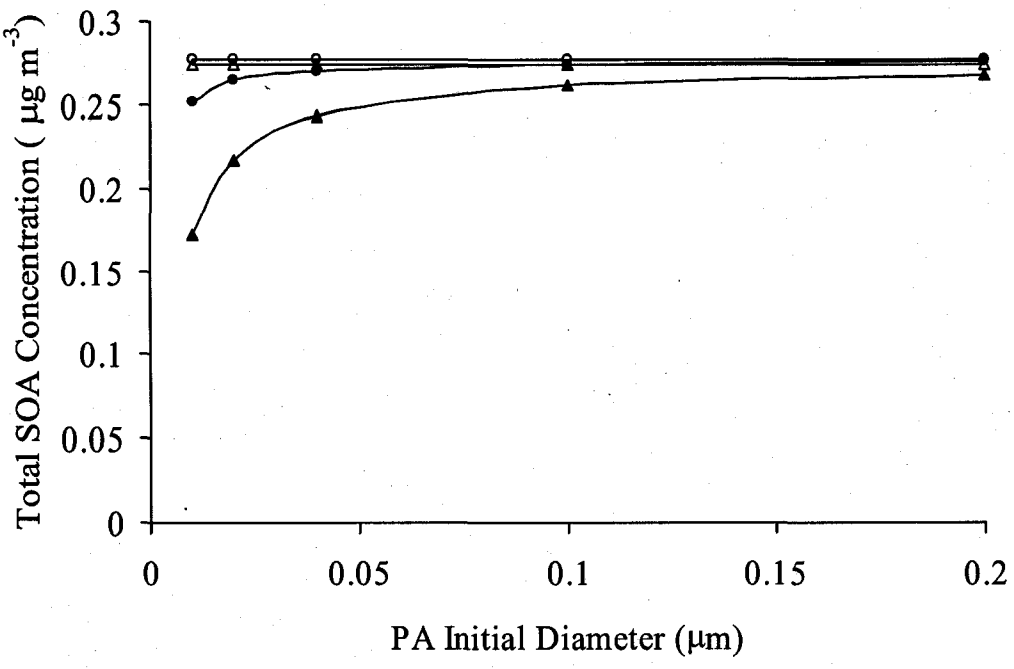

Figure 2.3. Total SOA concentration as a function of POA initial diameter in the polar-only PA (triangles) and mixed PA (circles) cases when the Kelvin effect is both considered (filled) and ignored (open).

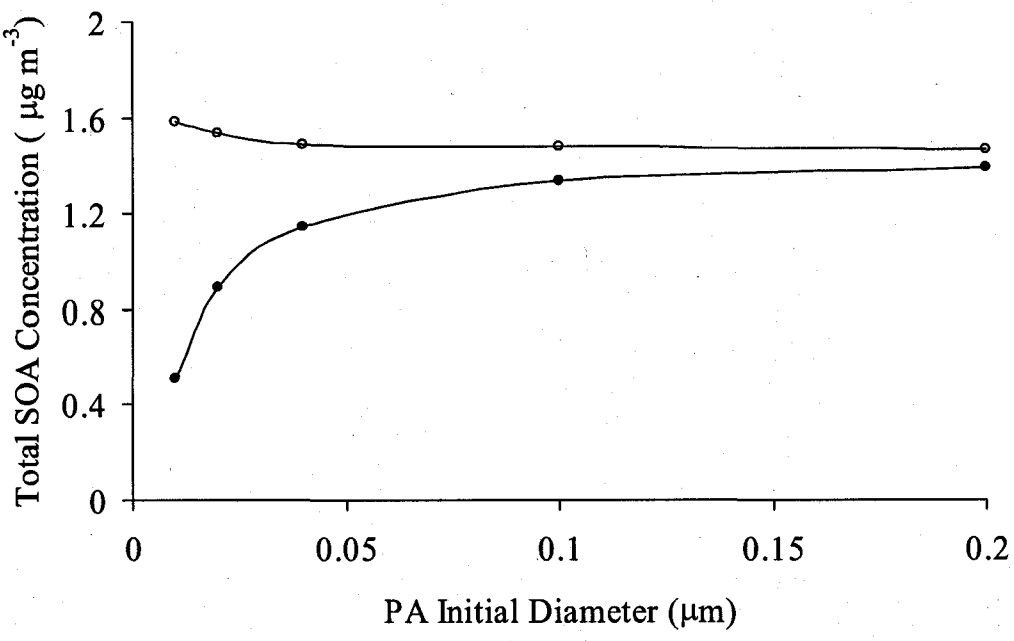

Figure 2.4. Total SOA concentration as a function of water aerosol initial diameter when the Kelvin effect is both considered (filled) and ignored (open).

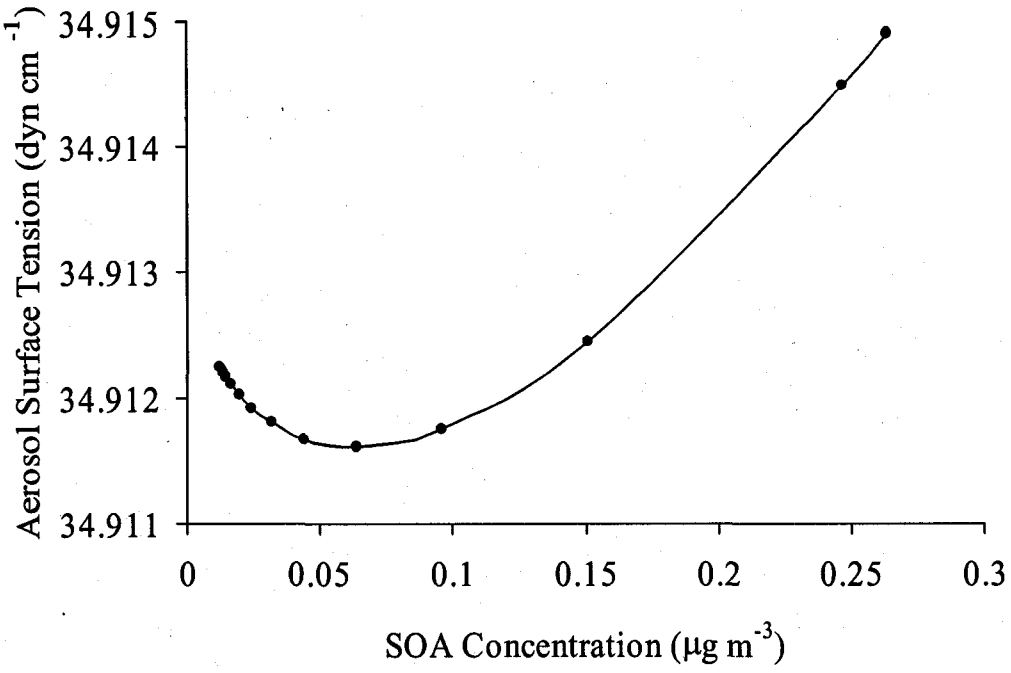

Figure 2.5. Aerosol surface tension as a function of total SOA concentration in the polar-only PA case.

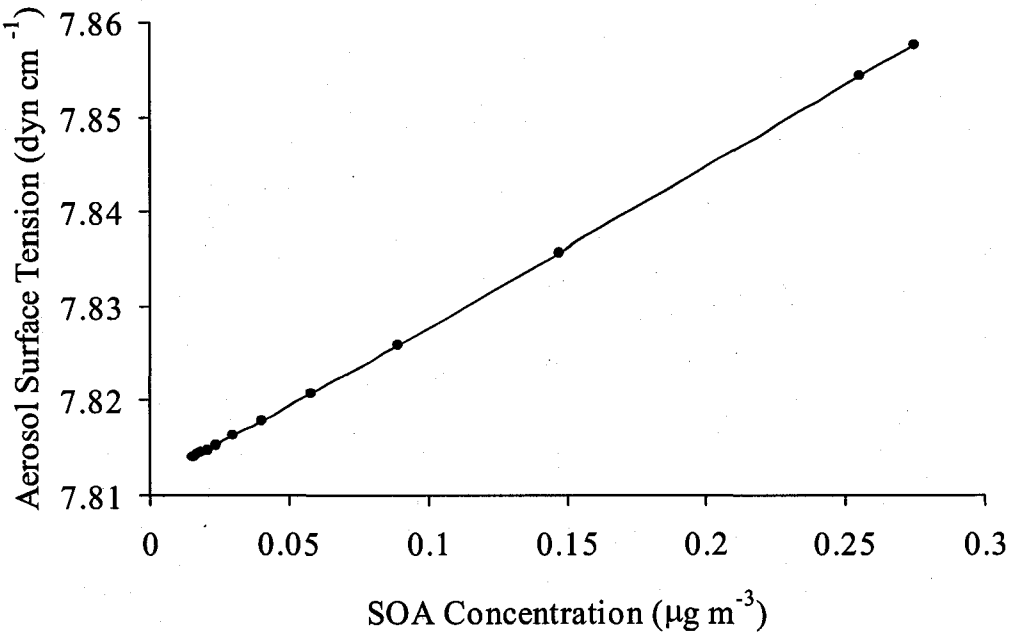

Figure 2.6. Aerosol surface tension as a function of total SOA concentration in the mixed PA case.

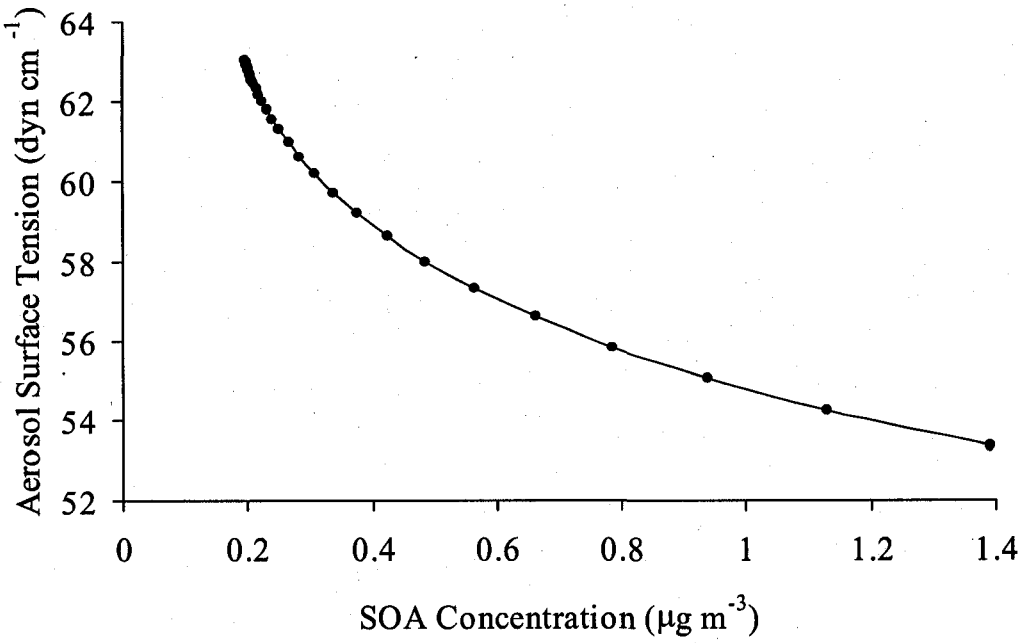

Figure 2.7. Aerosol surface tension as a function of total SOA concentration in the water aerosol case.

CHAPTER III

SECONDARY AEROSOL FORMATION FROM THE OXIDANT OF BIOGENIC HYDROCARBONS BY CHLORINE ATOMS

Introduction

Aerosol particles affect air quality and climate significantly. Epidemiological evidence links increased morbidity and mortality to increased concentrations of atmospheric particulate matter (PM) [*Lippmann et al.*, 2000]. Atmospheric particles also influence visibility degradation due to their light scattering capabilities [*Mazurek et al.*, 1997], alter the global radiative balance through scattering or absorption of incident solar radiation (direct effect of aerosol particles on climate) [*Charlson et al.*, 1992], and act as the cloud condensation nuclei around which clouds form, thereby changing the albedo of the Earth due to effects on cloud lifetime, droplet size, and number distribution (indirect effect of aerosol particles on climate) [*Twomey et al.,* 1978].

Organic aerosol (OA) is a ubiquitous constituent of atmospheric PM [*Murphy et al.*, 1998] and consists of primary organic aerosol (POA) and secondary organic aerosol (SOA). POA is emitted directly to the atmosphere from sources such as combustion processes [*Rogge et al.*, 1993; *Schauer et al.*, 1996]. Gas-phase oxidation of volatile organic compounds (VOCs) often yields non-and/or semi-volatile products. The partitioning of these non-and semi-volatile organic compounds (SVOCs) generally via

absorption into an OA phase or via dissolution into an aerosol aqueous phase leads to the formation of SOA [*Pankow*, 1994a; *Pankow*, 1994b; *Saxena and Hildemann,* 1996]. It has been estimated that a range of 20 to 80% of observed OA in the South Coast Air Basin (SoCAB) of California is secondary in nature [*Turpin and Huntzicker,* 1995; *Schauer et al.,* 1996]. Clearly, this fraction depends on many factors including specific location, time of day, and method of calculation. Higher concentrations and fractions of SOA generally indicate conditions conducive to photochemistry.

On a global scale, SOA is predicted to contribute significantly to the tropospheric aerosol burden. The modeling results of *Chung and Seinfeld* [2002] indicate that SOA generally constitutes 10 to 20% of the total OA at the Earth's surface. In polar regions, however, it is predicted to contribute up to 50%. *Tsigaridis and Kanakidou* [2003] estimate that the global annual SOA production from biogenic VOCs (BVOCs) ranges from 2.5 to 44.5 Tg yr^{-1} of organic matter, whereas that from anthropogenic VOCs ranges from 0.05 to 2.62 Tg yr^{-1}. *Griffin et al.* [1999a] obtained an estimate for atmospheric SOA formed annually from biogenic precursors of 18.5 Tg. The modeling results of *Lack et al.* [2004] show that global SOA production has significant seasonal variation. Maximum SOA concentrations are found over North America, Europe, and South America during the months of June to August. While minimum SOA concentrations over Asia are found in June, they remain high from September through December. In Africa, SOA concentrations are found to have less seasonal variability. Simulations using regional models also highlight the importance of SOA on smaller geographic scales [*Andersson-Skold and Simpson,* 2001; *Schell et al.,* 2001; *Griffin et al.*, 2002; *Pun et al.*, 2003; *Liousse et al.*, 2005].

BVOCs play an important role in tropospheric chemistry because of their large emission rates and their atmospheric reactivity [*Chameides et al.*, 1988; *McKeen et al.*, 1991; *Roselle et al.*, 1991; *Fehsenfeld et al.*, 1992]. They are important precursors to tropospheric ozone (O_3) [*Chameides et al.*, 1988; *Roselle et al.*, 1991; *Bell and Ellis*, 2004] and yield non- and/or semi-volatile secondary oxidation products that condense to form SOA [*Odum et al.*, 1996; *Hoffmann et al.*, 1997; *Griffin et al.*, 1999b]. *Kanakidou et al.* [2000] estimate that the emission rate of non-isoprene biogenic hydrocarbons is 210 Tg C yr^{-1}, comprised by 127 Tg C yr^{-1} of monoterpenes and 83 Tg C yr^{-1} of other reactive VOCs (ORVOCs). The most important monoterpenes on an emission basis are α-pinene, β-pinene, sabinene, and d-limonene, accounting for 40-80% of the overall terpene emission on a global scale [*Kanakidou et al.*, 2005]; each of these species also produce SOA upon oxidation. According to *Griffin et al.* [1999a], approximately 30% of the lumped biogenic ORVOCs have the potential to form SOA. Isoprene is by far the most abundant BVOC (emitted at a rate of approximately 500 Tg yr^{-1} globally) [*Guenther et al.*, 1995]. The ability of isoprene to form SOA upon oxidation has been identified only recently [*Claeys et al.*, 2004a; *Claeys et al.*, 2004b; *Kroll et al.*, 2005; *Lim et al.*, 2005; *Matsunaga et al.*, 2005], but characterization of its SOA formation potential is far from complete.

Due to the significant contribution of SOA to the regional and global tropospheric aerosol burdens, many studies have been conducted to attempt to understand the chemical reactions and thermodynamic processes that lead to its formation. The reader is referred to the review of *Seinfeld and Pankow* [2003]. These studies have focused on VOC oxidation by hydroxyl radicals (OH), O_3, oxygen atoms (O), and nitrate radicals (NO_3).

They have investigated yield, gas-phase products, aerosol speciation, product phase partitioning, and the effects of environmental variables such as temperature and relative humidity for multiple VOCs, most commonly aromatics and monoterpenes, using both experimental and computational techniques.

Another potential atmospheric oxidant of VOCs is the chlorine atom (Cl), which forms in coastal environments, near industrial sources, and in close proximity to swimming pools. It has been suggested that molecular chlorine (Cl_2) may be generated by sea salt aerosol reactions [*Spicer et al.,* 1998*; Knipping et al.*, 2000]. Cl_2 is then photolyzed to form Cl. Recent studies have shown the significant potential for Cl to act as an organic oxidant in coastal and industrialized areas [*Ganske et al.,* 1992*; Keene et al.,* 1996*; Spicer et al.,* 1998; *Canosa-Mas et al.,* 1999*; Finlayson-Pitts et al.*, 1999; *Tanaka et al.,* 2003]. At dawn, Cl-initiated oxidation of VOCs is estimated to be comparable with that initiated by OH [*Canosa-Mas et al.,* 1999; *Finlayson-Pitts et al.*, 1999]. Inclusion of Cl-VOC reactions in a three-dimensional air quality model for the SoCAB indicates increases of up to 10 ppb in O_3 mixing ratios in coastal locations when the release of Cl_2 from sea salt aerosol is parameterized [*Knipping and Dabdub*, 2003].

Because Cl reactions with VOCs have been demonstrated to affect O_3 in coastal and industrialized locations, it is hypothesized that such reactions trigger the formation of SOA in similar areas. Outside of the study of *Karlsson et al.* [2001], in which SOA formation from the Cl-initiated oxidation of toluene was studied, little work has been done to examine this phenomenon. The purposes of this paper are to test the hypothesis that the Cl-initiated oxidation of some typical BVOCs forms meaningful amounts of SOA

and to quantify the yield of SOA formation from the oxidation of BVOCs initiated by Cl in a laboratory environmental simulation chamber.

It is known that chlorine-catalyzed oxidation of organic compounds play important role in atmospheric chemistry, for example, evidence shows that in O_3 depletion events observed during sunrise in the Arctic, non-methane hydrocarbons and ozone may be destroyed by Cl-catalyzed oxidation [*Kieser et al.*, 1993; *Johnson et al.*, 1994; *Ariya et al.*, 1998; *Ariya et al.*, 1999]. In chlorine-catalyzed oxidation of organics, ClO acts as a catalyst; the rate of initiation step in this process is slower than that of propogation; and usually one of the net effects of the reaction cycle is the destruction of O_3 [*Lary and Toumi*, 1997]. However, this study is focused only on Cl-initiated oxidation of biogenic hydrocarbons because in our experiments, no O_3 is used.

Mechanism of SOA Formation

A large number of products typically is generated when a parent VOC with a large number of constituent carbon atoms is oxidized [*Atkinson*, 1994]. Some of these products distribute themselves between the gas and aerosol phases to form SOA, if in general, the parent VOC has at least 5 or 6 carbon atoms [*Seinfeld and Pankow*, 2003]. Consider a parent BVOC reacting with Cl. A variety of organic products (P_i) forms as follows:

(R1) BVOC + Cl → $\alpha_1 P_1 + \alpha_2 P_2 + \ldots$

(R2) P_i + Cl → additional products

The parameter α_i represents a stoichiometric coefficient relating the total concentration of product i formed to the total concentration of BVOC that reacts. In SOA studies, this constant is expressed typically on a mass, rather than the usual molar, basis. As shown in (R2), any of these products can further react with any of the available oxidants, in this case Cl, to create additional oxidation products. Those products with sufficiently low vapor pressure or high solubility form SOA through partitioning to the aerosol phase.

Fractional Aerosol Yield

Following the SOA formation model developed by *Pandis et al.* [1992], the concentration of SOA formed is related to the consumption of the parent BVOC by:

$$Y = \frac{\Delta M_0}{\Delta \text{BVOC}} \tag{1}$$

where ΔM_0 ($\mu g\ m^{-3}$) is the SOA mass concentration formed after the consumption of ΔBVOC ($\mu g\ m^{-3}$) of the given parent and Y (dimensionless) is the fractional aerosol yield. This yield is a convenient overall measure of the aerosol-forming potential of the secondary products of atmospheric oxidation of a parent organic molecule. As will be discussed subsequently, the aerosol mass may continue to increase despite the complete oxidation of the precursors. Thus, the yield defined by Equation (1) is time dependent. However, the yields determined in this work and previous studies are the final yields or the maximum yields, because the stabilized final aerosol mass concentrations are used to estimate the yields. This is a significant limitation of the yield approach. Based on the

theory of absorptive partitioning of *Pankow* [1994a; 1994b], the SOA yield is also expressed as a function of ΔM_0 by [*Odum et al.*, 1996]:

$$Y = \Delta M_0 \sum_i \left(\frac{\alpha_i K_{om,i}}{1 + \Delta M_0 K_{om,i}}\right) \quad (2)$$

where $K_{om,i}$ (m^3 μg^{-1}) is the equilibrium partitioning coefficient that describes the phase distribution of species *i* between the gas phase and absorbing organic material (om) in the aerosol phase. Yield data obtained from chamber experiments have been fit to Equation (2) using a two-product model developed by *Odum et al.* [1996], that is with parameters α_1, α_2, $K_{om,1}$, and $K_{om,2}$ [*Odum et al.*, 1996; *Hoffmann et al.*, 1997; *Odum et al.*, 1997a; *Odum et al.*, 1997b; *Griffin et al.*, 1999b; *Cocker et al.*, 2001a; *Cocker et al.*, 2001b; *Takekawa et al.*, 2003; *Keywood et al.*, 2004]. Although many products result from the atmospheric oxidation of a parent VOC, it has been shown that the two-product model is capable of generating curves that describe adequately the yield data generated in chamber experiments. Such a fitting technique also allows for easy comparison of yield curves under different scenarios. However, the fitted parameters for the two hypothetical products provide no specific information about the real oxidation products and ascribing meaning to them should be avoided. More recently, a multi-product fitting procedure has been applied to temperature-dependent chamber data [*Stanier and Pandis*, 2005], but no attempt to consider more than two hypothetical products is made here.

Combining Equation (1) and Equation (2), *Song et al.* [2005] obtained the relationship between the consumed hydrocarbon (ΔHC, μg m^{-3}) and the generated aerosol mass in chamber experiments:

$$\Delta M_0 = \frac{1}{2K_{om,1}K_{om,2}}\{K_{om,1}K_{om,2}(\Delta\mathrm{HC})(\alpha_1+\alpha_2)-(K_{om,1}+K_{om,2})+$$
$$[K_{om,1}^2K_{om,2}^2(\Delta\mathrm{HC})^2(\alpha_1+\alpha_2)^2+2K_{om,1}K_{om,2}(\Delta\mathrm{HC})(K_{om,1}-K_{om,2})(\alpha_1-\alpha_2) \quad (3)$$
$$+(K_{om,1}-K_{om,2})^2]^{1/2}\}$$

In applying Equation (3), however, it must be recognized that there is a threshold reacted precursor concentration (THC, μg m^{-3}) required for the formation of SOA [*Seinfeld and Pandis*, 1998; *Griffin et al.*, 1999c]. Setting ΔM_0 to zero, THC is determined from Equation (3) to be:

$$\mathrm{THC} = (\alpha_1 K_{om,1} + \alpha_2 K_{om,2})^{-1} \quad (4)$$

THC can be converted to a mixing ratio using the ambient temperature, the ideal gas constant, and the molecular weight of the compound. Thus, if ΔHC ≤ THC, $\Delta M_0 = 0$; if ΔHC > THC, ΔM_0 is a positive number determined by Equation (3). THC provides another simple metric for comparison of the SOA formation potentials of different VOCs under different scenarios. If pre-existing OA were to exist, however, there may be no THC simply because existing OA may provide material into which SVOCs may partition.

Chamber Studies

In this study, laboratory chamber experiments investigating SOA formation from three BVOCs are performed. Experimental conditions and results are detailed in Table 1. The three BVOCs are α-pinene, β-pinene, and d-limonene; the structures for these compounds are shown in Figure 1. Both α-pinene and β-pinene have one double bond, but the location of these double bonds is different: exo- versus endocyclic relative to the six-carbon ring. d-Limonene has two double bonds, one exocyclic and one endocyclic relative to the six-carbon ring. The difference in the number of double bonds in a molecular structure also partly determines the difference in the SOA yields because double bonds in molecules influence their reactivities and product formation [*Griffin et al.*, 1999b]. In all of the experiments described here, Cl is the only available oxidant, and the parent BVOC is consumed completely.

The experimental system constructed for this study is based on a 6-m^3 hemi-cylindrical chamber made of FEP Teflon® film and mounted on a metal framework approximately 0.30 m above the floor. A Shimadzu (Columbia, MD) GC-17A gas chromatograph (GC) with a flame ionization detector (FID) and an Agilent (Palo Alto, CA) DB-5 column is used to monitor the gas-phase mixing ratios of VOCs in the chamber. The temperature program for the GC-FID begins at 35°C, holds for 2 minutes, ramps from 35°C to 150°C at a rate of 12°C per minute, and holds for 5 minutes. The sample loop for the GC-FID has been modified to decrease the detection limit to approximately 1.0 ppb. The aerosol size distribution measurement system consists of a TSI (St. Paul, MN) 3012 ^{85}Kr neutralizer, a TSI 3010 condensation particle counter (CPC), and a TSI 3080 nano-differential mobility analyzer (DMA). The DMA operates

with sheath and excess flow rates of 5.8 L min^{-1} and aerosol and monodisperse flow rates of 0.3 L min^{-1}. Filtered chamber air is used as sheath air. A Labview program written in-house is used to monitor continuously and automatically the aerosol sampling process. Twenty 4-ft, 40-W Sylvania 350BL lights are used to generate 365-nm ultraviolet (UV) light to photo-dissociate gaseous Cl_2 to form Cl. Between experiments, the chamber is baked for 48 hours using the associated UV lamps and flushed for 36 hours with clean air. This clean air is also used to fill the chamber prior to experiments. The outflow from a TEI (Franklin, MA) 111 zero air generator is further stripped to ensure that the air is free of organics and NO_x species. NO_x species are removed by passing the airflow through an adsorbing Purafil ® column. Organic species are removed by passing the flow into a reactor containing a 500°C catalytic surface that converts hydrocarbons to water and carbon dioxide. The flow is also passed through an activated charcoal column. The water vapor in the outflow from the zero air generator is removed using a desiccant column and by passing the injection tube through a cooler packed with dry ice. The particle number concentration measured in the zero air in the chamber is less than 0.1 particle cm^{-3}. Blank experiments are conducted to verify that the concentrations of hydrocarbons, NO_x, and O_3 are all below the respective detection limits (generally 1.0 ppb).

The first step in the experimental protocol is the calibration of the GC-FID for the VOC of interest. Following the GC-FID calibration, the studied VOC is injected using a microliter syringe into a small glass tube connected to the chamber. The zero air flow is used to disperse the VOC into the chamber. Hexafluorobenzene (C_6F_6) is injected into the chamber in a manner identical to that of the parent hydrocarbon and is used as a non-

reactive internal standard for all experiments. Its mixing ratio in the chamber is approximately 100 ppb. After the VOC is mixed homogeneously in the chamber, its initial mixing ratio is measured using the GC-FID. Typically, three initial VOC samples are collected and averaged. The initial VOC mixing ratios in the chamber in this study are between 8 and 45 ppb. Like many previously reported chamber experiments, the mixing ratios of species used in the experiments in this study are generally higher than those in the real ambient atmosphere. For β-pinene (BP series in Table 1) and α-pinene (AP series in Table 1), the consumed mixing ratio is in the range of 12.3 to 27.8 ppb (67.4 to 152.2 $\mu g\ m^{-3}$) and 12.1 to 27.5 ppb (66.6 to 152.3 $\mu g\ m^{-3}$), respectively. For d-limonene, two sets of experiments have been conducted. In one set of experiments, referred to as HDL in Table 1, the consumed d-limonene mixing ratio is between 27.0 ppb and 44.4 ppb (149.4 $\mu g\ m^{-3}$ and 245.8 $\mu g\ m^{-3}$); in another set of experiments, referred to as LDL in Table 1, the consumed d-limonene mixing ratio is considerably lower: 8.0 ppb to 12.5 ppb (44.2 $\mu g\ m^{-3}$ to 69.1 $\mu g\ m^{-3}$). Cl_2 gas is injected into the chamber from a certified cylinder of approximately 1000 ppm in nitrogen. For all the experiments except the HDL experiments, the initial Cl_2 mixing ratio in the chamber is approximately 100 ppb. For the HDL experiments, the initial Cl_2 mixing ratio in the chamber is increased to approximately 200 ppb. Initial experiments (data not shown) showed that the yields for experiments in which the initial d-limonene mixing ratio is more than 20 ppb are very small when 100 ppb of Cl_2 is used. It is speculated that for the HDL experiments, 100 ppb Cl_2 may not lead to complete reaction of both double bonds and/or intermediate products. Thus, a mixing ratio of 200 ppb Cl_2 is used for the HDL experiments shown here. No variation of Cl_2 level was necessary for α-pinene and β-pinene. Once all of the

gases in the chamber are mixed homogeneously, the DMA/CPC program is initiated to monitor the particle number concentration and size distribution, the UV lights are illuminated to initiate the oxidation reactions in the chamber by photolyzing Cl_2, and the GC-FID is used to monitor the change of BVOC mixing ratio in the chamber. When both the aerosol mass reaches a plateau and the BVOC in the chamber is completely consumed, the experiment is terminated. Aerosol mass is calculated from the measured aerosol size distribution corrected for depositional loss and assuming an aerosol density of 1.0 g cm^{-3} [*Odum et al.*, 1996; *Hoffmann et al.*, 1997; *Griffin et al.*, 1999b; *Lim and Ziemann,* 2005; *Presto et al.*, 2005]. The aerosol loss rate is determined from the measured aerosol number concentration time series. It is assumed that when the number concentration of aerosol particles in the chamber started to decrease, the nucleation process is over and that decrease of the number concentration is due to the deposition process. A first order loss term is used to account for this loss. Compared to the aerosol formation rate, the wall loss rate of aerosol was usually less than 10% of the aerosol formation rate. *Presto et al.* [2005] assumed that the wall loss rate of gas-phase organics equaled the wall loss rate of aerosol. However, the wall loss of gas-phase species is not considered in this study because it is found that the wall loss of gas-phase parent organics in the chamber was less than 3% over a 2-hour blank experiment.

Results and Discussion

The SOA yields of the three BVOCs tested are summarized and described in Table 1, Table 2, and Figure 2. The total relative errors of SOA yields and generated aerosol masses in Figure 2 are estimated based on an assumed relative error for aerosol number

concentration of 5%, a resolution for the aerosol size measurement of 2 nm, and an error for the measurement of hydrocarbon mixing ratio of 1.0 ppb. The relative errors for all of the SOA yields shown in Figure 2 are in the range of 13.2 to 23.3%, and those for the aerosol masses are in the range of 9.8 to 14.4%.

Pinene Isomer Yields

It is seen in Figure 2 that α-pinene and β-pinene have similar yields when oxidized by Cl. For generated OA mass ranging from 8.0 μg m^{-3} to 35.0 μg m^{-3}, the yields range from 0.079 to 0.230. Table 2, however, shows that the stoichiometric parameters and equilibrium partitioning constants that describe SOA formation from α-pinene and β-pinene and that are found using a minimization fitting technique are quite distinct, even though their yields are generally similar. It should also be noted that the THC values of α-pinene and β-pinene are different (Table 2), with the THC for β-pinene being roughly two-thirds that of α-pinene for the conditions of this study. These disparities underscore the fact that no meaning should be attributed to these fitted parameters beyond a qualitative comparison.

Figures. 3 and 4 show the proposed addition pathways for β-pinene and α-pinene oxidation by Cl atom, respectively. Only the favored addition location is shown in each case. It is expected that H abstraction may account for a significant fraction of the reaction between a monoterpene and Cl [*Finlayson-Pitts et al.*, 1999]. However, for this discussion, it is assumed that the addition pathway dominates the initial oxidation. The final products of reactions BR1, BR2, and BR3 are quite similar to the final products of reactions AR1 and AR2. This may explain why the SOA yield curves of α-pinene and β-

pinene are similar. However, the SOA yield from the ozonolysis of α-pinene is much higher that that from the ozonolysis of β-pinene, as shown in Figure 5 and 6, which compares yields for different oxidants. This is because the double bond in α-pinene is endocyclic, so fragmentation does not generally reduce the product carbon number. The double bond in β-pinene is exocyclic, fragmentation eliminates either CH_2O or CH_2OO. Thus, the products from the ozonolysis of α-pinene probably more readily condense than those from the ozonolysis of β-pinene. This elimination of C and O is presumed to be the reason for the lower ozonolysis SOA yield for β-pinene. However, in the chlorine case, nopinone can be further oxidized by Cl leading to products similar to the α-pinene system. This is not the case for O_3.

d-Limonene Yields

The measured yields of the HDL experiments are significantly smaller than those of α-pinene and β-pinene. For generated aerosol mass ranging from 5.0 μg m^{-3} to 20.0 μg m^{-3}, the yields of α-pinene and β-pinene are nearly three times as large as those determined for the HDL experiments. However, the yields resulting from LDL experiments are larger than those of α-pinene and β-pinene. In d-limonene, there are two unsaturated carbon-carbon bonds, which allows for four sites (two for each double bond) for Cl addition. Because an increase in the number of potential sites for addition increases the possible number of functional groups, the yields of d-limonene are expected to be higher than those of α-pinene and β-pinene. The yields of the LDL support this hypothesis. It could be speculated that incomplete consumption of d-limonene in the HDL experiments leads to decreases in SOA yield. Figure 7 exhibits the d-limonene and

generated aerosol mass concentrations as a function of time for experiment HDL-2. Not only does Figure 7 confirm that d-limonene is consumed completely in this experiment, but it also indicates that particle growth continues after the point when the d-limonene mixing ratio approaches zero. Figure 7 is representative of all LDL and HDL experiments.

In the LDL and HDL sets of experiments, it is clear that both the initial d-limonene mixing ratio and the initial ratio of Cl_2 to d-limonene vary. In the LDL experiments, the ratio of the initial concentration of Cl_2 to d-limonene ranges from 8.0 to 12.5, while in the HDL experiments, it ranges from 4.5 to 7.4. These ratios theoretically affect the SOA formation process in the following way.

In the oxidation reaction system of a BVOC and Cl, the oxidation reactions R_1, R_2, ...,R_N have rate constants that depend on the structure of the BVOC and its products. Each of these reactions consumes Cl. For a certain amount of BVOC, if the Cl_2 level is high enough, all of the BVOC and reactive intermediate products can be consumed completely. The existing final products are only those that are not further oxidized significantly by Cl. The concentration ratio of Cl_2 to VOC in this situation is clearly a critical ratio. For systems with the concentration ratios of Cl_2 to VOC that are larger than this critical ratio (meaning that the Cl_2 concentration is large enough to ensure that the BVOC and intermediates are completely oxidized), the final components in these systems are likely to be the same final products as in the system when the Cl_2 to VOC concentration ratio is equal to the critical ratio. The relative abundance of the products is assumed to be the same as well. Thus, the relationship of yield and aerosol mass in this system should be the same as the system with the critical ratio because the SOA is

produced from the same products with the same relative abundance. On the contrary, for systems with a concentration ratio of Cl_2 to VOC that is smaller than the critical value (meaning that Cl_2 levels are not large enough to ensure that both the BVOC and the intermediates are completely oxidized), faster reactions consume the intermediate products involved, but relatively slower intermediate reactions do not completely consume the participating intermediate species. For example, a parent hydrocarbon A reacts with Cl to generate products P_1 and P_2. P_1 and P_2 are further oxidized by chlorine to form P_3 and P_4. If the reaction rate constant of P_1 is larger than that of P_2, for some low Cl mixing ratios, the P_3 concentration may be higher than that of P_4. If Cl concentration is high enough, the relative concentration distribution among P_1, P_2, P_3, and P_4 will keep the same in this system

$$A + Cl \rightarrow P_1 + P_2$$

$$P_1 + Cl \rightarrow P_3$$

$$P_2 + Cl \rightarrow P_4$$

Thus, the final components in these systems consist of both some intermediate products and some so-called final products. Both the components and their relative abundance in these systems are different from those in the system where the ratio is larger than or equal to the critical value. Theoretically, the yield-aerosol mass relationship in these systems should also be different. In some cases, where the relative concentration distribution of condensable intermediate and final products does not change with the varying of the initial concentration ratio of Cl to BVOC, other intermediate and final products may have little influence on aerosol formation. In these cases, any differences between yield curves at different oxidant levels may become

indistinguishable. This appears to be the case for the Cl-initiated reactions of α-pinene and β-pinene, probably because of the lack of a second (or more) unsaturated carbon-carbon bond.

There are several examples of SOA yield depending on the amount of oxidant available in the system. For a given mixing ratio of d-limonene, *Huff Hartz et al.* [2005] observe an increase in SOA yield with increasing O_3 in the O_3/d-limonene system until a plateau is reached; *Presto et al.* [2005] indicate an influence of the presence of NO_x on yields of SOA from the ozonolysis of other monoterpenes. Such behavior has also been observed for aromatic species. *Song et al.* [2005] found two aerosol yield curves for *m*-xylene for different ratios of *m*-xylene to NO_x in NO_x-containing photooxidation scenarios. In *Song et al.* [2005], plots of consumed hydrocarbon versus ΔM_0 show this phenomenon quite clearly. A similar plot for d-limonene in this study is shown in Figure 8. In this plot, points represent experimental data, while the curves are generated using Equation (3) with the parameters shown in Table 2. The points for experiments LDL-1 and LDL-3 deviate from the optimized M_0-ΔBVOC curve probably because of variations in the initial Cl and BVOC ratios for these two experiments. *Karlsson et al.* [2001] found a similar dependence of toluene SOA formation on the concentration ratio of initial chlorine to VOC. They found that both the number of particles and the volume of aerosol exhibit a steep rise as the initial chlorine atom level increases. Conversely, the number of particles displays a strong inverse dependence on the initial toluene, whereas the aerosol volume remains nearly unaffected by toluene level.

The key prerequisite for the argument of multiple SOA yield curves is the existence of different condensable intermediate products when the concentration ratio of VOC to

oxidant varied. This prerequisite may be more easily satisfied by VOCs with more than one double bond. For example, *Martinez et al.* [1999] found that the reaction of NO_3 with d-limonene proceeds predominantly via electrophilic addition of NO_3 to the C=CH double bond. Thus, it is likely that an intermediate oxidation product of d-limonene is formed when the NO_3 concentration is not high enough to oxidize completely both the C=CH bond and the $C=CH_2$ bond in d-limonene. Similar results have been found using theoretical calculations to estimate the preferential addition of OH to the endo-, rather than the exo-, cyclic double bond [*Ramirez-Ramirez and Nebot-Gil*, 2005].

Product studies also indicate preferential OH and O_3 oxidation of the endocyclic double bond [*Hakola et al.*, 1994]. In addition to structural differences, it is likely that secondary products will have different properties as well. Experiments in which a given mixing ratio of d-limonene is oxidized by a given O_3 mixing ratio at varying temperature indicate that at lower temperature, it is possible to generate higher yields of SOA from smaller initial mixing ratios of d-limonene [*Huff Hartz et al.*, 2005]. In addition, the SOA yields from higher concentration d-limonene experiments (7 ppb) have weaker temperature dependence than those from lower concentration d-limonene experiments (4 ppb) [*Huff Hartz et al.*, 2005]. This result indicates that the products forming SOA in the two sets of experiments are likely to have different vapor pressures. A similar phenomenon may occur, by analogy, in the Cl system described here.

The proposed addition pathways for reaction between d-limonene and chlorine are shown in Figure 9 and Figure 10. The first step of the oxidation reaction is for the Cl atom to attack the endocyclic double bond. The intermediate stable products P1 and P2 (limonaldehyde) are potentially condensable. The second step of the oxidation is for the

Cl atom to attack the exocyclic double bond, as hypothesized in Figure 10. If the mixing ratio of Cl is high enough to also oxidize the exocyclic double bond, then the potentially condensable products LP3 or other condensable products will also start to appear in the SOA phase. The SOA yield curve is then also determined by the presence of species in addition to LP1 and LP2. This makes the existence of two yield curves for the oxidation of d-limonene by Cl reasonable.

Much of the previous experimental work on SOA formation has investigated only the relationship between the amount of consumed parent hydrocarbon and the SOA yield for the parent hydrocarbon. The relationship between the SOA yield and the mixing ratio of oxidant is ignored. Also, the critical ratio is not found and theoretically discussed. The two-product model describing the formation of SOA has been used for the estimation of SOA concentration in some three-dimensional air quality models. Usually, only one set of parameters for the two-product model has been used because usually only one yield curve was found in the laboratory experiments. The multiple yield curves found in this paper require us to use several different sets of parameters for the two-product model depending on the VOC and oxidant ratio. The existence of multiple yield curves also indicate that different oxidation products of biogenic VOC may dominate the formation of SOA when the concentration ratio of VOC and oxidant varies.

The theorized explanation for the existence of multiple d-limonene SOA yield curves may not reflect the complexity of the oxidation reactions under ambient conditions. In the ambient atmosphere, oxidants compete with each other to consume the parent hydrocarbons as well as intermediate products; therefore, separating generations of oxidation products may not be straightforward. For example, in the Cl case, the products

of the first generation of oxidation may be oxidized further by species other than Cl. Also, these oxidants under ambient conditions may interact with each other. For example, Cl is observed to destroy O_3 in depletion events in Arctic areas [*Ariya et al.*, 1998; *Ariya et al.*, 1999].

Importance of Cl Reactions in SOA Formation

In order to evaluate the potential importance of Cl reactions in SOA formation, comparisons of SOA formation yields and estimated reaction rates for the studied monoterpenes with Cl, OH, O_3, and NO_3 have been made and are shown in Table 3. The reaction rates are determined by the mixing ratios of the parent hydrocarbon and the four oxidants:

$$R_{ij} = k_{ij}[BVOC_i][Oxidant_j] \qquad (5)$$

where [ ] represents a concentration, R_{ij} is the reaction rate between the *i*th *BVOC* and the *j*th oxidant; and k_{ij} is the reaction rate coefficient for the *i*th *BVOC* with the *j*th oxidant.

For the three monoterpenes of interest, the rate constants are listed in Table 4. The estimated peak concentrations of Cl in the marine boundary layer in the early morning are on the order of 10^3 to 10^5 cm^{-3} [*Singh and Kasting*, 1988; *Pszenny et al.*, 1993; *Wingenter et al.*, 1996; *Spicer et al.*, 1998]. The mixing ratio of Cl atom in coastal area in early morning for this discussion is assumed to be 10^4 cm^{-3}. The peak concentration of OH in the same time period is 5 x 10^5 cm^{-3} [*Brauers et al.*, 1996]. An O_3 mixing ratio of 20 ppb (4.9 x 10^{11} cm^{-3}) in the early morning in coastal areas is assumed [*Seinfeld and*

Pandis, 1998]. The NO_3 mixing ratio is low and is assumed to be 0.3 ppt (7.4×10^6 cm^{-3}) in the early morning [*Geyer et al.*, 2003]. The mixing ratios of α-pinene, β-pinene, and d-limonene are assumed to be 50ppt (1.253E+08 cm^{-3}), 50ppt (1.253E+08 cm^{-3}), and 5ppt (1.253E+07 cm^{-3}) respectively based on observed data from Appledore Island from the AIRMAP project at the University of New Hampshire [B. Sive, Personal Communication].

The pre-existing organic aerosol concentration in the atmosphere in a coastal area is assumed to be in the range of 1.0 to 5.0 μg m^{-3}. The SOA yields are calculated from the two-product model based on the parameters listed in Table 2 and Table 5. The data listed in Table 5 is from the experimental work of *Griffin et al.* [1999b]. For d-limonene, the yield from the HDL experiments is used for Y_{Cl}.

Table 5 indicates that for α-pinene and β-pinene, their reaction rates with Cl are quite similar to those of reactions with OH. Also, the SOA yields from the Cl initiated oxidation and the OH oxidation are comparable. However, the reaction rate of Cl oxidation of d-limonene is much smaller than that of OH oxidation of d-limonene, and the SOA yield of d-limonene from the oxidation initiated by OH is approximately four times of that from Cl reaction. Therefore, Cl is unlikely to be important in this scenario for SOA formation from d-limonene. Generally, in coastal areas in early morning, Cl may be important for α-pinene and β-pinene SOA formation. In the remote marine boundary layer, where the concentrations of NO_3 and O_3 are relatively lower, the Cl-initiated SOA formation maybe become relatively more important. The same can be said of significantly polluted areas, where the concentration of Cl may be relatively higher.

It is difficult to extrapolate the effects of a single oxidant to the real atmosphere because of several factors. First, the mixing ratios of monoterpene and oxidants in the experiments from which the data in Table 2, Table3, and Table 5 are generated are generally higher than those under ambient conditions. Second, the yield data used in this comparison are from two different chamber systems, one exposed to the ambient conditions and the other located in the laboratory. Any influence of ambient conditions on the previously measured SOA yields is not considered in this comparison. Third, in ambient conditions, the four oxidants may coexist, compete, and interact with each other, but in the experiments described here, no other oxidants were present in the chamber. Thus, the effect of multiple oxidants on SOA yields and the interaction of these oxidants are not considered.

Conclusions

Laboratory chamber simulation experiments indicate that the oxidation of α-pinene, β-pinene, and d-limonene by Cl generates significant amounts of SOA. α-Pinene and β-pinene exhibit similar SOA yields from the oxidation initiated by Cl. The d-limonene SOA yield from Cl-initiated oxidation, however, depends on the ratio between the initial Cl and d-limonene mixing ratios in the chamber. If this ratio is higher than ~7.5, the double bonds and reactive intermediate products in d-limonene are likely to be completely oxidized, and SOA yields from Cl-initiated oxidation are higher than those of α-pinene and β-pinene. Conversely, if this ratio is smaller than ~7.5, SOA yields from Cl-initiated oxidation are lower than those of α-pinene and β-pinene. Other researchers have noted a similar dependence of SOA yields on the oxidant level for both

monoterpenes and aromatic SOA precursors. It is argued, therefore, that multiple SOA yield curves are common for VOCs when the concentration ratio of VOC to the oxidant changes, especially for those species with multiple unsaturated carbon-carbon bonds. The SOA yields of α-pinene, β-pinene, and d-limonene when oxidized by Cl are generally comparable to other scenarios. In the marine boundary layer, coastal areas, or inland areas with industrial Cl sources, SOA formation from the Cl-initiated oxidation of the pine isomers could be a secondary source of OA in the early morning when considering Cl mixing ratio, the rate constants for the reaction of these BVOCs with Cl, and the SOA yields of these BVOCs from Cl-initiated oxidation.

Table 3.1. Initial conditions and data for Cl-initiated oxidation experiments.

Run	Parent Hydrocarbon	$(Cl_2/BVOC)_0$	T(K)	ΔBVOC (ppb)	ΔBVOC ($\mu g\ m^{-3}$)	ΔM_0 ($\mu g\ m^{-3}$)	Y
BP-1	β-pinene	6.0	297	16.7	91.2	9.4	0.103
BP-2	β-pinene	7.0	300	14.2	77.8	12.6	0.162
BP-3	β-pinene	8.1	298	12.3	67.4	11.2	0.166
BP-4	β-pinene	4.9	298	20.6	112.9	19.2	0.170
BP-5	β-pinene	4.0	299	25.0	136.8	27.5	0.201
BP-6	β-pinene	3.6	300	27.8	152.2	35.0	0.230
AP-1	α-pinene	5.5	299	18.3	101.3	8.0	0.079
AP-2	α-pinene	6.7	300	15.0	82.7	9.1	0.110
AP-3	α-pinene	8.3	300	12.1	66.6	10.0	0.150
AP-4	α-pinene	6.3	299	15.8	87.6	18.4	0.210
AP-5	α-pinene	4.6	298	21.9	121	25.4	0.210
AP-6	α-pinene	3.6	299	27.5	152.3	33.5	0.220
HDL-1	d-limonene	7.4	300	27.0	149.4	6.5	0.044
HDL-2	d-limonene	5.7	297	35.4	195.7	12.0	0.062
HDL-3	d-limonene	4.5	299	44.4	245.8	17.5	0.072
HDL-4	d-limonene	5.5	299	36.1	199.6	15.2	0.077
HDL-5	d-limonene	4.8	300	41.8	231.3	18.3	0.080
HDL-6	d-limonene	5.5	298	36.5	201.8	18.0	0.090
LDL-1	d-limonene	8.9	299	11.3	62.2	1.3	0.020
LDL-2	d-limonene	12.5	296	8.0	44.2	5.5	0.130
LDL-3	d-limonene	8.0	299	12.5	69.1	9.8	0.143
LDL-4	d-limonene	10.2	299	9.8	54.2	9.0	0.200
LDL-5	d-limonene	10.0	300	10.0	55.3	13.2	0.220
LDL-6	d-limonene	9.9	299	10.1	55.7	13.0	0.220

[a] $(Cl_2/BVOC)_0$ is the approximate initial ratio of Cl_2 and BVOC mixing ratios. The temperature refers to the average temperature during the course of the experiment. The temperature T in the laboratory is maintained at 23°C-27°C. Because this temperature range is small, the influence of temperature on the experimental results is neglected.

Table 3.2. SOA yield parameters for the Cl-initiated oxidation of monoterpenes.

BVOC	α_1	α_2	$K_{om,1}$ (m^3 μg^{-1})	$K_{om,2}$ (m^3 μg^{-1})	THC (ppb)
α-pinene	0.336	0.025	0.056	0.040	6.05
β-pinene	0.107	0.234	0.199	0.036	9.07
High-level d-limonene	0.123	0.055	0.062	0.024	20.14
Low-level d-limonene	0.301	0.168	0.076	0.048	5.82

Table 3.3. Comparison of reaction rates and SOA yields for the studied monoterpene reactions with Cl, OH, O_3, and NO_3 under assumed ambient conditions in coastal areas in early morning.

Parent Hydrocarbon	Oxidant	Reaction Rate (molecules cm^{-3} s^{-1})	SOA Yield
α-pinene	O_3	5.44E+03	0.043~0.120
α-pinene	OH	7.58E+02	0.020~0.042
α-pinene	Cl	5.89E+02	0.015~0.078
β-pinene	O_3	9.42E+02	0.017~0.037
β-pinene	OH	1.49E+03	0.018~0.071
β-pinene	NO_3	2.36E+03	0.021~0.170
β-pinene	Cl	6.64E+02	0.027~0.089
d-limonene	OH	1.07E+03	0.033~0.120
d-limonene	Cl	8.02E+01	0.008~0.035

Table 3.4. Reaction rate constants (k_j) for the oxidation of the three studied biogenic hydrocarbons. Units are cm^3 $molecules^{-1}$ s^{-1}. Data are from *Atkinson* [1997] and *Finlayson-Pitts et al.* [1999].

BVOC	$k_{Cl}*10^{10}$	$k_{OH}*10^{11}$	$k_{O3}*10^{17}$	$k_{NO3}*10^{12}$
α-pinene	4.7	1.21	8.66	1.19
β-pinene	5.3	2.38	1.5	2.51
d-limonene	6.4	17.1	20	12.2

Table 3.5. Aerosol yield parameters for O_3 oxidation, photooxidation, and NO_3 oxidation of α-pinene, β-pinene, and d-limonene.

BVOC	Oxidant	α_1	α_2	$K_{om,1}$[a] (m^3 μg^{-1})	$K_{om,2}$[a] (m^3 μg^{-1})	THC[b] (ppb)
α-pinene	O_3	0.125	0.102	0.228	0.2050	3.64
α-pinene	OH[c]	0.038	0.326	0.441	0.0104	8.92
β-pinene	O_3	0.026	0.485	0.506	0.0078	10.61
β-pinene	OH[c]	0.130	0.406	0.114	0.0127	9.00
β-pinene	NO_3	1.000	-	0.042	-	4.33
d-limonene	OH[c]	0.239	0.363	0.143	0.0138	4.59

[a]$K_{om,1}$ and $K_{om,2}$ are temperature corrected from *Griffin et al.* [1999b]. [b]THC values are calculated from Equation (4). [c]OH represents a photooxidation scenario in which OH, O_3, NO_3 and O are all present.

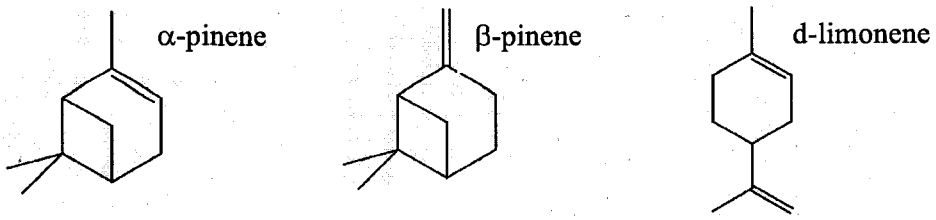

Figure 3.1. The molecular structures of α-pinene, β-pinene, and d-limonene.

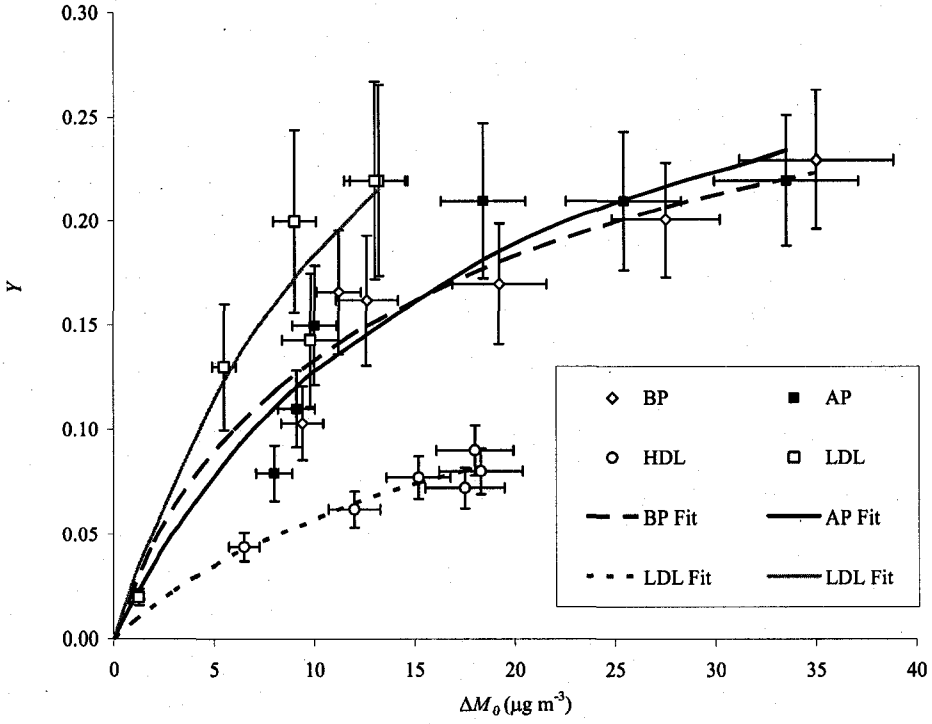

Figure 3.2. Summary of α-pinene (AP), β-pinene (BP), and d-limonene (LDL and HDL) SOA yields when oxidation is initiated by Cl. Points show experimental data. Fitted lines are based on the two-product model of *Odum et al.* [1996] with parameters listed in Table 2.

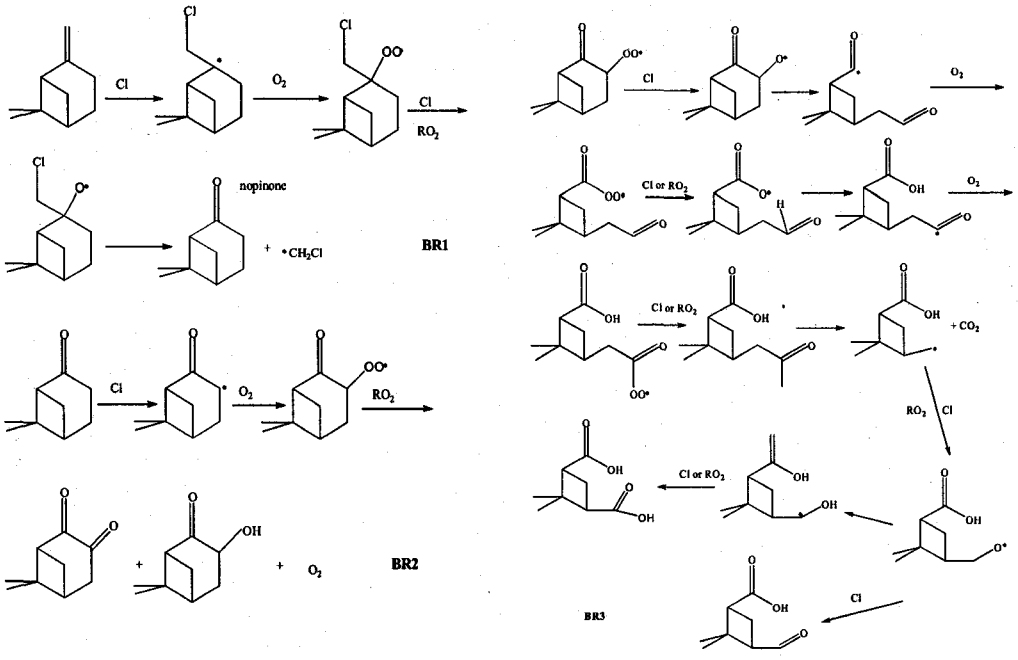

Figure 3.3. The proposed addition pathway for the reaction between β-pinene and Cl atom and for the reaction between nopinone and Cl.

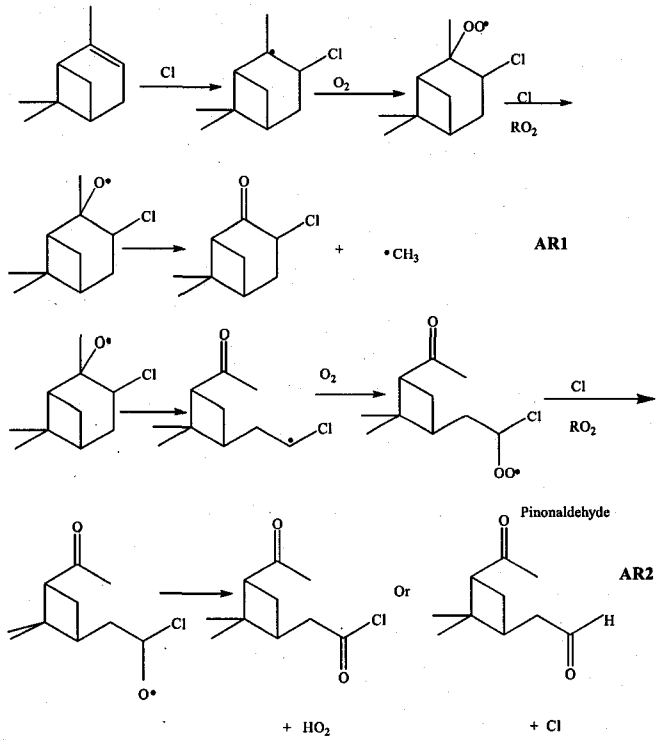

Figure 3.4. The proposed addition pathway for the reaction between α-pinene and Cl atom.

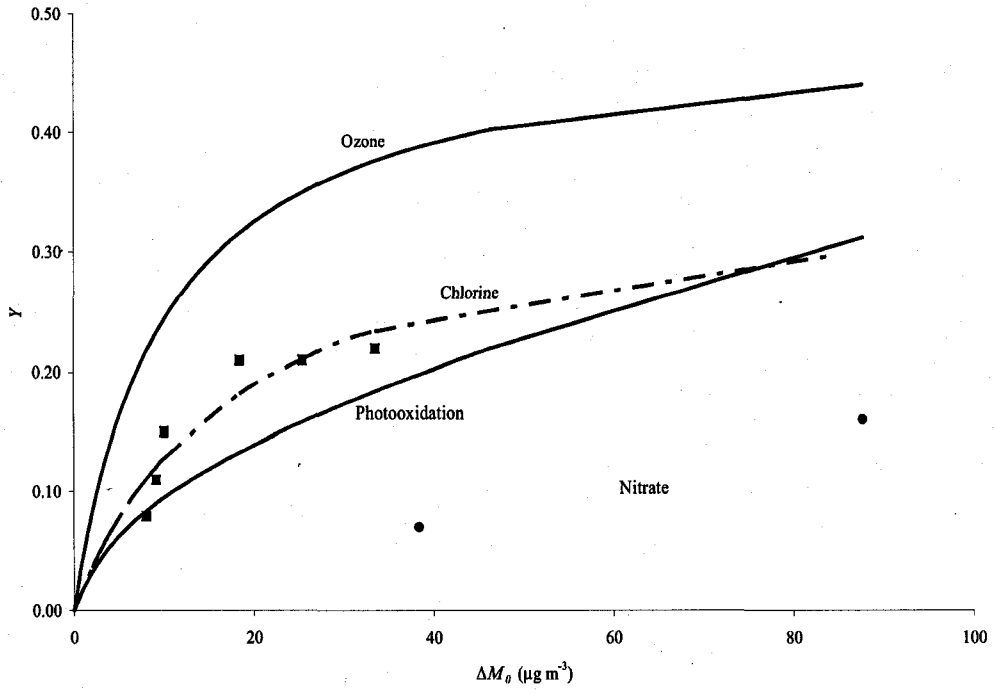

Figure 3.5. Comparison of SOA yields of α-pinene from different oxidants. The O_3 and photooxidation yield curves are from the fitted results from *Odum et al.* [1996] and *Griffin et al.* [1999b] that are corrected for temperature according to *Sheehan and Bowman* [2001]. Yields from two NO_3 experiments (filled circles) are taken from *Hallquist et al.* [1999]. The Cl yield curve is the fitted line of the chlorine yield data (solid squares) from this study using the parameters in Table 2.

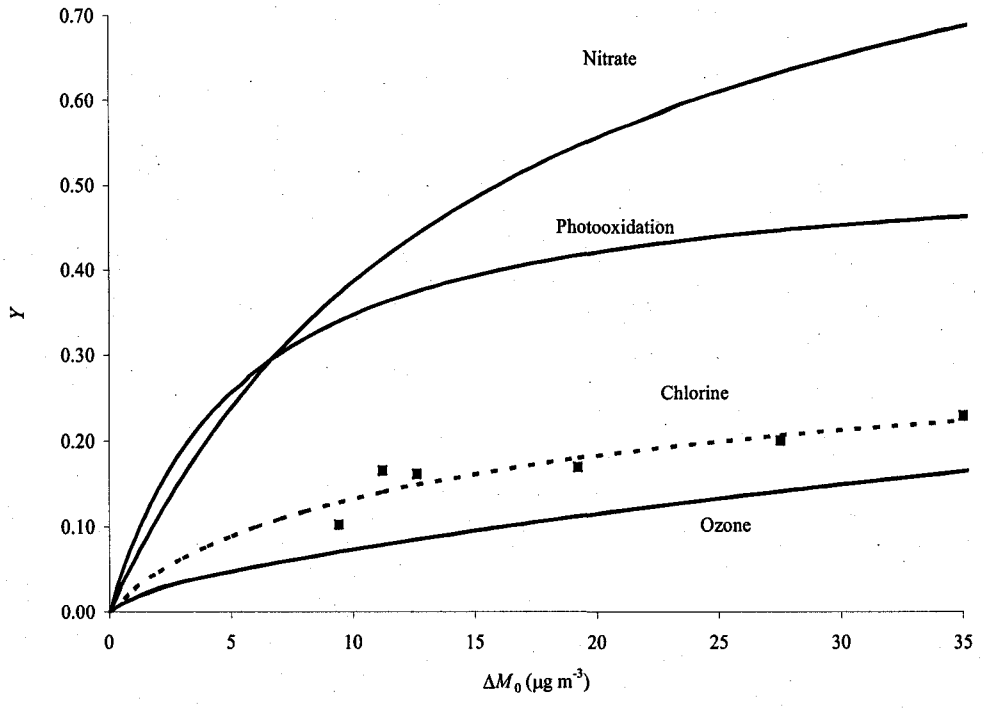

Figure 3.6. Comparison of SOA yields of β-pinene from different oxidants. The NO_3, O_3, and photooxidation yield curves are from the fitted results from *Griffin et al.* [1999b] that are corrected for temperature according to *Sheehan and Bowman* [2001]. The Cl yield curve is the fitted line of the yield data (solid squares) from this study using the parameters in Table 2.

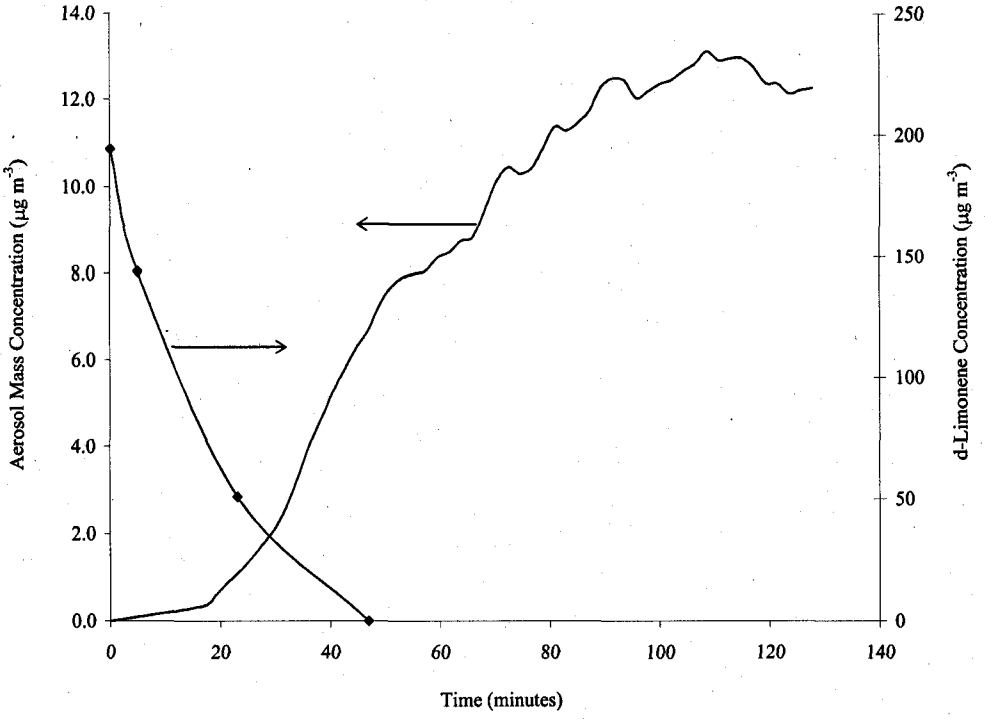

Figure 3.7. The temporal evolution of aerosol and d-limonene concentration in the chamber during experiment HDL-2. Aerosol concentration is corrected for wall loss.

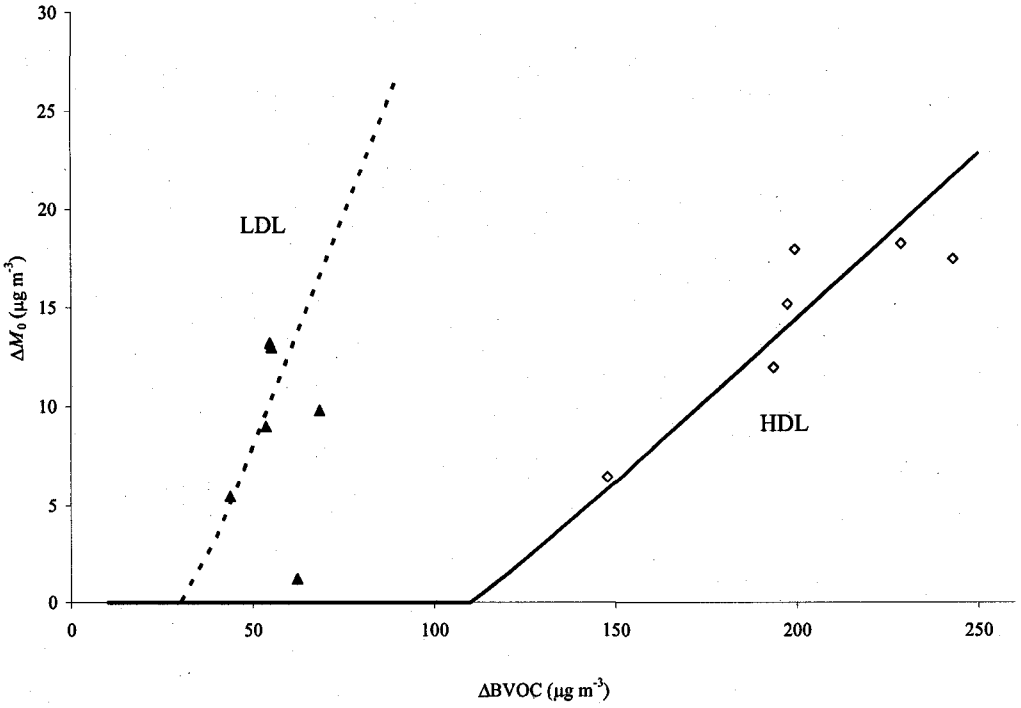

Figure 3.8. The relationship between ΔBVOC and the generated aerosol concentration of the LDL and HDL experiments.

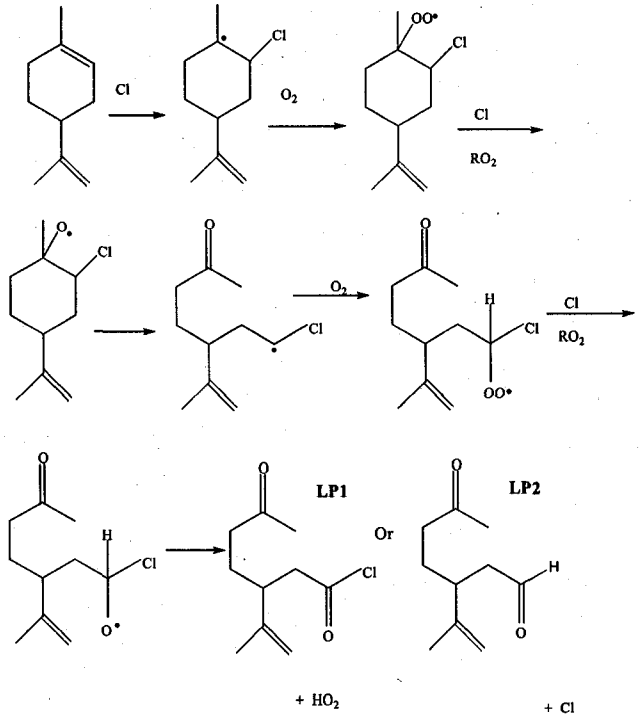

Figure 3.9. The proposed addition pathway for the reaction between d-limonene and Cl: the first attack of the endocyclic double bond.

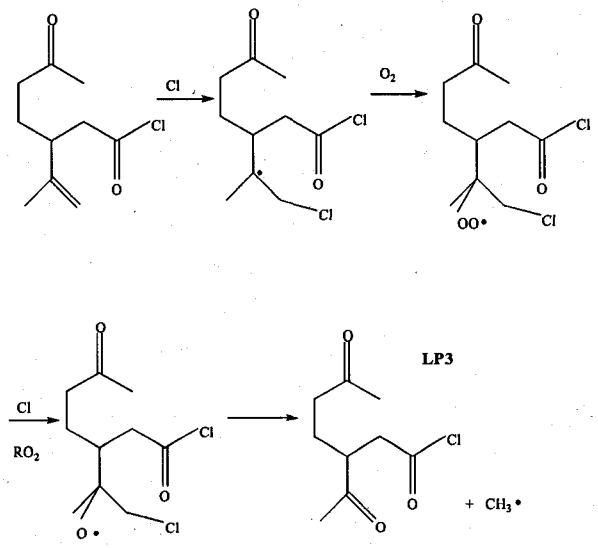

Figure 3.10. The proposed addition pathway for the reaction between d-limonene and Cl: the attack of the exocyclic double bond in product LP1.

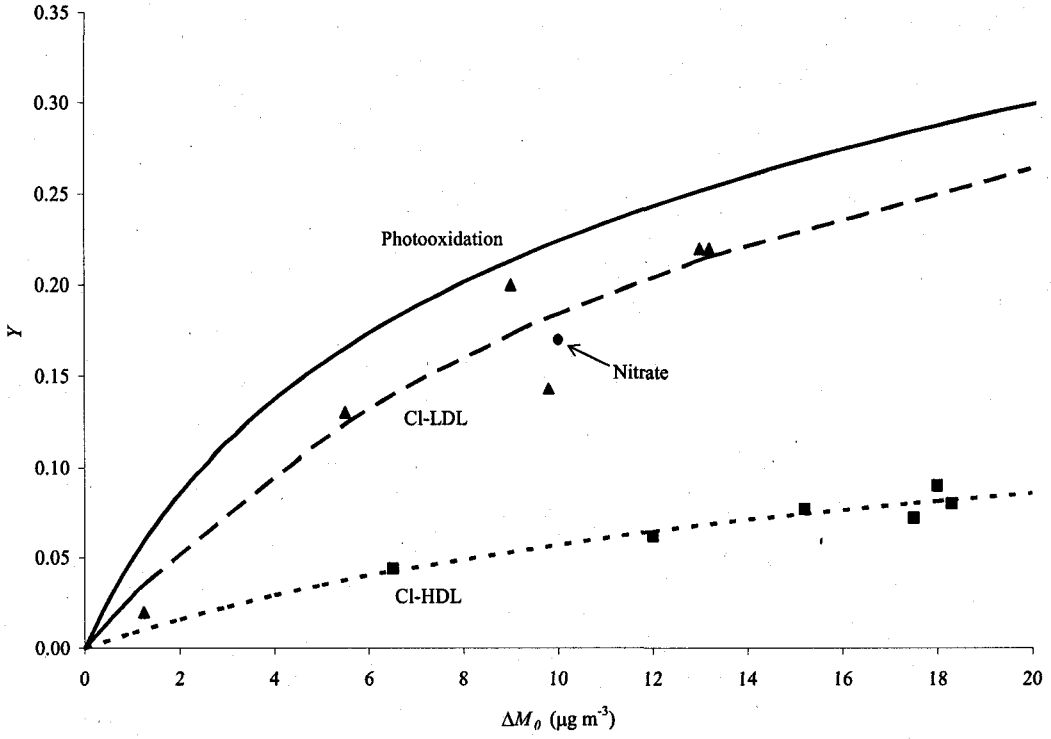

Figure 3.11. Comparison of SOA yields of d-limonene from different oxidants. The photooxidation yield curve is the fitted result from *Griffin et al.* [1999b] corrected for temperature according to *Sheehan and Bowman* [2001]. One nitrate yield (filled circle) from *Hallquist et al.* [1999] is shown. The yield curves for HDL and LDL experiments are the fitted lines of the yield data (solid squares and solid triangles, respectively) from this study using the parameters in Table 2.

CHAPTER IV

SECONDARY AEROSOL FORMATION FROM THE OXIDATION OF AROMATIC HYDROCARBONS BY CHLORINE ATOMS

Introduction

Atmospheric particulate matter (PM) influences human health, climate, and visibility (*1-4*). Organic aerosol (OA), much of which is believed to be secondary (*5*), is a ubiquitous component of PM (*6*). Secondary OA (SOA) is formed from partitioning of secondary non- and semi-volatile organic compounds (SVOCs) into organic and/or aqueous aerosol phases (*7,8*). Oxidation of volatile organic compounds (VOCs) or the gas-phase portion of SVOCs (*9*) results in products that form SOA. Due to the significant mass of OA in the troposphere, many studies have attempted to understand the chemical and thermodynamic processes that lead to its formation (*10*).

Aromatic hydrocarbons are important in the formation of urban photochemical smog because of their large emission rates, reactivities, and SOA forming capabilities (*11-18*). Toluene and the xylene isomers are major components of aromatic emissions (*19*), and SOA formed upon their oxidation accounts for the majority of simulated SOA from mobile sources in urban areas (*20*). Aromatic hydrocarbons in the atmosphere are oxidized by hydroxyl radicals (OH) that add to the ring or abstract a hydrogen atom (H) from alkyl substituents. Oxidation by chlorine atoms (Cl) is expected to proceed only via abstraction (*21*).

Efficient oxidation by chlorine atoms affects ozone (O_3) formation and likely leads to SOA formation in some areas of the troposphere (*13*, *22-27*). This study quantifies Cl-initiated SOA formation from two aromatics through calculation of the dimensionless SOA yield, *Y* (*28*):

$$Y = \frac{\Delta M_O}{\Delta \mathrm{VOC}} \tag{1}$$

where ΔM_O ($\mu g\ m^{-3}$) is the SOA mass concentration formed after the consumption of ΔVOC ($\mu g\ m^{-3}$) of the VOC. This yield is an overall measure of the SOA-forming potential of a VOC. Based on absorptive partitioning (*7*), *Y* is also expressed as (*12*):

$$Y = \Delta M_O \sum_i \left(\frac{\alpha_i K_{om,i}}{1 + \Delta M_O K_{om,i}}\right) \tag{2}$$

where $K_{om,i}$ ($m^3\ \mu g^{-1}$) is the distribution coefficient of product *i* between the gas phase and aerosol organic material (om) and α_i is its mass-based stoichiometric factor. Yield data obtained from chamber experiments have been fit to Equation (2) assuming two products (*12,16,18,26*). The four fitted parameters for this model are not associated with absolute physical meanings, but differences for yield curves between conditions and laboratories may be represented through such fits.

Experiments

The system for this study (*26*) includes a 6-m^3 hemi-cylindrical chamber made of FEP Teflon® film and mounted in a frame 0.30 meters above the floor. Pure air provided by a TEI (Franklin, MA) 111 zero air generator is dehumidified and stripped to reduce nitrogen oxides (NO_x) and VOCs. The number concentration measured in the zero air is less than 0.1 particles cm^{-3}. Blank experiments are conducted to verify that

concentrations of VOCs, NO_x, and O_3 are below detection limits (1.0 ppb). A Shimadzu (Columbia, MD) GC-17A gas chromatograph (GC) with a flame ionization detector (FID) and an Agilent (Palo Alto, CA) DB-5 column is used to monitor VOC mixing ratios. Aerosol size distributions are collected with a TSI (St. Paul, MN) 3012 ^{85}Kr neutralizer, a TSI 3010 condensation particle counter (CPC), and a TSI 3080 nano-differential mobility analyzer (DMA). In certain experiments, an Aerodyne (Billerica, MA) quadrupole Aerosol Mass Spectrometer (Q-AMS) (*29*) characterizes the SOA chemically. Twenty 4-ft, 40-W Sylvania 350BL lights are used to generate 365-nm ultraviolet (UV) light to photo-dissociate molecular chlorine (Cl_2) to form Cl. Between experiments, the chamber is conditioned for 48 hours with the UV lamps on and flushed for 36 hours in the dark with pure air.

The experimental protocol is similar to that published previously (*26*). Following a GC-FID calibration, the studied VOC is injected using a microliter syringe into a small glass tube and dispersed into the chamber using the zero air flow. After mixing, the initial VOC mixing ratio is measured by taking three replicates and averaging. Chlorine gas is injected from a certified cylinder of 1000 ppm in nitrogen.

Once all of the gases are mixed homogeneously, the DMA/CPC, GC-FID, and Q-AMS programs and the UV lights are started. When the aerosol mass reaches a plateau and the VOC in the chamber is consumed completely (indicating that ΔVOC is generally equal to the initial mixing ratio), the experiment is terminated. Aerosol mass is calculated from the measured aerosol size distributions corrected for particle depositional loss and assuming a unit density (*12,26*). Yields are not corrected for aerosol-phase hydrochloric acid (HCl) or chloride (*26*). In addition, loss of gases to chamber walls is

not considered because wall loss of gas-phase parent VOCs is less than 3% over a 2-hour blank experiment (*26,30*).

The ratio of the initial Cl_2 to VOC mixing ratios ($(Cl_2/VOC)_0$) is varied because previous studies (*13,26*) found that SOA yields depend positively on this value. *Cai and Griffin* (*26*) discuss in detail the relationship between this ratio and SOA yield. In the THR (toluene high ratio) set of experiments, $(Cl_2/VOC)_0$ is varied between 5.2 and 10.0; in the TLR (toluene low ratio) set of experiments, it is varied between 2.6 and 4.0. For *m*-xylene experiments (MX series), this ratio is varied from 2.9 to 7.4. Experimental data are given in Table 1. Larger initial mixing ratios (though similar values of $(Cl_2/VOC)_0$) are used in the Q-AMS experiments, leading to aerosol growth outside the DMA size range.

Results and Discussion

Yields

SOA yields of the two aromatics are described in Table 1, Table 2, and Figure 1. Figure 1 shows two yield curves for toluene depending on $(Cl_2/VOC)_0$. For THR experiments, the SOA yields range from 0.058 to 0.091 for generated aerosol mass ranging from 4.6 to 13.8 $\mu g\ m^{-3}$. In TLR experiments, the SOA yields range from 0.035 to 0.074, corresponding to a generated aerosol mass range of 3.5 to 12.7 $\mu g\ m^{-3}$. The yields associated with the two curves are similar, and the experimental error bars overlap. However, the observed yields and the predicted yield curve for THR experiments are systematically larger than those for TLR experiments. The two toluene SOA yield curves found in this study confirm the dependence of toluene SOA formation on $(Cl_2/VOC)_0$

observed by *Karlsson et al.* (*13*), who found that the number and volume concentrations of SOA exhibited an increase as the initial Cl_2 level increased.

Figure 1 also shows a comparison of toluene SOA yields from different oxidants. The experimental results suggest yields from Cl oxidation that are higher than those from OH oxidation alone (high NO_x (200 – 13,000 ppb)) (*14*) or OH, O_3, and nitrate radical (NO_3) oxidation (also high NO_x (122 – 1,609 ppb)) (*12*). More recent OH-oxidation data at low NO_x (< 1.0 ppb) indicate significantly larger SOA yields for toluene (0.17 to 0.30) (*18*). The experiments described in this manuscript are performed at low NO_x (<1.0 ppb) but exhibit smaller yields. It is believed that the yields in this study are greater than those shown for comparison in Figure 1 due to slightly lower temperature and significantly smaller NO_x concentrations (*16*). The decrease in the yields here compared to those of *Ng et al.* (*20*) likely results from Cl (unlike OH) only abstracting H from the methyl group (*21*). Therefore, less ring fragmentation chemistry (and therefore less SOA formation) is likely to occur in the Cl system, a hypothesis that would require product identification to be confirmed.

Measured *Y* values for *m*-xylene are similar to those for toluene and range from 0.068 to 0.120 for generated aerosol mass from 5.2 to 19.0 $\mu g\ m^{-3}$. This similarity is in contrast to *Odum et al.* (*12*) who observed a significant difference between the two. Unlike toluene, only one yield curve for *m*-xylene is obtained over the same $(Cl_2/VOC)_0$ range, indicating that the volatile first generation products of *m*-xylene are less likely than those of toluene to form SOA upon further Cl oxidation (*26*).

Figure 1 also compares *m*-xylene SOA yields from different oxidants. As with toluene, *m*-xylene SOA yields from OH-initiated oxidation depend on NO_x level. SOA

yields from Cl chemistry are generally larger than those from OH-initiated oxidation with significant NO_x (*12,16*). Again, significantly larger recent low-NO_x OH-initiated oxidation yield data for SOA (0.26 to 0.40) (*18*) are not shown in Figure 1. The differences between the *m*-xylene data presented here, those from previous studies shown in Figure 1, and those from *Ng et al.* (*18*) likely are caused by the same factors as those discussed for toluene.

Growth Dynamics

The mass of new particles from nucleation is small. Therefore, SOA growth in these experiments depends on condensation, which inherently includes diffusion and convection. For this system, the observed SOA growth curves can be fit to (*31*):

$$\Delta M(t) = \frac{1}{2}\Delta M_O erfc[\beta \frac{t_{1/2} - t}{\sqrt{t}}] \quad (3)$$

where $\Delta M(t)$ is the formed aerosol mass ($\mu g\ m^{-3}$) at time t (min), $t_{1/2}$ is the time (min) for aerosol concentration to reach one half of ΔM_O, and β is the only fitting parameter ($min^{-1/2}$). Parameters $t_{1/2}$ and β are included in Table 1.

A characteristic time for aerosol mass growth is represented by $t_{1/2}$, which is correlated strongly with $([VOC]_0[Cl_2]_0)^{1/2}$, where the brackets represent initial mixing ratios. Values of $t_{1/2}$ are controlled by concentrations at small initial reactant mixing ratios (Figure 2) because SOA formation is limited by availability of material. For larger initial mixing ratios, reactions proceed very quickly, and $t_{1/2}$ values are limited only by mass transfer. Figure 2 shows that $t_{1/2}$ values for THR experiments are smaller than those for TLR experiments, indicating that both the rate and amount of SOA formation are enhanced by higher oxidant levels (*18*).

A characteristic time for diffusion is related to β, with larger values for rapid diffusion. The fitted β values are correlated linearly to the initial VOC mixing ratios (Figure 3) because larger initial concentrations generate larger mixing ratios of condensable products; no such relationship was found with initial chlorine concentration, indicating that diffusion is controlled by the rapid VOC oxidation, not by the oxidant itself. The larger VOC mixing ratios produce a larger concentration gradient between the gas and the particle surface, leading to more rapid diffusion. Figure 3 demonstrates that the slope for THR experiments is essentially twice that for TLR experiments, indicating faster diffusion in THR experiments, consistent with smaller $t_{1/2}$ values.

Q-AMS

The Q-AMS provides size-resolved particle chemical composition (*29*). All data were analyzed using the tools of *Allan et al.* (*32*) with corrections to ensure that signal was attributed to chloride or organic mass.

Mass concentration and mass-based size distribution time series for an experiment with *m*-xylene are shown in Figure 4. In this experiment, the initial *m*-xylene mixing ratio is 51.9 ppb, and $(Cl_2/VOC)_0$ is 4.8. Figure 4 shows that the maximum concentration of SOA exceeds that of chloride (172 μg m^{-3} versus 3.6 μg m^{-3}), confirming that inorganic chloride is insignificant with respect to *Y*. Chloride growth continues after SOA growth has ceased. The time series in Figure 4 are not corrected for chamber wall deposition to underscore this fact. The organic concentration reaches a maximum and then decreases once the rate of loss due to particle deposition is greater than the rate of growth due to SOA chemistry. In contrast, the chloride curve continues to increase after

the time of the inflection in the organic curve. Continued gas-phase chemistry likely leads to larger HCl concentrations that partition to the aerosol without enhancing SOA. The size distributions in Figure 4 confirm that SOA and chloride likely are mixed internally given similar particle size distributions that peak between 100 and 200 nm in vacuum aerodynamic diameter. These phenomena were also observed in additional *m*-xylene and toluene experiments with the Q-AMS.

An ion series analysis (*15,33,34*) in which a delta value ($\Delta = m/z - 14n + 1$) is assigned to each mass-to-charge (*m/z*) ratio based on the nominal number of carbons (*n*) in the ion fragment provides the relative intensity for each Δ ($-7 \leq \Delta \leq 6$) from the spectrum. The relative intensity of Δ values from the spectrum provides insight into the likely size, nature, and volatility of the molecules analyzed. Larger values reflect oxidized material, and smaller numbers reflect cyclic and unsaturated fragments. Delta analysis can also be segregated based on estimated *n*. The results of a delta analysis for the same *m*-xylene experiment discussed previously and a toluene experiment are shown in Figure 5. In the toluene experiment, the initial toluene mixing ratio is 59.4 ppb, and $(Cl_2/VOC)_0$ is 4.2. Values were averaged over entire experiments.

The average delta pattern varies considerably between the *m*-xylene and toluene experiments, with a very large contribution from $\Delta = -2$ in the *m*-xylene experiment. The toluene pattern exhibits much stronger contributions from $\Delta = 2$ and $\Delta = 3$. The significant intensity at $\Delta = -2$ in the *m*-xylene system results from the large contribution of *m/z* 95. The large intensities of positive delta values in the toluene system result from strong contributions from *m/z* 43 and 44, where *m/z* 44 traditionally is associated with more oxidized material (*5*). When segmented by likely fragment size, the negative values

for larger n indicate a degree of aromaticity in the SOA from both *m*-xylene and toluene. When $(Cl_2/VOC)_0$ is increased or delta patterns are derived from the latter parts of an *m*-xylene experiment, the delta pattern shifts to considerably more positive values, indicating greater oxidation and a likely shift from *m/z* 95 to *m/z* 43 and 44. This is confirmed in Figure 6 in which size distributions of the mass concentration at *m/z* 44 and 95 over the course of the experiment are shown.

A potential explanation for this shift from larger to smaller fragments is that some of the mass of the species that lead to *m/z* 95 remains in the gas phase and is subject to further oxidation. When this oxidation occurs, the mass in the particle phase evaporates to maintain thermodynamic equilibrium. A second explanation is that heterogeneous or particle-phase reactions lead to the formation of the species that form smaller fragments. Other experiments with *m*-xylene, with varying $(Cl_2/VOC)_0$, showed similar temporal behavior. Experiments with toluene did not exhibit such behavior, with *m/z* 43 and 44 making significant contributions to OA from the start, indicating a key difference between the SOA reaction mechanisms for toluene and *m*-xylene. Without product identification or detailed numerical simulations, it is not possible to explain this mechanistic difference.

Bahreini et al. (*15*) performed a Q-AMS analysis of the SOA generated by *m*-xylene via OH-initiated oxidation that focused on only the latter parts of the experiments. The previously published spectra are dominated by signals at *m/z* 43 and 44, with a delta analysis showing all positive values when segmented by n (confirming a larger degree of oxidation and less aromaticity). When a regression between the spectra published by *Bahreini et al.* (*15*) (y-axis) and that derived here (x-axis) is performed, the slope is not

greatly different than unity (1.1). The regression coefficient is not large (R^2 = 0.5), with deviation from linearity driven almost exclusively by *m/z* 43, 44, and 95. If one were to focus on the latter part of the experiment presented here, the contribution of *m/z* 43 and 44 increases and that of *m/z* 95 decreases, leading to strong linearity and indicating that aged SOA from *m*-xylene from different oxidation scenarios is spectrally similar.

Cl Reaction Importance in SOA Formation

Calculations of SOA formation rates from Cl- and OH-initiated oxidation in a hypothesized coastal urban area are made to evaluate their relative importance. If first-generation products condense instantaneously to form SOA, SOA formation rates (R_{ij}) for VOC *i* and oxidant *j* are then the product of the SOA yield for the appropriate system (Y_{ij}) and the gas-phase reaction rate determined by reaction rate coefficients (k_{ij}) and the mixing ratios of the VOC and the oxidants:

$$R_{ij} = k_{ij}[VOC_i][oxidant_j]Y_{ij} \quad (4)$$

The rate constants are 6.2e-11 and 1.4e-10 cm^3 $molecules^{-1}$ sec^{-1} for toluene and *m*-xylene with Cl, respectively (*21*). Corresponding values for OH oxidation are 5.63E-12 and 2.31E-11 (*35*).

Estimated peak early morning concentrations of Cl in marine areas are 10^4 molecules cm^{-3} (*23*). A coincident concentration of OH of 5e5 molecules cm^{-3} is assumed (*36*). Based on data from urban areas (*35*), toluene and *m*-xylene mixing ratios of 30 ppbC (~15 μg m^{-3}) and 10 ppbC (~4 μg m^{-3}), respectively, are assumed. The preexisting OA concentration in this hypothetical area is assumed to be 5.0 μg m^{-3}. SOA yields are calculated from the two-product model based on the parameters listed in Table 2 (high-

NO_x OH-initiated oxidation and TLR). For OH-initiated oxidation, the yields used are 0.006 and 0.008 for toluene and *m*-xylene, respectively. Corresponding values for Cl oxidation are 0.050 and 0.063.

Values of R_{ij} range from 7.3 to 14.6 ng m^{-3} hr^{-1}, with slightly larger values for Cl oxidation and *m*-xylene. The order of magnitude difference in gas-phase reaction rates (OH > Cl) is offset by the order of magnitude difference in SOA yields (Cl > OH-initiated). Thus, Cl oxidation of aromatics may contribute a significant fraction of OA mass growth under appropriate conditions in the early morning.

Table 4.1. Initial conditions and data for Cl-initiated oxidation yield experiments.

Experiment	Parent Hydrocarbon	$(Cl_2/VOC)_0$ (ppb ppb^{-1})	ΔVOC (ppb)	ΔVOC (μg m^{-3})	ΔM_O (μg m^{-3})	Y	$t_{1/2}$ (min)	β (min$^{-1/2}$)
THR-1	toluene	9.0	22.1	84.8	4.8	0.058	26.7	0.235
THR-2	toluene	5.2	19.4	74.3	4.6	0.062	61.0	0.192
THR-3	toluene	7.0	17.9	68.7	5.9	0.085	36.2	0.175
THR-4	toluene	9.5	18.4	70.3	6.3	0.090	33.0	0.213
THR-5	toluene	10.0	30.0	114.9	8.6	0.091	20.2	0.245
THR-6	toluene	6.7	37.1	142.3	12.7	0.089	27.7	0.269
THR-7	toluene	10.0	39.2	150.3	13.8	0.091	22.0	0.288
TLR-1	toluene	3.5	23.9	91.4	3.5	0.038	66.0	0.159
TLR-2	toluene	2.6	28.7	110.1	3.7	0.035	64.0	0.187
TLR-3	toluene	3.1	23.9	91.6	4.6	0.056	68.2	0.171
TLR-4	toluene	3.9	19.4	74.3	6.6	0.060	58.5	0.164
TLR-5	toluene	3.2	31.7	121.4	7.5	0.062	41.5	0.191
TLR-6	toluene	3.5	35.4	135.6	8.9	0.066	57.0	0.214
TLR-7	toluene	4.0	49.5	189.6	12.7	0.074	23.0	0.224
MX-1	*m*-xylene	2.9	17.3	76.6	5.2	0.068	83.0	0.156
MX-2	*m*-xylene	4.4	23.0	88.1	6.9	0.078	79.8	0.238
MX-3	*m*-xylene	3.8	26.3	116.0	11.5	0.098	55.4	0.151
MX-4	*m*-xylene	3.5	28.7	127.0	11.7	0.092	50.0	0.182
MX-5	*m*-xylene	7.4	34.0	150.3	14.4	0.095	41.5	0.232
MX-6	*m*-xylene	7.1	35.3	156.2	19.0	0.120	22.2	0.302

The temperature is the average during the course of the experiment. Laboratory temperature is maintained at 23°C-27°C. The influence of this small range on the experimental results is neglected. ΔVOC equals the initial VOC concentration, as discussed in the text.

Table 4.2. Aerosol yield parameters for oxidation of aromatics.

VOC	Oxidant	α_1	α_2	$K_{om,1}$ (m^3 μg^{-1})	$K_{om,2}$ (m^3 μg^{-1})
Toluene (THR)	Cl	0.114	0.001	0.324	0.203
Toluene (TLR)	Cl	0.095	0.017	0.148	0.262
Toluene[a]	OH	0.006	0.058	0.281	0.010
Toluene[b]	OH + O_3 + NO_3	0.071	0.138	0.053	0.002
m-xylene	Cl	0.083	0.064	0.115	0.217
m-xylene[b]	OH + O_3 +NO_3	0.038	0.167	0.042	0.001

[a]*Hurley et al. (14).* [b]*Odum et al. (12).*

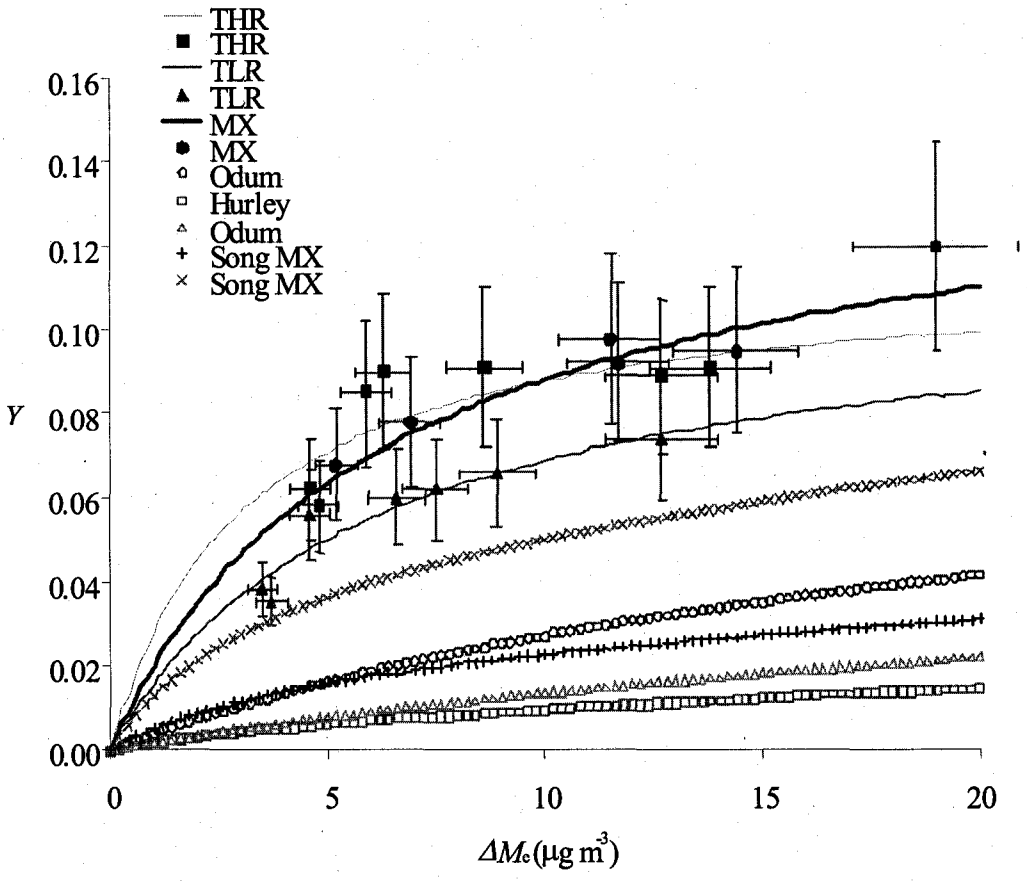

Figure 4.1. Summary of toluene (TOL, TLR, and THR) and *m*-xylene (MX) SOA yields including error bars for the current study. Points show experimental data from this study, and fitted cures are based on the two-product model of *Odum et al.* (*12*) with parameters listed in Table 2. The Hurley curve is from the fitted results from the group A OH experimental data in *Hurley et al.* (*14*). The Odum curves are for $O_3 + NO_3 + OH$ (*12*). The Song curves are also for $NO_3 + O_3 + OH$ (*16*) under different NO_x to VOC ratios (Hi or Lo). Data from the study of *Ng et al.* (*18*) are not included due to the scale of the *y*-axis.

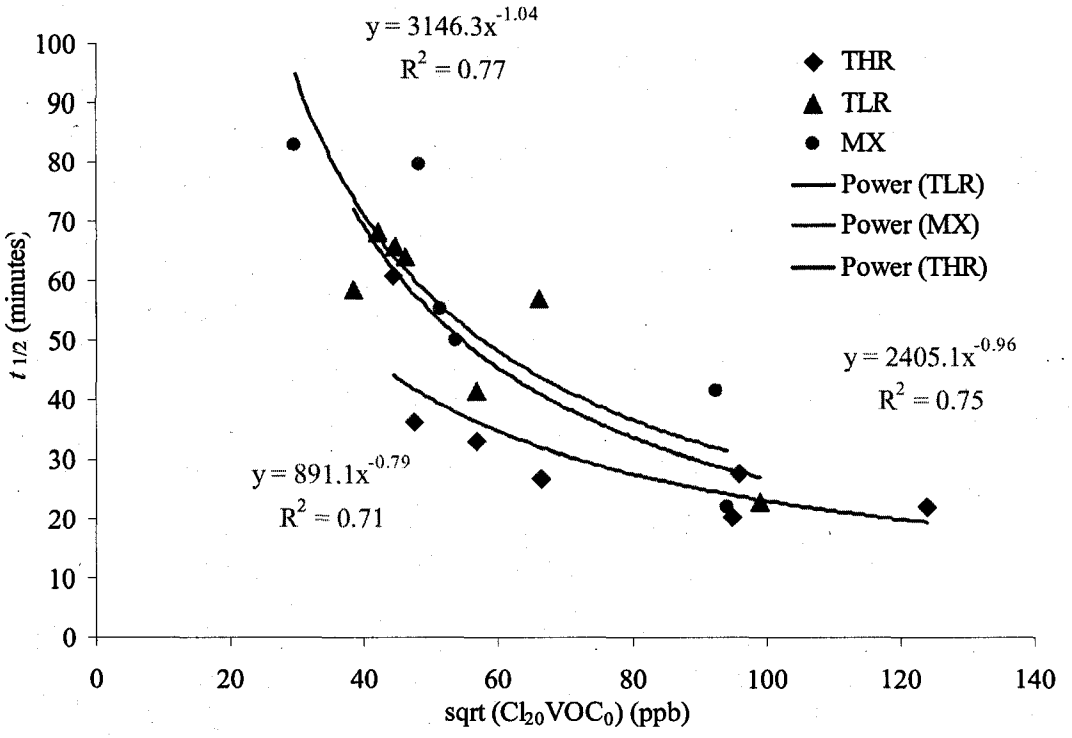

Figure 4.2. The correlation between the fitted $t_{1/2}$ values and the square roots of the products of initial VOC and Cl_2 mixing ratios.

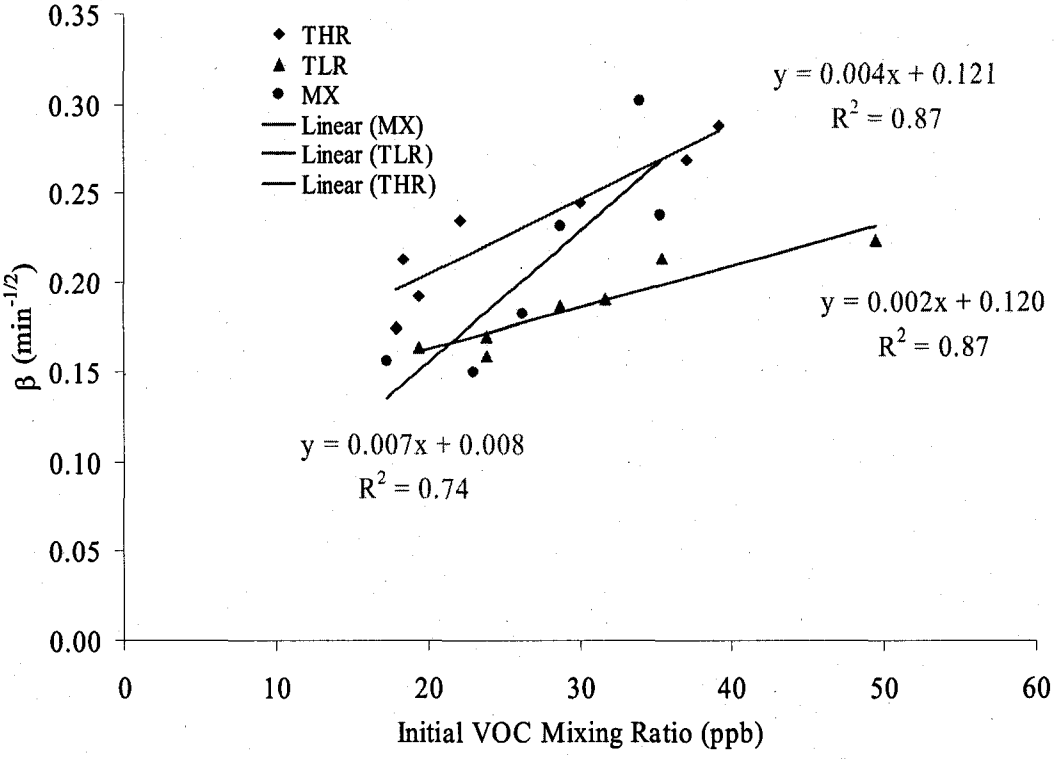

Figure 4.3. The correlation between the initial VOC mixing ratios and the fitted β values.

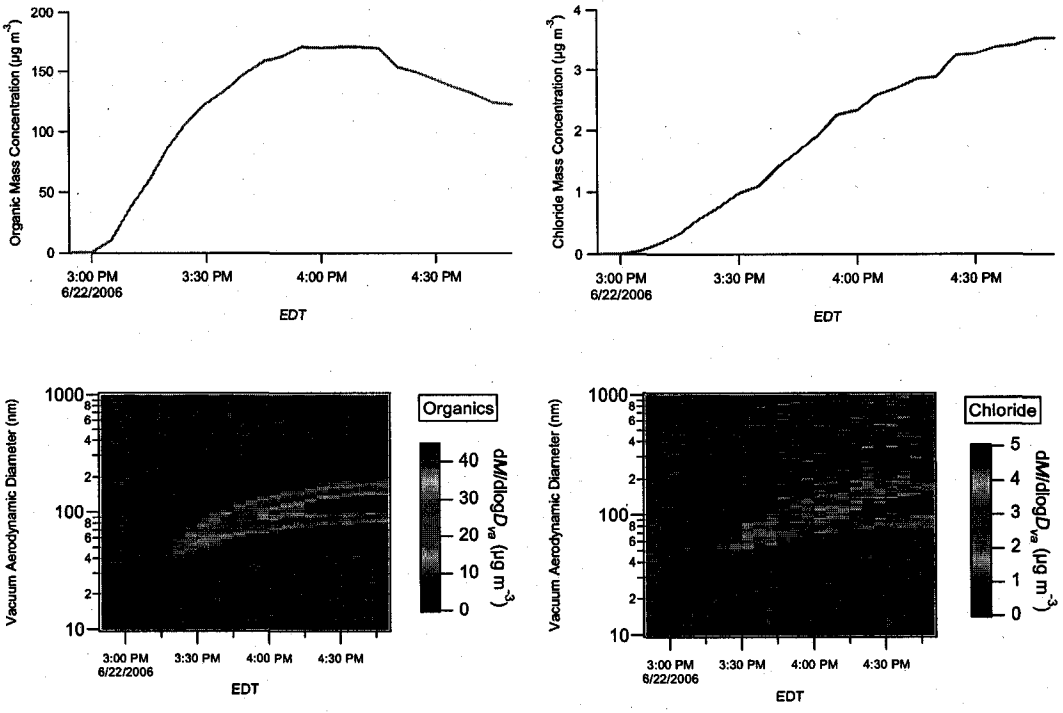

Figure 4.4. Aerosol mass concentration and size distribution time series as measured by the Q-AMS in an *m*-xylene-Cl oxidation experiment.

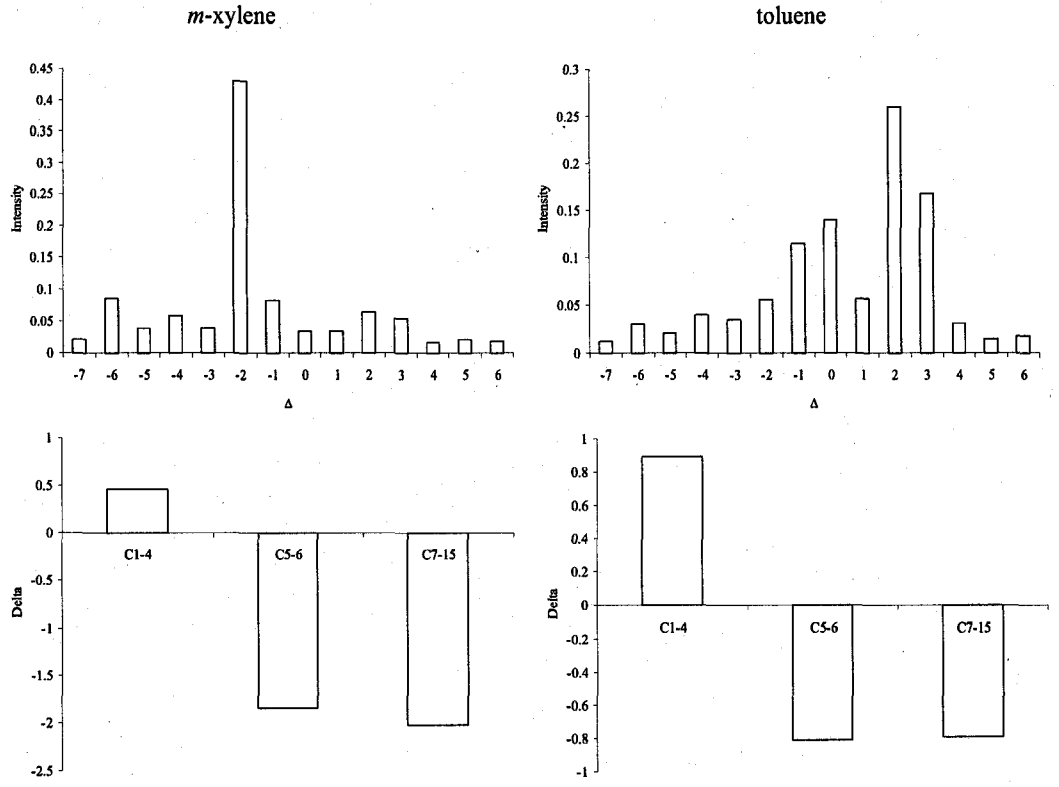

Figure 4.5. Results of a delta analysis averaged over the entire *m*-xylene experiment described in Figure 4 and for a toluene experiment with a similar $(Cl_2/VOC)_0$.

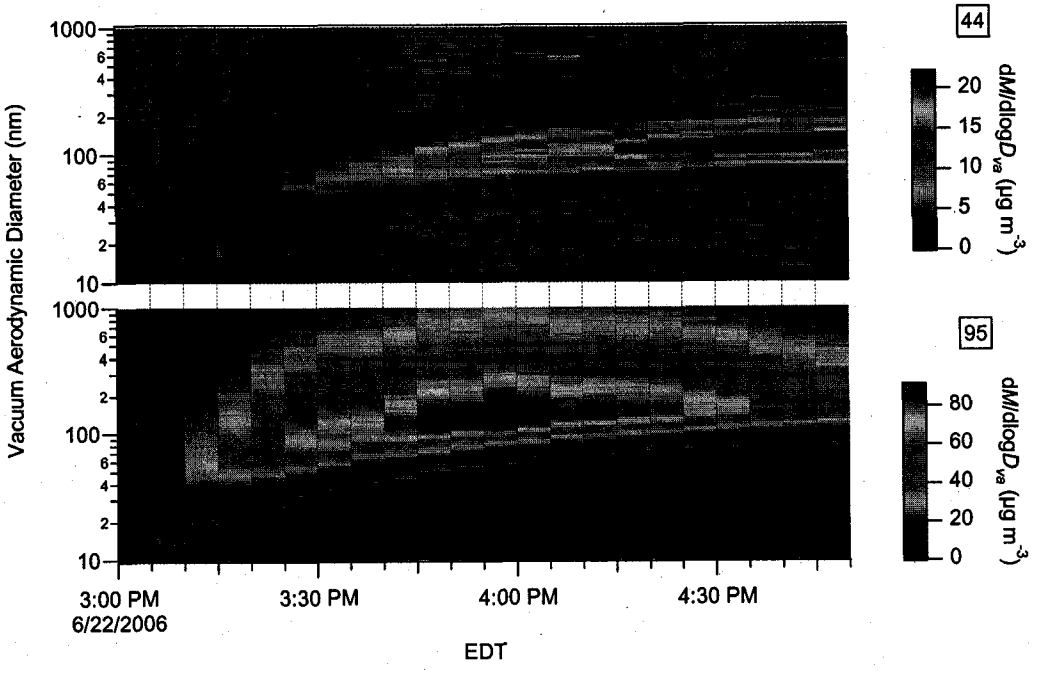

Figure 4.6. Size distribution time series for *m/z* 44 and *m/z* 95 as measured with the Q-AMS for the experiment described in Figure 4.

CHAPTER V

ZERO-DIMENSIONAL MODELING OF AEROSOL FORMATION FROM CL-INITIATED OXIDATION OF MONOTERPENES AND TOLUENE

Introduction

Secondary organic aerosol (SOA) is thought to constitute an important fraction of total fine aerosol mass in the troposphere [*Artaxo et al.,* 1988, 1990; *Saxena and Hildemann*, 1996; *Andreae and Cruzen*, 1997; *Roberts et al.*, 2001; *Putaud et al.,* 2004]. The formation mechanisms for SOA have been studied increasingly in recent years because particles, including SOA, increase human morbidity and mortality rates [*Dockery et al.*, 1993], cause visibility degradation in the troposphere [*Mazurek et al.*, 1997], and exert significant effects on regional and global climate [*Twomey et al.*, 1979; *Charlson et al.*, 1992]. In general, field-observed concentrations of what is thought to be SOA are much larger than those state–of–the-art SOA models predict in the troposphere [*de Gouw et al.*, 2005; *Heald et al.*, 2005; *Johnson et al*, 2006; *Volkamer et al.,* 2006]. Therefore, new modeling approaches can be used to identify sources and processes of SOA formation that may reconcile these inconsistencies.

Chlorine atom (Cl) is an efficient atmospheric oxidant in coastal areas, near industrial sources, and close to swimming pools [*Ganske et al.*,1992; *Finlayson-Pitts*, 1993; *Keene et al.,* 1996; *Spicer et al.*, 1998; *Canosa-Mas et al.*, 1999; *Tanaka et al.*, 2003a, *Wingenter et al.*, 2005; *Pszenny et al.*, 2007]. The Cl reactivity of volatile organic

compounds (VOCs) at dawn in coastal areas is estimated to be comparable to that with respect to hydroxyl radical (OH) [*Canosa-Mas et al.,* 1999; *Finlayson-Pitts et al.*, 1999]. Modeling results suggest that Cl-VOC reactions cause an increase of ozone (O_3) mixing ratio up to 10 parts per billion (ppb) in the South Coast Air Basin of California when Cl-initiated oxidation of VOCs is included in a three-dimensional air quality model [*Knipping and Dabdub*, 2003]. Cl-initiated oxidation of monoterpenes and aromatic VOCs recently has been shown to result in the formation of SOA [*Karlsson et al.*, 2001; *Cai and Griffin*, 2006; *Cai et al.*, 2007]. To estimate the importance of Cl-initiated SOA formation for regional and global air quality, a better understanding of the chemical mechanisms of SOA formation from Cl-initiated oxidation of VOCs through computational simulation is needed.

The main goal of the present study is to develop and evaluate reaction mechanisms of Cl with α-pinene, β-pinene, d-limonene, and toluene so that they may be implemented into air quality models. The detailed mechanisms are proposed under the framework of the Caltech Atmospheric Chemistry Mechanisms (CACM) [*Griffin et al.*, 2002a] driven by the protocol of *Jenkin et al.* [1997]. To verify the developed mechanisms, a mechanistic approach for SOA formation modeling [*Griffin et al.*, 2002b, 2003, 2005; *Pun et al.*, 2002] is used to simulate SOA formation experiments performed in a chamber [*Cai and Griffin*, 2006; *Cai et al.*, 2007]. This approach has been successful previously [*Kamens et al.*, 1999; *Kamens and Jaoui,* 2001; *Colville and Griffin*, 2004ab; *Jenkin*, 2004; *Chen and Griffin*, 2005].

Gas-phase Oxidation Mechanisms

The kinetics of the reactions between Cl and several VOCs have been studied [*Bierbach et al.*, 1996; *Kaiser and Wallington*, 1996; *Atkinson et al.*, 1997; *Bedjanian et al.*, 1998; *Finlayson-Pitts et al.*, 1999; *Fantechi et al.*, 2004; *Wang et al.*, 2005]. However, little work to date has elucidated explicitly the potential detailed reaction mechanisms involving the reactions between Cl and α-pinene, β-pinene, d-limonene, and toluene, which are model compounds for other monoterpenes and aromatic hydrocarbons. In the present study, the Cl-initiated oxidation mechanisms of these four species are proposed based on the organic degradation protocol established by *Jenkin et al.* [1997], the principles adopted by *Griffin et al.* [2002a] in the development of CACM, experimental work detailing SOA formation from these reactions [*Karlsson et al.*, 2001; *Cai and Griffin*, 2006; *Cai et al.*, 2007], other experimental studies on Cl-initiated oxidation of alkenes [*Bierbach et al.*, 1996; *Kaiser and Wallington*, 1996; *Atkinson et al.*, 1997; *Bedjanian et al.*, 1998], and analogy with the mechanisms for reactions between OH and VOCs [*Noziere et al.*, 1999; *Larsen et al.*, 2001; *Aschmann et al.*, 2002; *Capouet et al.*, 2004; *Jaoui et al.*, 2006]. The host gas-phase chemistry model is the updated CACM [*Chen and Griffin*, 2005], which contains approximately 580 reactions and 360 species prior to the additions discussed here.

Simplifications are made to balance the number of reactions and species in the system, the computational cost, and the accuracy of the proposed mechanisms. Previous studies suggest that the oxidation of alkenes by Cl is dominated by the addition pathway even though the abstraction pathway may account for a significant part of the reaction [*Kaiser and Wallington*, 1996; *Bierbach et al.*, 1996; *Atkinson et al.*, 1997; *Bedjanian et*

al., 1998; *Finlayson-Pitts et al.*, 1999]. Therefore, in most cases, the abstraction pathway is ignored in the mechanisms developed for alkenes in this study. In addition, the number of predicted products is limited by disregarding those pathways with a probability of less than 5% [*Jenkin et al.,* 1997]. Fourth generation products are considered non-reactive [*Griffin et al.*, 2002a], and oxidation products with similar molecular structures are lumped using a surrogate approach [*Griffin et al.*, 2002a]. The self-reactions and permutation reactions of a given organic peroxy radical (RO_2) are represented by a single parameterized reaction, in which an operator term, RO_2T (the sum of all organic peroxy radicals), is used [*Jenkin et al.*, 1997; *Griffin et al.*, 2002a]. Finally, photolysis of hydroperoxides in the chamber simulations is not considered because of their small photolysis rates at the wavelength of the associated lamps [*Jet Propulsion Laboratory*, 1997].

Most rate constants used in the present study are adopted based on the recommendations from *Jenkin et al.* [1997]. Due to the lack of kinetic data for the reactions between Cl and specific peroxy radicals, the rate constants for the formation of the corresponding alkoxy radicals and Criegee biradicals are assumed to be 1.50E-11 and 1.35E-10 cm^3 $molecules^{-1}$ s^{-1}, respectively [*Maricq et al.*, 1994]. The rate constant used for the reactions between Cl and aldehydes is 2.50E-10 cm^3 $molecules^{-1}$ s^{-1} based on the measured average values for aldehydes containing seven to ten carbon atoms [*Thevenet et al.*, 2000]. For the reaction between nopinone and Cl, the rate constant assigned is 1.8E-10 cm^3 $molecules^{-1}$ s^{-1} by analogy to cyclohexanone [*Notario et al.*, 1999]. For other reactions such as the reactions of Cl with alcohols, acids, and benzoquinones, the

available rate constants for compounds with similar molecular structures are used [*Nelson et al.*, 1990; *Olariu et al.*, 2000; *Aranda et al.*, 2003].

α-Pinene

The proposed Cl-initiated oxidation mechanism for α-pinene includes 62 reactions involving 12 organic radicals and 23 organic non-radical species. The reaction list includes those involving only inorganic species but does not include those reactions already included in CACM. These reactions and the molecular structures of the radicals and the stable products are described in Tables 1 and 2. The major initial steps for the proposed mechanism are shown in Figure 1.

By analogy to OH-initiated oxidation of α-pinene, Cl addition to the double bond of α-pinene is assumed to form a tertiary or secondary β-chloro peroxy radical (PRO21 and PRO22) [*Larsen et al.*, 2001; *Capouet et al.*, 2004; *Jenkin*, 2004]. According to *Noziere et al.* [1999], the channels for the tertiary and secondary radical formation account for 65% and 35% of the reaction, respectively. The reaction of PRO21 with RO_2T leads to the formation of the chloro-alcohol product AP1. The chloro-hydroperoxide AP2 forms when PRO21 reacts with hydroperoxy radical (HO_2). The ketone product AP3 and alcohol product AP4 are formed from the reaction of PRO22 with RO_2T. PRO22 reacts with HO_2 to generate hydroperoxide AP5. Peroxy radicals PRO21 and PRO22 are converted into corresponding alkoxy radicals upon reactions with Cl and NO. (While NO is not present at significant levels in the chamber experiments, these reactions are included for completeness for extension to three dimensions.) These alkoxy radicals generate condensable products such as pinonaldehyde, acid AP13

(pinonic acid), ketone AP6, and hydroperoxide AP8. Another channel for the reaction between Cl and PRO22 is the formation of Criegee intermediate CB-RO22, which upon reaction with water is likely to lead to the corresponding ketone [*Jenkin et al.*, 1997]. Pinonaldehyde, product AP10, and product AP11 may further be attacked by Cl at multiple reactive sites, generating radicals that follow chemistry similar to that described here.

β-Pinene

The proposed Cl-initiated mechanisms for β-pinene include 84 reactions involving 16 organic radicals and 32 organic non-radical products. The reaction list includes those involving only inorganic species but does not include those reactions already included in CACM. Tables 3 and 4 and Figure 2 give a description of these reactions and species.

The addition of Cl to the double bond of β-pinene leads to the formation of two peroxy radicals: a tertiary β-chloro peroxy radical (BRO21) and a primary β-chloro peroxy radical (BRO22). The first oxidation channel is assumed to be favored over the second in relative amounts of 80% and 20%, respectively, using the analogy of the OH chemistry [*Larsen et al.*, 2001; *Davis et al.*, 2005]. Peroxy radical BRO21 reacts with Cl or NO, leading to the formation of nopinone (BP1). Hydroperoxide BP2 and alcohol BP3 are generated from the reaction of BRO21 with HO_2 and RO_2T, respectively. The primary peroxy radical BRO22 undergoes reaction with RO_2T, leading to the formation of acid BP4. Hydroperoxide BP5 is generated from the reaction of BRO22 with HO_2. BRO22 reactions with NO or Cl also lead eventually to nopinone. Another pathway for the reaction between BRO22 and Cl proceeds via the formation of Criegee biradical

CB-RO22, which will react with water to form the corresponding acid [*Jenkin et al.*, 1997].

Nopinone has been identified as the major product from the reactions of β-pinene with OH [*Hakola et al.*, 1994]. 9-Hydroxynorpinonic acid and pinic acid are found to be two major components formed from OH-initiated oxidation of β-pinene [*Larsen et al.*, 2001]. They are believed to be produced from abstraction of an H atom from nopinone [*Larsen et al.*, 2001]. By analogy, the abstraction pathway of nopinone is assumed to be a key channel for the formation of SOA generated from the reaction of β-pinene with Cl, as shown in Figure 3.

The abstraction of an H atom from nopinone leads to the formation of a bicyclic C_9-β-carbonyl secondary radical, which reacts with RO_2T, NO, or Cl to form the corresponding alkoxy radical. The alkoxy radical fragments by ring opening to form an acyl radical, which is converted rapidly to the C_9-acyl-peroxy radical as shown in Figure 3. Further reaction of the C_9-acyl-peroxy radical leads to pinic acid.

d-Limonene

The Cl-initiated oxidation mechanisms of d-limonene are constructed based on previous experimental and theoretical studies of OH-initiated photooxidation of d-limonene [*Larsen et al.*, 2001; *Ramirez-Ramirez et al.*, 2005; *Jaoui et al.*, 2006]. The constructed mechanisms consist of 107 reactions, involving 21 organic radical and 41 organic non-radical species including lumped radicals and products, which are described in Tables 5 and 6 and Figure 4. The reaction list includes those involving only inorganic species but does not include those reactions already included in CACM. In order to reduce the number of reactions and minimize the computational cost, all compounds

involving the oxidation of the same double bond in first (and subsequent) generation products are lumped into a single product. The lumping scheme employed in the d-limonene mechanism is described in the Appendix.

Addition of Cl to the endocyclic double bond is favored over that to the exocyclic one, but both pathways are significant [*Larsen et al.,* 2001; *Ramirez-Ramirez et al.*, 2005]. Addition of Cl to the endocyclic double bond leads to the formation of a tertiary β-chloro peroxy radical (LRO21) and a secondary β-chloro peroxy radical (LRO22). Criegee biradical CB-RO22 is generated from the second channel from the reaction between LRO22 and Cl. If Cl attacks the exocyclic double bond, a tertiary β-chloro peroxy radical (LRO23) and a primary β-chloro peroxy radical (LRO24) are formed. Based on the yield of limonaldehyde and limona ketone from OH-initiated d-limonene oxidation, which were found to be 0.3 and 0.2 [*Hakola et al.*, 1994], respectively, the endocyclic and exocyclic addition channels are assumed to account for 60% and 40% of the reaction, respectively. The primary and the secondary peroxy radical pathways are assumed to contribute 10% of the reaction. LRO21 reacts with Cl and is converted into the corresponding alkoxy radical, which undergoes decomposition to yield secondary α-chloro peroxy radical LRO25. Alcohol product LP1 and hydroperoxide product LP2 are generated from the reaction of LRO21 with RO_2T and HO_2, respectively. LRO22 is converted into secondary α–chloro peroxy radical LRO26 via the reaction with Cl or NO. LRO22 reacts with HO_2 to form LP5 (hydroperoxide product), and alcohol LP3 and ketone LP4 are generated from the reaction of LRO22 with RO_2T. LRO23 reacts with Cl, NO, and RO_2, yielding limona ketone (LP6), which is observed in OH-initiated oxidation experiments of d-limonene [*Hakola et al.*, 1994]. The remaining reactions proceed in

ways similar to those described above, according to the protocol established by *Jenkin et al.* [1997].

The reaction of peroxy radical LRO26 with Cl, NO, or RO_2T leads to the formation of an acyl radical that is lumped into TZRO21. This acyl radical can be converted into limononic acid or keto-limononic acid, which have been identified as SOA components formed from OH-initiated oxidation of d-limonene [*Larsen et al.*, 2001]. LRO25 participates in further reactions, resulting in the formation of condensable oxidation products LP14 (alcohol), LP15 (hydroperoxide), and LP16 (limonaldehyde). Limona ketone (LP6) undergoes ring- opening reactions in a manner similar to α-pinene.

For reactions with multiple pathways, generic products are used to represent all final products when detailed branching ratio data are not available. In reaction LR42 and LR52 (Table 6), the abstraction of aldehydic H atom is described explicitly because this pathway is an important SOA source.

Toluene

The development of mechanisms for Cl-initiated oxidation of toluene is based on previous experiments and simple mechanisms of the reaction of toluene with Cl [*Fantechi et al.*, 1998; *Karlsson et al.*, 2001; *Wang et al.*, 2005]. The ring-retaining OH-initiated oxidation mechanisms of toluene [*Calvert et al.*, 2001] also are used partially as an analogy for those of Cl –initiated oxidation of toluene. The proposed oxidation mechanism in this study includes 60 reactions with 8 organic radicals and 16 organic non-radical species that are described in Tables 7 and 8 and Figure 5. The reaction list includes those involving only inorganic species but does not include those reactions already included in CACM.

The Cl-initiated oxidation of toluene proceeds via H atom abstraction from the methyl group attached to the aromatic ring [*Finlayson-Pitts and Pitts*, 2000; *Wang et al.*, 2005]. H-atom abstraction from the methyl group of toluene leads to the formation of benzyl peroxy radical, which is converted to the corresponding alkoxy radical via its reactions with Cl or NO. This alkoxy radical reacts with molecular oxygen to create benzaldyhyde and HO_2. Benzyl peroxy radical may also undergo self-reaction, yielding either benzyl alkoxy radical, benzaldehyde, and benzyl alcohol, or a benzyl dimer. The branching ratios for these three pathways are assumed to be 40%, 40% and 20%, respectively [*Karlsson et al.*, 2001]. Benzylhydroperoxide is generated from the reaction of benzyl peroxy radical with HO_2. Assuming that H-atom abstraction is the dominant pathway, the reaction of benzyl peroxy radical with Cl leads to the formation of a benzyl Criegee biradical, which is assumed to react with water to form benzoic acid. Benzaldehyde, benzyl alcohol, and benzylhydroperoxide are found to be the three major gas-phase products in reactions of toluene with Cl [*Fantechi et al.*, 1998; *Karlsson et al.*, 2001; *Wang et al.*, 2005]. The abstraction of the aldehydic H of benzaldehyde leads to the formation of a benzyl acyl radical, which leads to 1,4 benzoquinone, hydrobenzoquinone, and the hydroperoxide benzoquinone. The two endocyclic double bonds of benzoquinone products may then be further oxidized by Cl. Due to the existence of multiple reactive sites on the molecules of benzoquinone products, three generic products are used to represent the final products for their reaction with Cl. The vapor pressures of these products are estimated by fitting SOA formation data. The adducts for degradation of benzoquinone products are believed to be condensable [*Dubtsov et al.*, 2006].

Photolysis of Molecular Chlorine (Cl_2)

In the chamber experiments [*Cai and Griffin*, 2006, *Cai et al.*, 2007], molecular chlorine (Cl_2) is chosen as the photolytic source of Cl. In this modeling study, the rate of photolysis for Cl_2 is calculated using the approach of *Tanaka et al.* [2003b]. In this approach, the photolysis rate for Cl_2 is scaled directly to the rate constant for NO_2 photolysis based on the empirical relationship:

$$j_{Cl2} = 0.264\, j_{NO2} \qquad (1)$$

where j_{Cl2} and j_{NO2} are the photolysis rates for Cl_2 and NO_2 at noon-time under a clear-sky condition, respectively. An ultraviolet (UV) factor is used to estimate the UV strength of lights in the chamber system. A factor of 0.125 is adopted to correct for the difference between the actual solar spectrum and the chamber UV light spectrum based on the measured UV light spectrum [*Cocker et al.*, 2001; *Carter et al.*, 2005].

Equilibrium Absorptive Partitioning Model

Secondary organic aerosol is assumed to form primarily from the partitioning of the gas-phase semi-volatile oxidation products of parent hydrocarbons into a particle phase [*Seinfeld and Pankow*, 2003]. However, other physical and chemical processes such as polymerization and cloud processing also have been shown to lead to the formation of SOA [*Blando and Turpin*, 2000; *Jang et al.*, 2002; *Kalberer et al.*, 2004]. The equilibrium absorptive partitioning model developed by *Pankow* (1994) conventionally has been employed to simulate SOA formation under laboratory and ambient conditions [*Odum et al.*, 1996; *Hoffmann et al.*, 1997; *Griffin et al.*, 1999, *Kamens et al.*, 1999; *Kamens and Jaoui*, 2001; *Pankow et al.*, 2001; *Griffin et al.*, 2002b].

The equilibrium gas/particle partitioning coefficient $K_{om,i}$ (m^3 μg^{-1}) for condensable component *i* is determined by [*Pankow*, 1994; *Pankow et al.*, 2001]:

$$K_{om,i} = \frac{A_i}{G_i M_0} = \frac{RT}{MW_{om} 10^6 \gamma_i p^0_{L,i}} \quad (2)$$

where A_i and G_i are the aerosol and gas-phase concentrations ($\mu g\ m^{-3}$) , respectively, of specie *i*, M_0 ($\mu g\ m^{-3}$) is the total organic absorbent mass concentration (including both secondary and primary organic aerosol if present), R is the ideal gas constant (8.2×10^{-5} m^3 atm mol^{-1} K^{-1}), T is temperature (K), MW_{om} is the average molecular weight ($g\ mol^{-1}$) of the absorbing organics (including both primary organic compounds and secondary products), and $p^0_{L,i}$ is the pure component sub-cooled liquid vapor pressure (atm) of specie *i* at temperature *T*. The activity coefficient of specie *i* in the aerosol phase is represented by γ_i. For chamber experiments, M_0 is the sum of the aerosol-phase concentrations of all *N* secondary semi-volatile species. If the pre-existing organic aerosol concentration ($\mu g\ m^{-3}$) is A_0, the total aerosol mass is:

$$M_0 = (\sum_{i=1}^{N} A_i) + A_0 \quad (3)$$

For each specie *i*, a mass balance is:

$$C_i = G_i + A_i \quad (4)$$

where C_i is the total concentration of specie *i*.

Combining Equations (2) through (4) results in an implicit equation for M_0:

$$(\sum_{i=1}^{N} \frac{K_{om,i} C_i}{1 + K_{om,i} M_0}) + \frac{A_0}{M_0} - 1 = 0 \quad (5)$$

Equations (2) through (5) are solved numerically to evaluate the total equilibrium aerosol-phase concentration and the aerosol-phase concentration for each specie. The iteration procedures are to: (1) provide an initial estimate for MW_{om}; (2) calculate $K_{om,i}$ from Equation (2) assuming unit activity coefficient [*Seinfeld et al.*, 2001]; (3) evaluate M_0 by solving Equation (5) using C_i values from the gas-phase mechanism; (4) evaluate A_i and G_i by solving simultaneously Equations (2) and (4); and (5) calculate MW_{om} to see if it agrees with the initial value or to get a new estimate for MW_{om}. Procedures (2) through (5) are repeated until each equation has a tolerable error.

The humidity in the chamber experiments used in this work is smaller than 5% [*Cai and Griffin*, 2006; *Cai et al.*, 2007]. Therefore, the liquid water content is assumed negligible. The sub-cooled liquid vapor pressures for most species in the SOA system are not available. The group contribution method of Joback is employed to estimate vapor-liquid critical temperatures, pressures, and boiling points, and the Riedel corresponding-states method is adopted to calculate sub-cooled liquid vapor pressures [*Poling et al.*, 2000]. However, the estimated vapor pressures are used as reference parameters and adjusted by modeling SOA formation data. The calibrated vapor pressures are usually two or three magnitudes of order smaller than the estimated ones. A single universal scaling factor is first applied to all products so that the threshold for SOA formation is reached. The vapor pressures for only those compounds that have been identified previously in the aerosol phase are then adjusted to fit the observed data. The vapor pressures for generic products are treated in a manner similar to that for these products identified in laboratory studies previously. This heuristic optimization approach is constrained by the observed time-dependent decay of precursor hydrocarbon

concentrations, SOA mass growth data, and previous speciation data on SOA compositions. A single universal scaling factor could not be applied to all products to lead to a reasonable fitting for observed aerosol mass [*Johnson et al.*, 2006]. Numerical experiments indicate that including products with only a small tendency to condense into the aerosol phase usually causes great inconsistency between experiments. A similar corrective approach was adopted in previous studies [*Colville and Griffin*, 2004b; *Jenkin*, 2004; *Chen and Griffin*, 2005].

Modeling Results

For each of the four compounds in this study, data from one experiment are used to calibrate modeling parameters such as vapor pressures, and the calibrated SOA formation model is employed to simulate the remaining experiments. A total of 24 separate chamber experiments is thus simulated using the developed SOA formation mechanisms. The initial conditions for the simulated experiments are listed in Table 9.

α-Pinene

Figures 6a and 6b show the modeling results for the α-pinene mixing ratio profile and SOA mass growth for experiment AP-5. The α-pinene mixing ratio profile is very well reproduced, indicating that the proposed gas-phase mechanisms can describe generally the formation and consumption of Cl and the consumption of α-pinene.

Figure 6b is a typical modeling result for SOA mass growth, which shows that the developed mechanisms can well reproduce the steady-state aerosol mass concentration at the end and at the onset of the experiment. SOA formation is overestimated early in the simulation. *Chen and Griffin* [2005] report similar results for SOA mass generated from

ozonolysis of α-pinene. Because the partitioning model is an equilibrium model, the SOA mass concentration in the final stage can be well modeled. The over-prediction of SOA formation earlier in the simulation may be caused by the assumption that the fourth generation products are non-reactive, as their reaction may lead to less volatile products that would remain in the gas phase. In addition, mass transfer effects associated with smaller particles may limit SOA formation earlier in the experiments [*Cai and Griffin*, 2005].

Salient features shown on Figure 6a and 6b are that α-pinene in this experiment has been consumed completely within approximately 40 minutes, the simulated SOA mass stops growing within 35 minutes, and the observed SOA formation terminates around 90 minutes. These facts indicate that SOA formation may involve kinetic processes or that second-, third-, etc. generation SVOCs may contribute significantly to SOA formation. These reactions may not be included in the proposed mechanism appropriately.

The comparison of the simulated and observed final SOA concentrations for all α-pinene experiments is shown in Figure 6c. Five of the six simulated SOA concentrations are within ±25% of the observed SOA concentrations, suggesting that most experimental conditions and results are self-consistent and that the developed mechanisms can predict reasonably the measured yields.

The predicted SOA components are AP2, AP6, AP7, AP9, AP10, AP12, AP13, AP17, and AP20 (Table 1). These compounds are dicarboxylic acids, hydroperoxides, and alcohols. Most of them are generated from the reactions of PRO24 and PRO25 with Cl, HO_2, and RO_2T. For experiment AP-5, the major components are AP13 (pinonic

acid), AP17 (generic), and AP20 (norpinonic acid), which account for 12%, 44%, and 16%, respectively, of the predicted final equilibrium aerosol mass. In the early stage, AP9 and AP10 comprise totally approximately 40% of the aerosol mass. Their mass in the aerosol phase decreases with time, and they are not present in the final equilibrium aerosol mass despite being observed (in the case of AP9) in OH-initiated oxidation experiments of α-pinene [*Noziere et al.*, 1999].

β-pinene

Figure 7 shows the modeling results for β-pinene. For Experiment BP-4, the temporal behavior of the β-pinene concentration profile is adequate (Figure 7a), but the simulated concentrations are systematically larger than those observed, indicating that the Cl mixing ratio in the chamber is likely somewhat underestimated. SOA formation is well reproduced during the onset and final stage of the experiment and is over-predicted in the middle stage (Figure 7b), similar to what was observed for α-pinene. Simulated final SOA concentrations are within 20% of observed SOA concentrations for most β-pinene experiments, showing consistency among the six experiments (Figure 7c).

The components in the aerosol phase are found to be BP2, BP4, BP14, BP15, BP18, BP19, BP20 (pinic acid), BP23 (norpinic acid), and BP24 (Table 3). These compounds are aldehydes, dicarboxylic acids, and hydroperoxides. In the simulated final equilibrium aerosol mass for experiment BP-4, BP4, BP20, BP23, and BP24 make up 10.5%, 39.5%, 26%, and 10%, respectively. Although the simulated aerosol concentrations for these compounds increase with time, their distribution is consistent. Most of the aerosol components are formed via the reaction of BP1 (nopinone) with Cl.

d-Limonene

Figure 8a and 8b show the comparison of observed and simulated d-limonene and SOA concentration evolution in Experiment LDL-6. The decay of d-limonene is reasonably simulated, which indicates that Cl concentration in the chamber is well reproduced in the model. The SOA concentration is overestimated before the end of the experiment (Figure 8b). This result is consistent with those from α-pinene and β-pinene.

The final SOA concentrations obtained from HDL experiments and LDL experiments are reasonably reproduced by the developed mechanisms (Figure 8c and Figure 8d). In HDL experiments, the initial d-limonene concentrations are larger than those in LDL experiments. The relative errors for the simulation of most of the experiments are less than ±50%. The discrepancy between SOA yields from HDL and LDL experiments is well reproduced by the developed mechanisms.

For experiment LDL-5, the predicted SOA components are the products (lumped into T1P1) formed from the oxidation of the exocyclic double bond in LP13, LP14,the series of TZ products, and the products (lumped in T2P2 and T2P5) generated from the oxidation of the endocyclic double bond in LP6 through LP12. LP27 is also a significant SOA contributor. These compounds consist of aldehydes, hydroperoxides, and dicarbonxylic acids. In the simulated final equilibrium aerosol mass, the oxidation products (lumped into T1P1) of LP13 and LP14 account for 45% and 15%, respectively. LP27 and the oxidation products (lumped into T1P1) of the TZ series make up 9% and 21% of the final equilibrium aerosol mass, respectively. These compounds result from the reactions of PRO21 and the reactions of LP16, LP17, and LP18 with Cl. The aerosol concentrations for reactive intermediate products in the aerosol phase decrease with time

and disappear in the final equilibrium state. The aerosol concentrations for non-reactive stable products gradually increase with time and reach the maximum values in the final equilibrium state.

The simulated T1P1 mass concentrations in LDL experiments are relatively larger than those for the HDL experiments at the same elapsed time. This difference was largest at approximately 60 minutes after initiation of the experiments and disappeared after approximately 120 minutes. This fact appears to be responsible for the difference in observed SOA yields in the two sets of experiments.

Toluene

For experiment TLR-5, the toluene mixing ratio evolution is well reproduced (Figure 9a). The SOA formation is also well simulated in the first 40 minutes and at the end of the experiment (Figure 9b). From 40 to 80 minutes after the initiation of experiment, the proposed mechanism overestimates SOA mass, as was observed in the simulations for the monoterpenes. Modeling results for final SOA mass concentrations for all THR and TLR experiments are shown in Figure 9c and Figure 9d, respectively. (The initial concentration ratios of Cl_2 to toluene in THR experiments are larger than those in TLR). The overall relative errors for the simulation of all of THR and TLR experiments are ±25% and ±50%, respectively, indicating good reproducibility and consistency among these experiments.

For experiment TLR-5, the optimized calibration indicates that SOA consists of TP1 (benzaldehyde), TP2 (benzyl alcohol), TP14, TP15, and TP16. The last three compounds are hypothesized generic products from the further oxidation of benzoquinone-like products. Benzaquinone products are formed from the reaction of

TRO24 with Cl, NO, and RO_2T. TP2, TP14, TP15, and TP16 account for 15%, 60%, 7%, and 9% of the simulated final equilibrium aerosol mass, respectively.

The simulated benzaldehyde concentrations in THR experiments are observably larger than those in TLR experiments at the same elapsed time. However, numerical simulation shows that the difference for the benzaldehyde concentrations between the two sets of experiments becomes significant when the initial concentration ratio of Cl_2 to toluene is larger than 12.0.

Conclusions

The mechanisms for the reactions of three monoterpenes (α-pinene, β-pinene, and d-limonene) and one representative aromatic hydrocarbon (toluene) with Cl have been developed within the framework of CACM. The proposed mechanisms are evaluated by simulating SOA formation in chamber studies. For the four compounds of interest, the developed mechanisms combined with an absorptive partitioning model can well reproduce the measured precursor decay curves and predict reasonably time-dependent SOA concentrations. Simulation results suggest that the approach used may overestimate SOA concentration in the middle stages of experiments.

Table 5.1. Chemical species in the mechanism of the Cl-initiated oxidation of α-pinene.

Notation	Structure	Notation	Structure	Notation	Structure
Radical	Species	Radical	Species	Radical	Species
PRO21	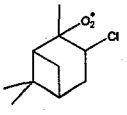	PRO22	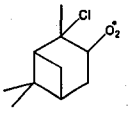	PRO23	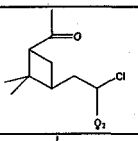
PRO24	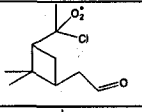	PRO25	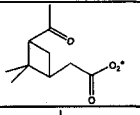	PRO26	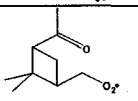
PRO27	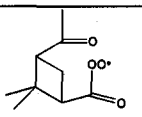	PRO28	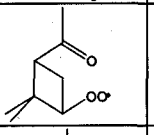	CB-RO22	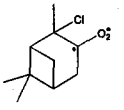
CB-RO23	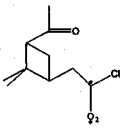	CB-RO26	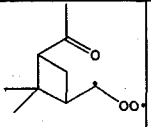	CB-RO28	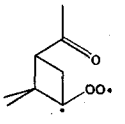
Non-radical	Products	Non radical	Products	Non radical	Products
AP1	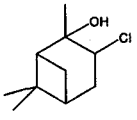	AP2	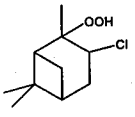	AP3	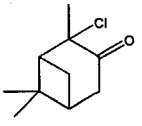
AP4	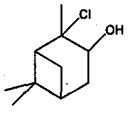	AP5	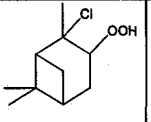	AP6	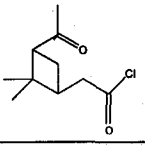
AP7	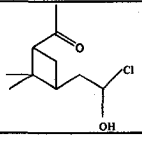	AP8	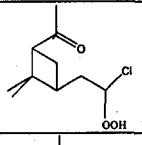	AP9	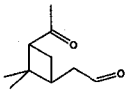
AP10	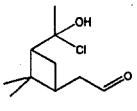	AP11	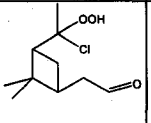	AP12	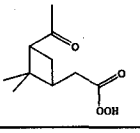
AP13	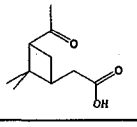	AP14	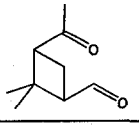	AP15	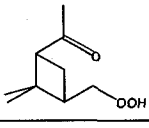

Table 5.1 Continued.

AP16	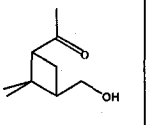	AP17	No Specific Structure	AP18	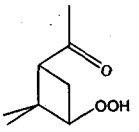
AP19	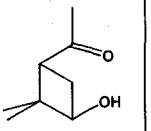	AP20	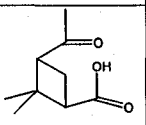	AP21	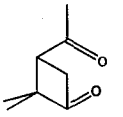
PAN25	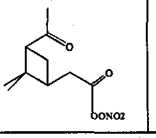	PAN27	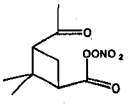		

Table 5.2. Chemical reaction mechanism for Cl-initiated oxidation of α–pinene.

Num	Reactants	Reaction Products	Rate Constant (cm^3 $molecule^{-1}$ s^{-1} or s^{-1})
RA1	α-pinene + Cl	fPRO21 + (1-f)PRO22 + RO_2T According to *Noziere et al.* [1999], f=0.65	4.7E-10[a]
RA2	PRO21 + Cl	PRO23 + ClO + RO_2T	1.5E-11[b]
RA3	PRO21 +RO_2T	0.7 PRO23 + 0.3 AP1 + 1.7 RO_2T	9.2E-14[c]
RA4	PRO21 + NO	PRO23 + NO_2 + RO_2T	(4.1E-12)*EXP(180/T)[c]
RA5	PRO21 + HO_2	AP2	(3.0E-13)*EXP(1250/T)* [1-EXP(-3.4)][c]
RA6	PRO22 + Cl	CBRO22 + HCl	1.35E-10[b]
RA7	CBRO22+H_2O	H_2O_2 + AP3	6.0E-18[c]
RA8	PRO22 + Cl	PRO24 + ClO + RO_2T	K2
RA9	PRO22 + RO_2T	0.6PRO24+ 0.2AP4 + 0.2AP3 + 1.6RO_2T	8.8E-13[c]
RA10	PRO22 + NO	PRO24 + NO_2 + RO_2T	K4
RA11	PRO22 + HO_2	AP5	K5
RA12	PRO23 + Cl	ClO + AP6 + HO_2	K2
RA13	PRO23 + Cl	CBRO23 + HCl	K6
RA14	CBRO23+H_2O	AP6 + H_2O_2	K7
RA15	PRO23 +RO_2T	0.8AP6 + 0.2AP7 + 0.6HO_2 + RO_2T	K9
RA16	PRO23 + NO	AP6 + NO_2 + HO_2	K4
RA17	PRO23 + HO_2	AP8	(3.0E-13)*EXP(820/T)[c]
RA18	PRO24 + Cl	AP9 + Cl + ClO	K2
RA19	PRO24+ RO_2T	0.7AP9 + 0.7Cl + 0.3AP10 + RO_2T	K3
RA20	PRO24 + NO	AP9 + Cl + NO_2	K4
RA21	PRO24 + HO_2	AP11	K17
RA22	AP9 + Cl	HCl + PRO25 + RO_2T	2.5E-10[d]
RA23	AP9 + hv	HO_2 + CO + PRO26 + RO_2T	3.1E-05[e], corrected for UV light strength and spectrum

Table 5.2. Continued.

RA24	PRO25 + NO_2	PAN25	5.8E-11[e]
RA25	PAN25	PRO25 + NO_2 + RO_2T	0.0102[e]
RA26	PRO25 + Cl	ClO + CO_2 + PRO26 + RO_2T	K2
RA27	PRO25 + NO	NO_2 + CO_2 + PRO26 + RO_2T	2.7*(4.1E-12)*EXP(180/T)[c]
RA28	PRO25 + HO_2	0.71AP12 + 0.29AP13 + 0.29O_3	(4.3E-13)*EXP(1040/T)[c]
RA29	PRO25 +RO_2T	0.3AP13+0.7CO_2+0.7PRO26 + 1.7RO_2T	(5.0E-12)[c]
RA30	PRO26 + Cl	ClO + HO_2 + AP14	K2
RA31	PRO26 + Cl	CBRO26 + HCl	K6
RA32	CBRO26+H_2O	AP14 + H_2O_2	K7
RA33	PRO26 + NO	NO_2 + HO_2 + AP14	(4.1E12)*EXP(180/T)* EXP(-0.17*8)[c]
RA34	PRO26 + HO_2	AP15	(3.0E-13)*EXP(1250/T)* [1-EXP(-0.34*9)][c]
RA35	PRO26 + RO_2T	0.8AP14 + 0.6HO_2 + 0.2AP16 + RO_2T	(1.3E-12)[c]
RA36	AP10 + Cl	AP17	K22
RA37	AP10 + hv	AP17	K23
RA38	AP11 + Cl	AP17	K22
RA39	AP11 + hv	AP17	K23
RA40	AP14 + Cl	PRO27 + HCl + RO_2T	K22
RA41	AP14 + hv	CO + HO_2 + PRO28 + RO_2T	K23
RA42	PRO27 + Cl	ClO + CO_2 + PRO28 + RO_2T	K2
RA43	PRO27 + NO_2	PAN27	K24
RA44	PAN27	NO_2 + PRO27 + RO_2T	K25
RA45	PRO27 + NO	NO_2 + CO_2 + PRO28 + RO_2T	K27
RA46	PRO27 + HO_2	0.7AP18 + 0.3AP19 + 0.3O_3	K28
RA47	PRO27 + RO_2T	0.7PRO28+0.7CO_2+ 0.3AP20 + 1.7RO_2T	K29

Table 5.2. Continued.

RA48	PRO28 + Cl	ClO + HO_2 + AP21	K2
RA49	PRO28 + Cl	HCl + CBRO28	K6
RA50	CBRO28+H_2O	AP21 + H_2O_2	K7
RA51	PRO28 + NO	AP21 + NO_2 + HO_2	(4.1E12)*EXP(180/T)* EXP(-0.17*7)[c]
RA52	PRO28 + HO_2	AP18	(3.0E-13)*EXP(1250/T)* (1-EXP(-0.34*8))[c]
RA53	PRO28 +RO_2T	0.8AP21 + 0.6HO_2 + 0.2AP19 + RO_2T	(2.5E-13)[c]
RA54	H_2O_2 + hv	2OH	0, for 365nm UV light[f]
RA55	Cl + O_3	ClO + O_2	(2.9E-11)*EXP(-260/T)[f]
RA56	HO_2 + Cl	HCl + O_2	(1.8E-11)*EXP(170/T)[f]
RA57	HO_2 + Cl	OH + ClO	(4.1E-11)*EXP(-450/T)[f]
RA58	HO_2 + ClO	HOCl + O_2	(4.8E-13)*EXP(700/T)[f]
RA59	HOCl + hv	OH + Cl	6.25E-06[f], Corrected for UV light strength and spectrum.
RA60	OH + HCl	H_2O + Cl	(2.6E-12)*EXP(-350/T)[f]
RA61	OH + HOCl	H_2O + ClO	(3.0E-12)*EXP(-500/T)[f]
RA62	Cl_2 + hv	2Cl	3.28E-03[g], Corrected for UV light strength and spectrum.

a: *Finlayson-Pitts et al.* [1999]; b: *Karlsson et al.* [2001]; c: *Jenkin et al.* [1997]; d: *Thevenet et al.* [2000]; e: *Griffin et al.* [2002a]; f: *Jet Propulsion Laboratory* [1997]; g: *Tanaka et al.* [2003a].

Table 5.3. Chemical species in the mechanism of the Cl-initiated oxidation of β-pinene.

Notation	Structure	Notation	Structure	Notation	Structure
Radical	Species	Radical	Species	Radical	Species
BRO21	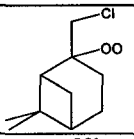	BRO22	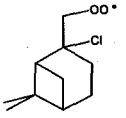	BRO23	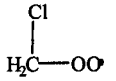
BRO24	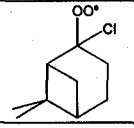	BRO25	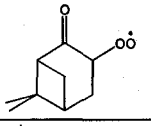	BRO26	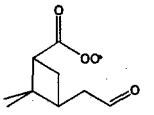
BRO27	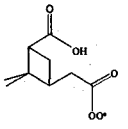	BRO28	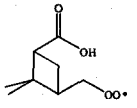	BRO29	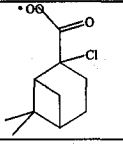
BRO210	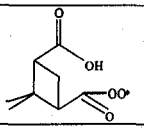	BRO211	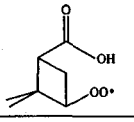	CB-RO22	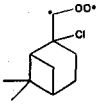
CB-RO23	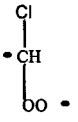	CB-RO25	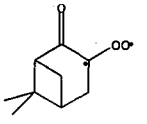	CB -RO28	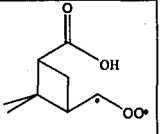
CB-RO211	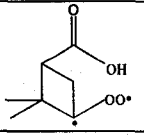				
Non-radical	Products	Non radical	Products	Non radical	Products
BP1	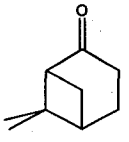	BP2	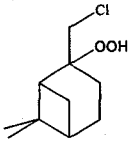	BP3	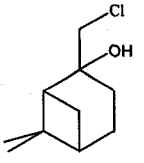
BP4	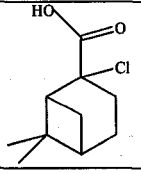	BP5	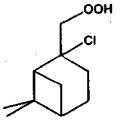	BP6	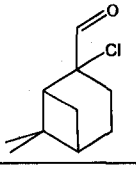
BP7	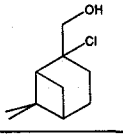	BP8	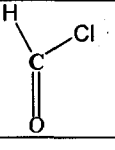	BP9	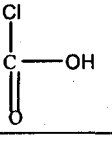

Table 5.3. Continued.

BP10	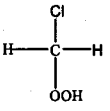	BP11	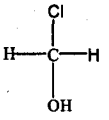	BP12	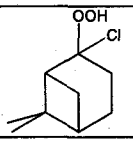
BP13	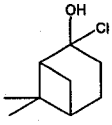	BP14	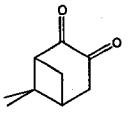	BP15	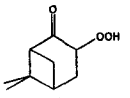
BP16	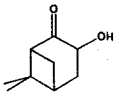	BP17	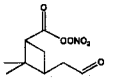	BP18	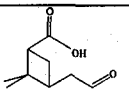
BP19	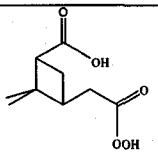	BP20	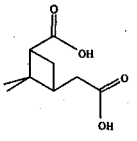	BP21	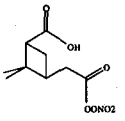
BP22	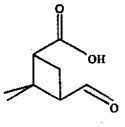	BP23	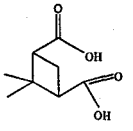	BP24	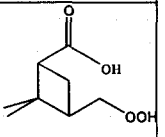
BP25	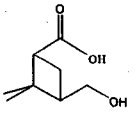	BP26	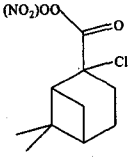	BP27	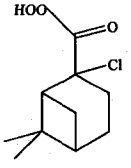
BP28	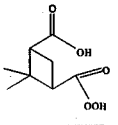	BP29	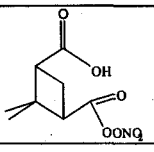	BP30	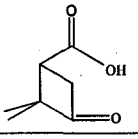
BP31	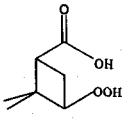	BP32	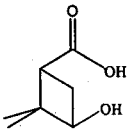		

Table 5.4. Cl-initiated oxidation mechanism for β-pinene.

Num	Reactants	Reaction Products	Rate Constant (cm^3 $molecule^{-1}$ s^{-1} or s^{-1})
BR1	β-Pinene + Cl	f BRO21 + (1-f)BRO22 + RO_2T According to *Davis et al.* [2005], f=0.80	5.3E-10[a]
BR2	BRO21 + Cl	BP1 + ClO + BRO23 + RO_2T	1.5E-11[b]
BR3	BRO21 + NO	NO_2 + BP1 + BRO23 + RO_2T	(4.1E-12)*EXP(180/T)[c]
BR4	BRO21 + HO_2	BP2	(3.0E13)*EXP(1250/T)* (1.0-EXP(-3.4))[c]
BR5	BRO21 + RO_2T	0.3BP3 + 0.7BP1 + 0.7 BRO23 + 1.7RO_2T	9.2E-14[c]
BR6	BRO22 + Cl	HCl + CB-RO22	1.35E-10[b]
BR7	CB-RO22 +H_2O	H_2O + BP4	1.0E-17[c]
BR8	BRO22 + Cl	ClO + BRO24 + HCHO + RO_2T	K2
BR9	BRO22 + NO	NO_2 + BRO24 + HCHO + RO_2T	K3
BR10	BRO22 + HO_2	BP5	K4
BR11	BRO22+ RO_2T	0.2BP6+0.2BP7+0.6BRO24 +0.6HCHO+1.6RO_2T	2.0E-12[c]
BR12	BRO23 + Cl	BP8 + HO_2 + ClO	K2
BR13	BRO23 + Cl	HCl + CB-RO23	K6
BR14	CB-RO23 +H_2O	H_2O + BP9	K7
BR15	BRO23 + NO	NO_2 + HO_2 + BP8	2.2*(4.1E-12)* EXP(180/T)[c]
BR16	BRO23 + HO_2	BP10	(3.3E-13)*EXP(820/T)[c]
BR17	BRO23 + RO_2T	0.33HO_2 + 0.33BP11 + 0.665BP8 + RO2T	K11
BR18	BRO24 + Cl	ClO + Cl + BP1	K2
BR19	BRO24 + NO	NO_2 + Cl + BP1	K3

Table 5.4. Continued.

BR20	BRO24 + HO_2	BP12	K16
BR21	BRO24 +RO_2T	0.7BP1 + 0.7Cl + 0.3BP13 + RO_2T	K5
BR22	BP1 + Cl	BRO25 + HCl + RO2T	1.8E-10[d] , by analogy to cyclohexanone.
BR23	BRO25 + Cl	ClO + BRO26 + RO_2T	K2
BR24	BRO25 + Cl	CB-RO25 + HCl	K6
BR25	CB-RO25+H_2O	BP14 + H_2O_2	6.0E-18[c]
BR26	BRO25 + NO	BRO26 + NO_2 + RO_2T	(4.1E-12)*EXP(180/T)* EXP(-0.17*8)[c]
BR27	BRO25 + HO_2	BP15	(1.36E-13)*EXP(1250/T)[c]
BR28	BRO25 + RO_2T	0.2BP16 + 0.2BP14+0.6BRO26 + 1.6RO_2T	8.8E-13[c]
BR29	BRO26 + Cl	ClO + BRO27 + RO_2T	K2
BR30	BRO26 + NO	NO_2 + BRO27 + RO_2T	2.7*(4.1E-12)* EXP(180/T)[c]
BR31	BRO26 + NO_2	BP17	5.8E-11[e]
BR32	BP17	BRO26 +NO_2 + RO_2T	0.0102[e]
BR33	BRO26 + HO_2	BP18 + 0.29O_3 (Lumping)	(4.3E-13)*EXP(1040/T)[c]
BR34	BRO26 +RO_2T	0.3BP18 + 0.7BRO27 + 1.7RO_2T	5.0E-12[c]
BR35	BRO27 + Cl	CO_2 + ClO + BRO28 + RO_2T	K2
BR36	BRO27 + NO	NO_2 + CO_2 + BRO28 +RO_2T	K30
BR37	BRO27 + HO_2	0.71BP19 + 0.29BP20 + 0.29O_3	K33
BR38	BRO27 + RO_2T	0.7BRO28 + 0.7CO_2 + 0.3BP20 +1.7RO_2T	K34
BR39	BRO27 + NO_2	BP21	K31
BR40	BP21	BRO27 + NO_2 +RO_2T	K32
BR41	BRO28 + Cl	ClO + HO_2 + BP22	K2
BR42	BRO28 + Cl	HCl + CB-RO28	K6

Table 5.4. Continued.

BR43	CB-RO28+H_2O	H_2O + BP23	K7
BR44	BRO28 + NO	HO_2 + NO_2 +BP22	(4.1E-12)*EXP(180/T)* EXP(-0.17*7)[c]
BR45	BRO28 + HO_2	BP24	(3.0E-13)*EXP(1250/T)* (1-EXP(-0.34*8))[c]
BR46	BRO28 + RO_2T	0.2BP25 +0.6HO_2 +0.8BP22+RO_2T	1.30E-12[c]
BR47	BP6 + hv	BRO24 + CO + HO_2 +RO_2T	3.1E-05[e], Corrected for UV light strength and spectrum
BR48	BP6 + Cl	HCl + BRO29 + RO_2T	2.5E-10[f]
BR49	BRO29 + Cl	ClO + CO_2 + BRO24 + RO_2T	K2
BR50	BRO29 + NO	NO_2 + CO_2 + BRO24 + RO_2T	K30
BR51	BRO29 + NO_2	BP26	K31
BR52	BP26	NO_2 + BRO29+RO_2T	K32
BR53	BRO29 + HO_2	0.71BP27 + 0.29O_3 +0.29BP4	K33
BR54	BRO29 + RO_2T	0.3BP4 + 0.7CO_2 + 0.7BRO24 +1.7RO_2T	K34
BR55	BP8 + hv	HO_2 + CO + Cl	K47
BR56	BP8 + Cl	HCl +CO+Cl	K48
BR57	BP16 + Cl	HCl + BRO27 + RO_2T	K48
BR58	BP16 + hv	BRO28 + HO_2 + CO + RO_2T	K47
BR59	BP22 + Cl	BRO210 + HCl + RO_2T	K48
BR60	BP22 + hv	HO_2 + CO + BRO211 + RO_2T	K47
BR61	BRO210 + Cl	ClO + CO_2 + BRO211 + RO_2T	K2
BR62	BRO210 + NO	NO_2 + BRO211 + CO_2 + RO_2T	K30
BR63	BRO210 + HO_2	0.71BP28 + 0.29BP23+0.29O_3	K33
BR64	BRO210+ RO_2T	0.3BP23+0.7BRO211+0.7C O_2+1.7RO_2T	K34

Table 5.4. Continued.

BR65	BRO210 + NO_2	BP29	K31
BR66	BP29	BRO210 + NO_2 +RO_2T	K32
BR67	BRO211 + Cl	HCl + CB-RO211	K6
BR68	CB-RO211 + H_2O	H_2O_2 + BP30	K25
BR69	BRO211 + Cl	BP30+ HO_2 +ClO	K2
BR70	BRO211 + NO	NO_2 + HO_2 +BP30	(4.1E-12)*EXP(180/T)* EXP(-0.17*6)[c]
BR71	BRO211 + HO_2	BP31	(3.0E-13)*EXP(1250/T)* (1-EXP(-0.34*7))[c]
BR72	BRO211+ RO_2T	0.8BP30 + 0.6HO_2 + 0.2BP32 + RO_2T	2.5E-13[c]
BR73	HCHO + Cl	HCl + CO + HO_2	K48
BR74	HCHO + hv	CO + 2HO_2	4.53E-05[g], Corrected for UV light strength and spectrum.
BR75	HCHO + hv	H_2 + CO	6.95E-05[g], Corrected for UV light strength and spectrum
BR76	H_2O_2•••hv•	2OH	0.0 for 365nm UV light[g]
BR77	Cl + O_3	ClO + HO_2	(2.9E-11)*EXP(-260/T)[g]
BR78	HO_2 + Cl	HCl + O_2	(1.8E-11)*EXP(170/T)[g]
BR79	HO_2 + Cl	OH + ClO	(4.1E-11)*EXP(-450/T)[g]
BR80	HO_2 + ClO	HOCl + O_2	(4.8E-13)*EXP(700/T)[g]
BR81	HOCl + hv	OH + Cl	6.25E-06[g], Corrected for UV light strength and spectrum.
BR82	OH + HCl	H_2O + Cl	(2.6E-12)*EXP(-350/T)[g]
BR83	OH + HOCl	H_2O + ClO	(3.0E-12)*EXP(-500/T)[g]
BR84	Cl_2 + hv	2Cl	J(Cl_2)=3.28E-03[g], Corrected for UV light strength and spectrum.

a: *Finlayson-Pitts et al.* [1999] or *Finlayson-Pitts and Pitts* [2000]; b: *Karlsson et al.* [2001]; c:*Jenkin et al.* [1997]; d: *Notario et al.* [1999]; e: *Griffin et al.* [2002a]; *f*: *Thevenet et al.* [2000]; g: *Jet Propulsion Laboratory* [1997]; *h*: *Tanaka et al.* [2003b].

Table 5.5. Chemical species in the mechanism for Cl-initiated oxidation of d-limonene.

Notation	Structure	Notation	Structure	Notation	Structure
Radical	Species	Radical	Species	Radical	Species
LRO21	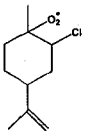	LRO22	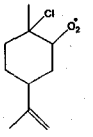	LRO23	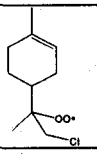
LRO24	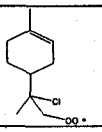	LRO25	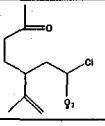	LRO26	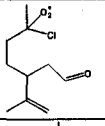
LRO27	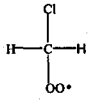	LRO28	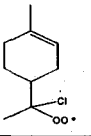	LP9RO2	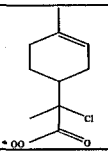
TZRO21	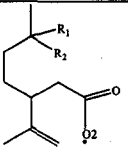	TZRO22	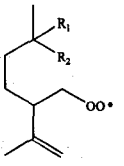	TZRO23	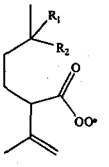
TZRO24	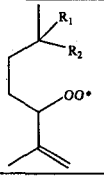	TL1RO2 (Lumped)	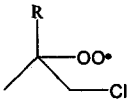	TL2-RO21 (Lumped)	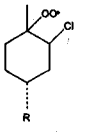
TL2-RO22 (Lumped)	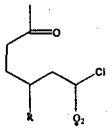	CB-RO22	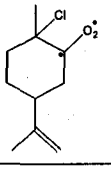	CB-RO24	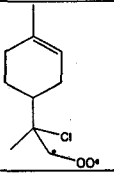
CB-RO25	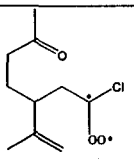	CB-RO27	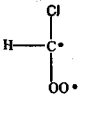	CB-TL2RO22 (Lumped)	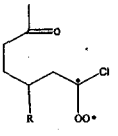
Non-radical	Products	Non radical	Products	Non radical	Products
LP1	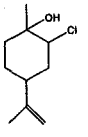	LP2	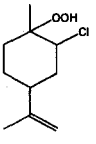	LP3	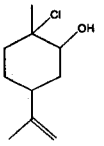

Table 5.5. Continued.

LP4	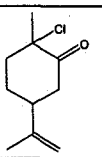	LP5	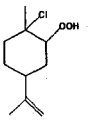	LP6	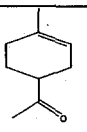
LP7	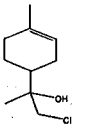	LP8	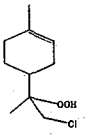	LP9	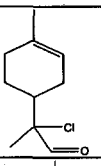
LP10	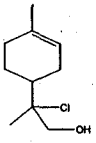	LP11	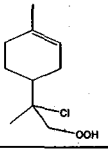	LP12	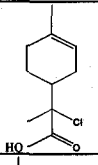
LP13	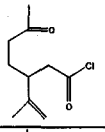	LP14	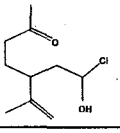	LP15	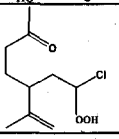
LP16	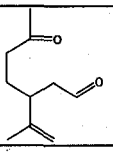	LP17	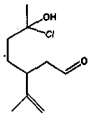	LP18	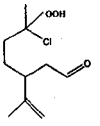
LP19		LP20		LP21	
LP22		LP23	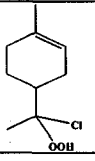	LP24	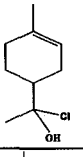
LP25	No Specific Structure	LP9P1	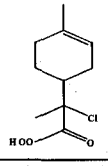	LP9P2	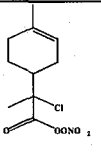
LP26	No Specific Structur	TZP1	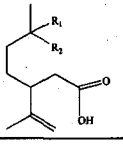	TZP2	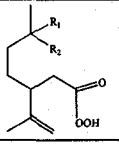

Table 5.5. Continued.

TZP3	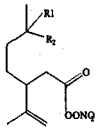	TZP4	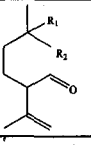	TZP5	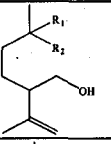
TZP6	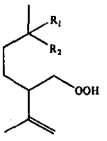	LP27	No Specific Structure	TZP7	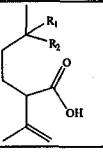
TZP8	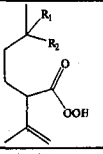	TZP9	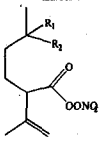	TZP10	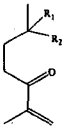
TZP11	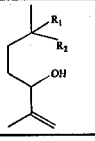	TZP12	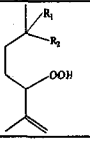	T1P1	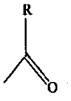
T1P2 (Lumped)	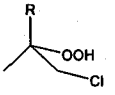	T1P3 (Lumped)	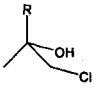	T2P1 (Lumped)	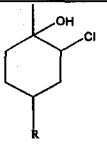
T2P2 (Lumped)	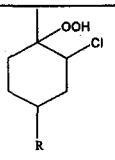	T2P3 (Lumped)	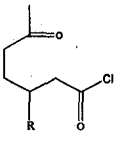	T2P4 (Lumped)	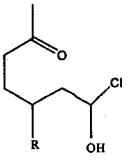
T2P5 (Lumped)	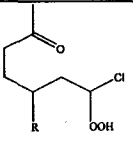				

Table 5.6. Cl-initiated oxidation mechanism for d-limonene.

Num	Reactants	Reaction Products	Rate Constant (cm^3 $molecule^{-1}$ s^{-1} or s^{-1})
LR1	d-limonene + Cl	0.5LRO21 + 0.1LRO22 + 0.3LRO23 + 0.1LRO24 + RO_2T Stochiometric coefficients are determined based on *Hakola et al.* [1994] and *Noziere et al.* [1999].	6.4E-10[a]
LR2	LRO21 + Cl	LRO25 + ClO + RO_2T	1.5E-11[b]
LR3	LRO21 + RO_2T	0.7LRO25 + 0.3LP1 + 1.7RO_2T	9.2E-14[c]
LR4	LRO21+ NO	LRO25 + NO_2 + RO_2T	(4.1E-12)*EXP(180/T)[c]
LR5	LRO21 + HO_2	LP2	(3.0E-13)*EXP(1250/T)* (1-EXP(-3.4))[c]
LR6	LRO22 + Cl	LRO26 + ClO + RO_2T	K2
LR7	LRO22 + RO_2T	0.6 LRO26 + 0.2LP3 + 0.2LP4 + 1.6RO_2T	8.8E-13[c]
LR8	LRO22 + NO	LRO26 + NO_2 + RO_2T	K4
LR9	LRO22 + HO_2	LP5	K5
LR10	LRO22 + Cl	HCl + CB-RO22	1.35E-10[b]
LR11	CB-RO22 + H_2O	H_2O_2 + LP4	6.0E-18[c]
LR12	LRO23 + Cl	LP6 + ClO + LRO27 + RO_2T	K2
LR13	LRO23 + RO_2T	0.7LP6 + 0.7LRO27+ 0.3LP7 + 1.7RO_2T	K3
LR14	LRO23 + NO	LP6 + NO_2 + LRO27 + RO_2T	K4
LR15	LRO23 + HO_2	LP8	K5
LR16	LRO24 + Cl	ClO + HCHO + LRO28 + RO_2T	K2
LR17	LRO24 + NO	NO_2 + HCHO + LRO28+RO_2T	K4
LR18	LRO24 + RO_2T	0.2LP9+0.2LP10+0.6LRO28+ 0.6HCHO+1.6RO_2T	2.0E-12[c]
LR19	LRO24 + HO_2	LP11	K5
LR20	LRO24 + Cl	HCl + CB-RO24	K10

Table. 5.6. Continued.

LR21	CB-RO24 + H_2O	H_2O + LP12	1.0E-17[c]
LR22	LRO25 + Cl	ClO + HO_2 + LP13	K2
LR23	LRO25 + RO_2T	0.8LP13 + 0.2LP14 + 0.6 HO_2 + RO_2T	K7
LR24	LRO25 + NO	LP13 + HO_2 + NO_2	K4
LR25	LRO25 + HO_2	LP15	(3.3E-13)*EXP(820/T)[c]
LR26	LRO25 + Cl	HCl + CB-RO25	K10
LR27	CB-RO25 + H_2O	H_2O_2 + LP13	K11
LR28	LRO26 + Cl	LP16 + Cl + ClO	K2
LR29	LRO26 + RO_2T	0.7 LP16 + 0.7Cl + 0.3LP17 + RO_2T	K3
LR30	LRO26 + NO	LP16 + Cl + NO_2	K4
LR31	LRO26 + HO_2	LP18	K25
LR32	LRO27 + Cl	ClO + HO_2 + LP19	K2
LR33	LRO27 + NO	NO_2 + HO_2 + LP19	2.2*(4.1E-12)* EXP(180/T)[c]
LR34	LRO27 + HO_2	0.6LP20 + 0.4LP19	K25
LR35	LRO27 + RO_2T	0.665LP19 + 0.33HO_2 + 0.335LP21 + RO_2T	K18
LR36	LRO27 + Cl	HCl + CB-RO27	K10
LR37	CB-RO27 + H_2O	H_2O + LP22	K21
LR38	LRO28 +Cl	ClO + Cl +LP6	K2
LR39	LRO28 + NO	NO_2 + Cl + LP6	K4
LR40	LRO28 + HO_2	LP23	K25
LR41	LRO28 + RO_2T	0.7LP6 + 0.7Cl + 0.3LP24 + RO_2T	K3
LR42	LP9 + Cl	0.33LP25 + 0.67LP9RO2 + HCl + 1.67RO2T	4.6E-10[a] + 2.5E-10[d] (K85 + K51)

Table 5.6. Continued.

LR43	LP9 + hv	CO + HO_2 +LRO28 +RO_2T	3.1E-05[e], Corrected for UV light strength and UV spectrum.
LR44	LP9RO2 + Cl	ClO + CO_2 +LRO28 +RO2T	K2
LR45	LP9RO2 + NO	NO_2 + CO_2 + LRO28 + RO2T	K4*2.7[c]
LR46	LP9RO2 +RO2T	0.7CO_2 +0.7LRO28 + 0.3LP9P1+1.7RO2T	5.0E-12[c]
LR47	LP9RO2+H O_2	0.71LP9P2 + 0.29LP9P1 + 0.29O_3	4.3E-13*EXP(1040/T)[c]
LR48	LP9RO2 + NO_2	LP9P3	5.8E-11[c]
LR49	LP9P3	LP9RO2 + NO_2 + RO2T	0.036[e]
LR50	LP19 + hv	HO_2 +Cl+CO	K43
LR51	LP19 + Cl	HCl +Cl +CO	2.5E-10[d]
LR52	TLP0 + Cl	0.45LP26 + 0.55HCl + 0.55TZRO21 + 1.55RO2T	5.5E-10 (K80 + K51)
LR53	TLP0 + hv	CO + HO2 + TZRO22 + RO2T	K43
LR54	TZRO21 + Cl	ClO + CO_2 + TZRO22 + RO2T	K2
LR55	TZRO21 + NO	NO2 + CO_2 + TZRO22 + RO2T	K45
LR56	TZRO21 + RO2T	0.7CO_2 + 0.7TZRO22 + 0.3 TZP1 + 1.7RO2T	K46
LR57	TZRO21 + HO_2	0.71TZP2 + 0.29TZP1 + 0.29O_3	K47
LR58	TZRO21 + NO_2	TZP3	K48
LR59	TZP3	TZRO21 + NO_2 + RO2T	K49
LR60	TZRO22 + Cl	ClO + TZP4 + HO_2	K2
LR61	TZRO22 + NO	NO_2 + TZP4 + HO_2	4.1E-12*EXP(180/T)* EXP(-0.17*8)[c]
LR62	TZRO22 + RO2T	0.8TZP4 + 0.6HO_2 + TZP5 + RO2T	1.3E-12[c]
LR63	TZRO22 + HO_2	0.6TZP6 + 0.4TZP4	3.0E-13*EXP(1250/T)* [1-EXP(-0.34*8)][c]
LR64	TZRO22 + Cl	CB-TZRO22 + HCl	1.35E-10[b]

Table 5.6. Continued.

LR65	CB-TZRO22 + H_2O	H_2O + TZP1	1.0E-17[c]
LR66	TZP4 + Cl	0.45LP27 + 0.55HCl + 0.55TZRO23 + 1.55RO2T	K52
LR67	TZP4 + Hv	CO + HO_2 + TZRO24 + RO2T	K43
LR68	TZRO23 + Cl	ClO + CO_2 + TZRO24 + RO2T	K2
LR69	TZRO23 + NO	NO_2 + CO_2 + TZRO24 + RO2T	K45
LR70	TZRO23 + RO2T	0.7CO_2 + 0.7TZRO24 + 0.3TZP7+ 1.7RO2T	K46
LR71	TZRO23 + HO_2	0.71TZP8 + 0.29TZP7 + 0.29O_3	K47
LR72	TZRO23 + NO_2	TZP9	K48
LR73	TZP9	TZRO23 + NO_2 + RO2T	K49
LR74	TZRO24 + Cl	ClO + TZP10 + HO_2	K2
LR75	TZRO24 + NO	NO_2 + TZP10 + HO_2	4.1E-12*EXP(180/T)* EXP(-0.17*7)[c]
LR76	TZRO24 + RO2T	0.8TZP10 + 0.6HO_2 + 0.2TZP11+ RO2T	2.5E-13[c]
LR77	TZRO24 + HO_2	0.6TZP12 + 0.4TZP10	3.0E-13*EXP(1250/T)* [1-EXP(-0.34*8)][c]
LR78	TZRO24 + Cl	HCl + CB-TZRO24	K64
LR79	CB-TZRO24 + H_2O	H_2O_2 + TZP10	6.0E-18[c]
LR80	TLP1 + Cl	TL1RO2 + RO_2T	K80 = K85*(0.40/0.60)
LR81	TL1RO2 + Cl	T1P1 +ClO +LRO27+RO_2T	K2
LR82	TL1RO2 + NO	T1P1+NO_2+LRO27+RO_2T	K4
LR83	TL1RO2 + HO_2	T1P2	K5
LR84	TL1RO2 + RO_2T	0.7T1P1+0.7LRO27+0.3T1P3+ 1.7RO_2T	K3
LR85	TLP2 +Cl	TL2RO21 + RO_2T	4.6E-10[a], By analogy to α-pinene
LR86	TL2RO21 + Cl	TL2RO22 + ClO + RO_2T	K2

Table 5.6. Continued.

LR87	TL2RO21 + RO_2T	0.7TL2RO22 + 0.3T2P1 + 1.7RO_2T	K3
LR88	TL2RO21 + NO	TL2RO22 +NO_2 + RO_2T	K4
LR89	TL2RO21 + HO_2	T2P2	K5
LR90	TL2RO22 + Cl	ClO +T2P3+HO_2	K2
LR91	TL2RO22 + Cl	HCl +CB-TL2RO22	K10
LR92	CB-TL2RO22 + H_2O	H_2O_2 +T2P3	K11
LR93	TL2RO22 +RO_2T	0.8T2P3 +0.6HO_2 +0.2T2P4+RO_2T	K7
LR94	TL2RO22 + NO	T2P3 +HO_2 +NO_2	K4
LR95	TL2RO22 + HO_2	T2P5	K25
LR96	HCHO + Cl	HCl + CO + HO_2	K42
LR97	HCHO + hv	CO + 2HO_2	4.53E-05[g], Corrected for UV light strength and spectrum.
LR98	HCHO + hv	H_2 + CO	6.95E-05[g], Corrected for UV light strength and spectrum
LR99	H_2O_2 + hv	2OH	0.0 for 365nm UV light[f]
LR100	Cl + O_3	ClO + O_2	(2.9E-11)*EXP(-260/T)[f]
LR101	HO_2 + Cl	HCl + O_2	(1.8E-11)*EXP(170/T)[f]
LR102	HO_2 + Cl	OH + ClO	(4.1E-11)*EXP(-450/T)[f]
LR103	HO_2 + ClO	HOCl + O_2	(4.8E-13)*EXP(700/T)[f]
LR104	HOCl + hv	OH + Cl	6.25E-06[f], Corrected for UV light strength and spectrum.

Table 5.6. Continued.

LR105	OH + HCl	H_2O + Cl	(2.6E-12)*EXP(-350/T)[f]
LR106	OH + HOCl	H_2O + ClO	(3.0E-12)*EXP(-500/T)[f]
LR107	Cl_2 + hv	2Cl	3.28E-03[g], Corrected for UV light strength and spectrum.

a: *Finlayson-Pitts et al.* [1999] or *Finalyson-Pitts and Pitts* [2000]; b: *Karlsson et al.* [2001]; c:*Jenkin et al.* [1997]; d: *Thevenet et al.* [2000]; e: *Griffin et al.* [2002a]; f: *Jet Propulsion Laboratory* [1997]; g: *Tanaka et al.* [2003b]

Table 5.7. Chemical species in the mechanism of the Cl-initiated oxidation of toluene.

Notation	Structure	Notation	Structure	Notation	Structure
Radical	Species	Radical	Species	Radical	Species
TRO21	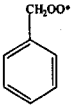	CB -TRO21	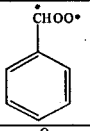	TRO22	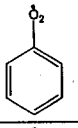
TRO23	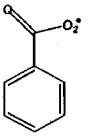	TRO24	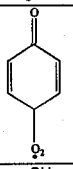	CB -TRO24	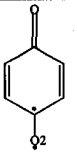
ZTRO21	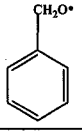	TR-1	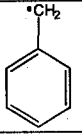		
Non-radical	Products	Non radical	Products	Non radical	Products
TP1	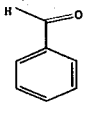	TP2	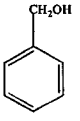	TP3	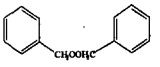
TP4	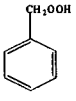	TP5	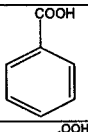	TP6	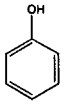
TP7	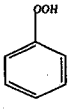	TP8	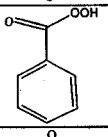	TP9	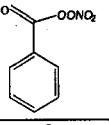
TP10	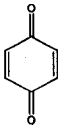	TP11	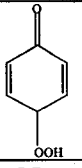	TP12	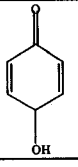
TP13	No Specific Structure	TP14	No Specific Structure	TP15	No Specific Structure
TP16	No Specific Structure				

Table 5.8. Cl-initiated oxidation mechanism for toluene.

Num	Reactants	Reaction Products	Rate Constant (cm^3 $molecule^{-1}$ s^{-1} or s^{-1})
TR1	RCH3 + Cl	HCl + TR-1	6.10E-11 [a]
TR2	TR-1 + O_2	TRO21 + RO2T	1.4E-12 [a]
TR3	TR-1 + TRO21	2ZTRO21	5.0E-11 [a]
TR4	TR-1 + NO	Products	9.5E-12 [a]
TR5	ZTRO21 + ZTRO21	F4TP1 + F4TP2 + (1-F4)TP3, F4=0.67	3.0E-11 [a], by analogy to the self-reaction of toluic peroxy radical.
TR6	ZTRO21 + NO	0.2TP1 + 0.2HNO + 0.8RCH_2ONO	6.0E-11 [a]
TR7	TRO21 + Cl	ZTRO21 + ClO	1.50E-11 [a]
TR8	TRO21 + Cl	CB-TRO21 + HCl	1.35E-10 [a]
TR9	TRO21 + RO2T	0.6ZTRO21 + 0.2TP1 + 0.2TP2 + RO2T	1.3E-12 [b]
TR10	TRO21 + HO_2	TP4 + O_2	1.0E-11 [a]
TR11	TRO21 + NO	ZTRO21 + NO_2	2.7E-11 [a]
TR12	CB-TRO21 + H_2O	TP5 + H_2O	1.0E-17 [b]
TR13	ZTRO21 + O_2	TP1 + HO_2	(2.5E-14)*EXP(-300/T) [c]
TR14	ZTRO21	HCHO + TRO22 + RO2T	(5.0E+13)*EXP(-9108/T)[c]
TR15	TP1 + Cl	HCl + TRO23 + RO2T	2.5E-10 [f]
TR16	TP1 + hv	HO_2 + CO + TRO22 + RO2T	3.1E-05[g], corrected for UV light strength and spectrum.
TR17	TRO22 + Cl	ClO + TRO24 + RO2T	K7
TR18	TRO22 + NO	NO_2 + TRO24 + RO2T	(4.1E-12)*EXP(180/T)* Exp(-0.17*5) [b]
TR19	TRO22 + RO2T	0.7TRO24 + 0.3TP6 + 1.7RO2T	(6.7E-15)*EXP(416/T) [b]
TR20	TRO22 + HO_2	TP7 + O_2	(3.0E-13)*EXP(1250/T)* [1-exp(-0.34*6)] [b]

Table 5.8. Continued.

TR21	TRO23 + RO2T	0.3TP5 + 0.7CO_2 + 0.7TRO22 + 1.7RO2T	(5.0E-12)[b]
TR22	TRO23 + Cl	ClO + CO_2 + TRO22 + RO2T	K7
TR23	TRO23 + HO_2	0.71TP8 + 0.71O_2 + 0.29TP5 + 0.29O_3	(4.3E-13)*EXP(1040/T)[b]
TR24	TRO23 + NO	CO_2 + TRO22 + NO_2 + RO2T	2.7*(4.1E-12)*EXP(180/T)[b]
TR25	TRO23 + NO_2	TP9	5.8E-11[g]
TR26	TP9	TRO23 + NO_2 + RO2T	0.0102[g]
TR27	TRO24 + Cl	ClO + HO_2 + TP10	K7
TR28	TRO24 + Cl	CB-TRO24 + HCl	K8
TR29	CB-TRO24 + H_2O	H_2O_2 + TP10	1.0E-18[b]
TR30	TRO24 + NO	NO_2 + HO_2 + TP10	(4.10E-12)*EXP(180/T)*Exp(-0.17*5)[b]
TR31	TRO24 + HO_2	TP11 + O_2	(3.0E-13)*EXP(1250/T)*[1-EXP(-0.34*6)][b]
TR32	TRO24 + RO2T	0.8TP10 + 0.6HO_2 + 0.2TP12 + RO2T	(2.5E-13)[b]
TR33	TP2 + Cl	TP1 + HCl + HO_2	4.79E-11[h]
TR34	TP3 + hv	2ZTRO21	0, for 365nm UV light[k]
TR35	TP4 + Cl	TRO21 + HCl + RO2T	(2.9E-11)*EXP(190/T)[b], Based on observed data, for toluene, K_{Cl}~10.0K_{OH}.
TR36	TP4 + hv	OH + HO_2 + TP1	1.42E-07[b], corrected for UV light strength and spectrum.
TR37	TP5 + Cl	HCl + CO_2 + TRO22 + RO2T	(1.3E-13)*EXP(1600/T)[i]
TR38	TP6 + Cl	TRO24 + HCl + RO2T	K33
TR39	TP7 + Cl	HCl + TRO22 + RO2T	K35
TR40	TP7 + hv	OH + TRO24 + RO2T	K36
TR41	TP8 + Cl	TRO23 + HCl + RO2T	K39

Table 5.8. Continued.

TR42	TP8 + hv	OH + CO_2 + TRO22 + RO2T	K40
TR43	TP10 + Cl	TP13	4.60E-11[j], Based on observed data, for toluene, K_{Cl}~10.0K_{OH}.
TR44	TP11 + Cl	TP14	K43
TR45	TP11 + hv	OH + HO_2 + TP10	K40
TR46	TP12 + Cl	TP15	K44
TR47	TP10 + OH	TP16	4.60E-12[j]
TR48	TP11 + OH	TP16	K47
TR49	TP12 + OH	TP16	K47
TR50	RCH3 + OH	TP16	5.96E-12[k]
TR51	H_2O_2 + hv	2OH	0, for 365nm UV light. (JPL Data, pp157)
TR52	HCHO + hv	$2HO_2$ + CO	K16
TR53	HCHO + hv	H_2 + CO	K16
TR54	HCHO + Cl	HCl + CO + HO2	K15
TR55	Cl + O_3	ClO + O_2	(2.9E-11)*EXP(-260/T)[k]
TR56	HO_2 + Cl	HCl + O_2	(1.8E-11)*EXP(170/T)[k]
TR57	HO_2 + Cl	OH + ClO	(4.1E-11)*EXP(-450/T)[k]
TR58	HO_2 + ClO	HOCl + O_2	(4.8E-13)*EXP(700/T)[k]
TR59	HOCl + hv	OH + Cl	6.25E-06[k], Corrected for UV light strength and spectrum.
TR60	OH + HCl	H_2O + Cl	(2.6E-12)*EXP(-350/T)[k]
TR61	OH + HOCl	H_2O + ClO	(3.0E-12)*EXP(-500/T)[k]
TR62	Cl_2 + hv	2Cl	3.28E-03[l], Corrected for UV light strength and spectrum.

a: *Karlsson et al.* [2001]; *b*: *Jenkin et al.* [1997]; c: *Atkinson* [2007]; *d*: *Atkinson* [1994]; *e*: *Niki et al.* [1981]; *f*:*Thevenet et al.* [2000]; *g*: *Griffin et al.* [2002a]; *h*: *Nelson et al.* [1990]; *i*: *Aranda et al.* [2003]; *j*: *Olariu et al.* [2000]; *k*: *Jet Propulsion Laboratory* [1997]; *l*: *Tanaka et al.* [2003a].

Table 5.9. Initial conditions and data for Cl-initiated oxidation experiments.

Run	Parent Hydrocarbon	[a](Cl$_2$/VOC)$_0$ (ppb ppb^{-1})	[b]T(K)	ΔVOC (ppb)	ΔVOC (μgm^{-3})	ΔM_0 (μgm^{-3})	Y
BP-1	β-pinene	6.0	297	16.7	91.2	9.4	0.103
BP-2	β-pinene	7.0	300	14.2	77.8	12.6	0.162
BP-3	β-pinene	8.1	298	12.3	67.4	11.2	0.166
BP-4	β-pinene	4.9	298	20.6	112.9	19.2	0.170
BP-5	β-pinene	4.0	299	25.0	136.8	27.5	0.201
BP-6	β-pinene	3.6	300	27.8	152.2	35.0	0.230
AP-1	α-pinene	5.5	299	18.3	101.3	8.0	0.079
AP-2	α-pinene	6.7	300	15.0	82.7	9.1	0.110
AP-3	α-pinene	8.3	300	12.1	66.6	10.0	0.150
AP-4	α-pinene	6.3	299	15.8	87.6	18.4	0.210
AP-5	α-pinene	4.6	298	21.9	121.0	25.4	0.210
AP-6	α-pinene	3.6	299	27.5	152.3	33.5	0.220
HDL-1	d-limonene	7.4	300	27.0	149.4	6.5	0.044
HDL-2	d-limonene	5.7	297	35.4	195.7	12.0	0.062
HDL-3	d-limonene	4.5	299	44.4	245.8	17.5	0.072
HDL-4	d-limonene	5.5	299	36.1	199.6	15.2	0.077
HDL-5	d-limonene	4.8	300	41.8	231.3	18.3	0.080
HDL-6	d-limonene	5.5	298	36.5	201.8	18.0	0.090
LDL-1	d-limonene	8.9	299	11.3	62.2	1.3	0.020
LDL-2	d-limonene	12.5	296	8.0	44.2	5.5	0.130
LDL-3	d-limonene	8.0	299	12.5	69.1	9.8	0.143
LDL-4	d-limonene	10.2	299	9.8	54.2	9.0	0.200
LDL-5	d-limonene	10.0	300	10.0	55.3	13.2	0.220
LDL-6	d-limonene	9.9	299	10.1	55.7	13.0	0.220

[a](Cl$_2$/VOC)$_0$ is the approximate initial ratio of Cl$_2$ and VOC mixing ratios.
[b]T(K) is the average temperature under which the experiments are conducted.

Table 5.9. Continued

Experiment	Parent Hydrocarbon	$(Cl_2/VOC)_0$ (ppb ppb^{-1})	Temperature (K)	ΔVOC (ppb)	ΔVOC (μg m^{-3})	ΔM_O (μg m^{-3})	Y
THR-1	toluene	9.0	297.0	22.1	84.8	4.8	0.058
THR-2	toluene	5.2	300.0	19.4	74.3	4.6	0.062
THR-3	toluene	7.0	298.0	17.9	68.7	5.9	0.085
THR-4	toluene	9.5	298.0	18.4	70.3	6.3	0.090
THR-5	toluene	10.0	298.5	30.0	114.9	8.6	0.091
THR-6	toluene	6.7	299.5	37.1	142.3	12.7	0.089
THR-7	toluene	10.0	298.5	39.2	150.3	13.8	0.091
TLR-1	toluene	3.5	299.5	23.9	91.4	3.5	0.038
TLR-2	toluene	2.6	300.0	28.7	110.1	3.7	0.035
TLR-3	toluene	3.1	299.0	23.9	91.6	4.6	0.056
TLR-4	toluene	3.9	298.0	19.4	74.3	6.6	0.060
TLR-5	toluene	3.2	299.0	31.7	121.4	7.5	0.062
TLR-6	toluene	3.5	299.5	35.4	135.6	8.9	0.066
TLR-7	toluene	4.0	297.0	49.5	189.6	12.7	0.074

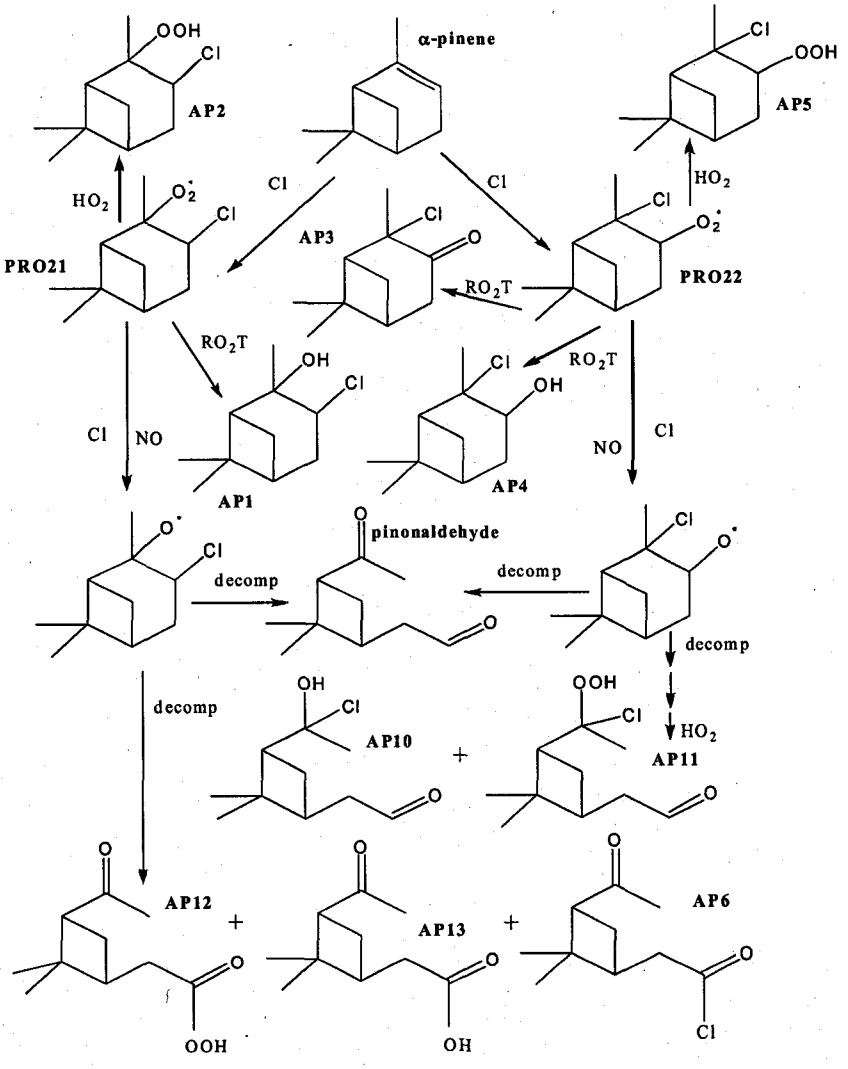

Figure 5.1. Proposed mechanism for the reaction of α-pinene with Cl. See Table 2 for notation. Decomposition reactions are denoted as "decomp." For the sake of brevity, not all steps are shown.

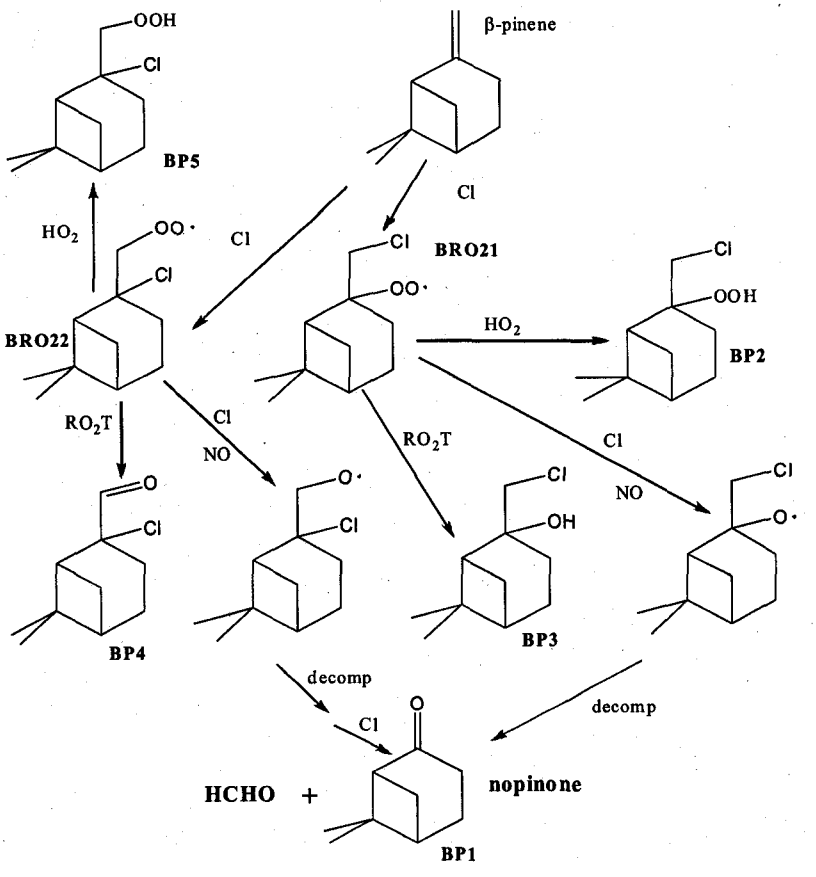

Figure 5.2. Proposed mechanism for the reaction of β-pinene with Cl. See Table 4 for notation. Decomposition reactions are denoted as "decomp." For the sake of brevity, not all steps are shown.

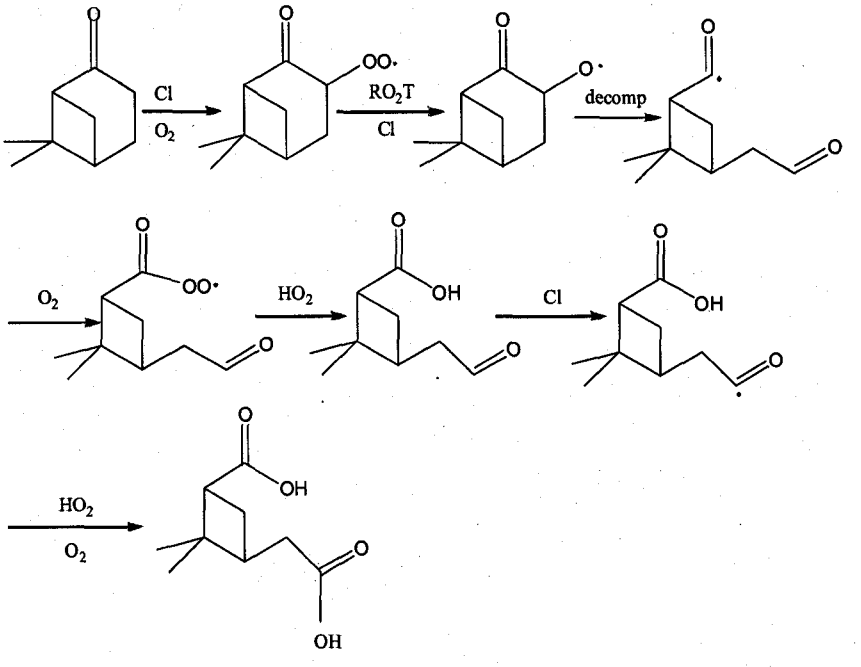

Figure 5.3. Proposed mechanism for the reaction of nopinone with Cl. Decomposition reactions are denoted as "decomp." For the sake of brevity, not all steps are shown.

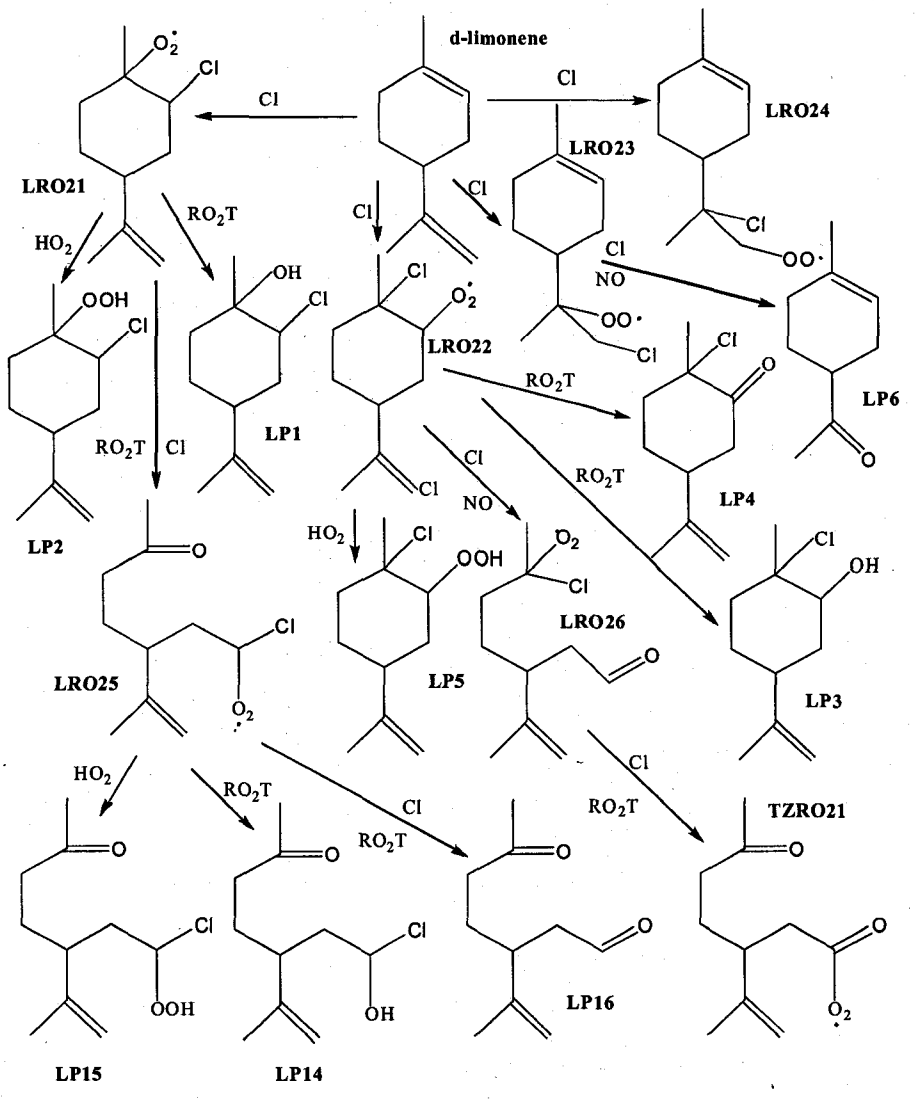

Figure 5.4. Proposed mechanism for the reaction of d-limonene with Cl. See Table 6 for notation. For the sake of brevity, not all steps are shown.

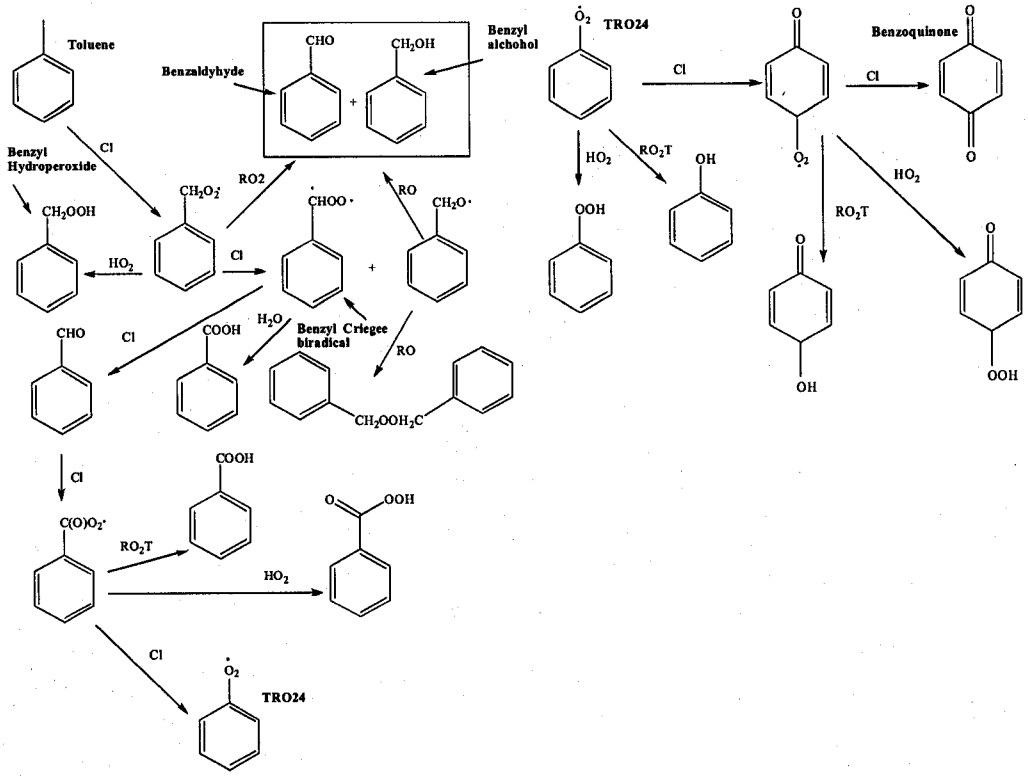

Figure 5.5. Proposed mechanism for the reaction of toluene with Cl.

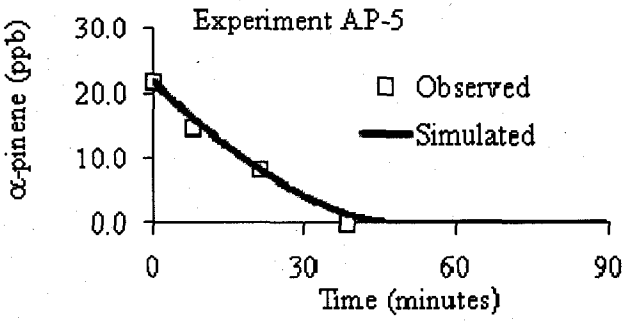

(a)

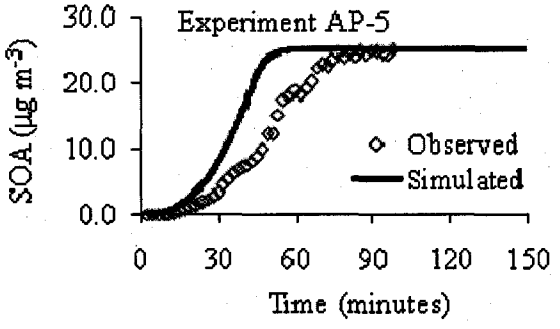

(b)

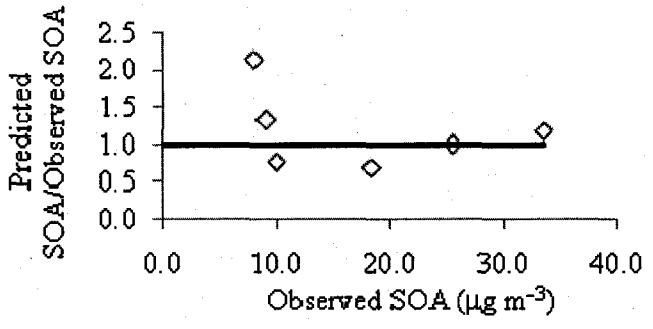

(c)

Figure 5.6. Modeling results for α-pinene: (a) simulated and observed α-pinene mixing ratios; (b) simulated and observed SOA mass concentration evolution; and (c) simulated and observed final SOA mass concentration for all α-pinene experiments.

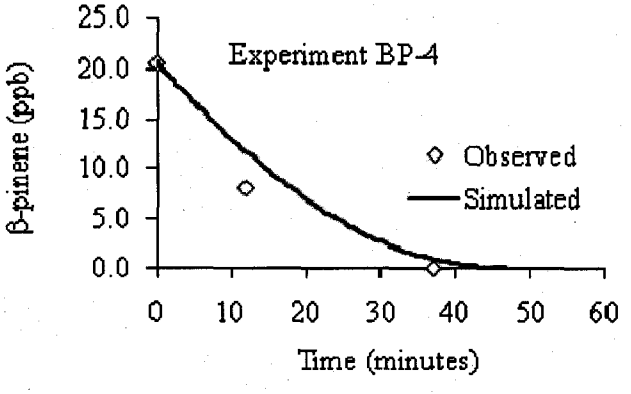

(a)

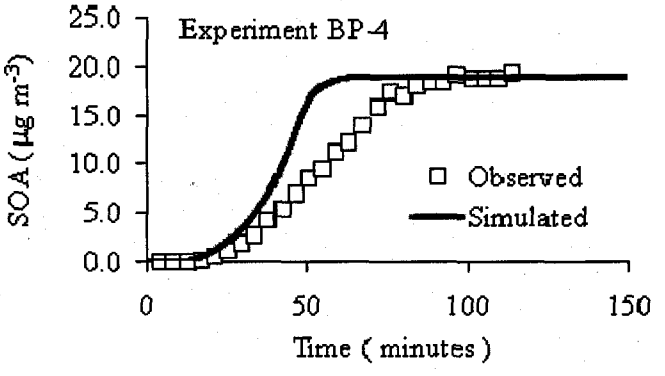

(b)

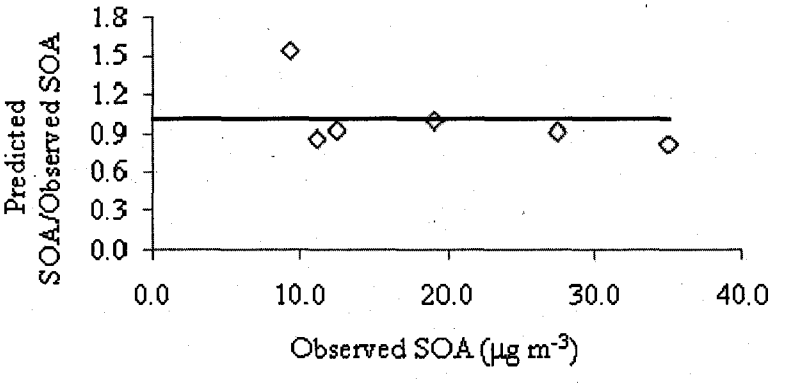

(c)

Figure 5.7. Modeling results for β-pinene: (a) simulated and observed β-pinene concentration profile; (b) simulated and observed SOA concentration evolution; and (c) simulated and observed final SOA mass concentrations for all β-pinene experiments.

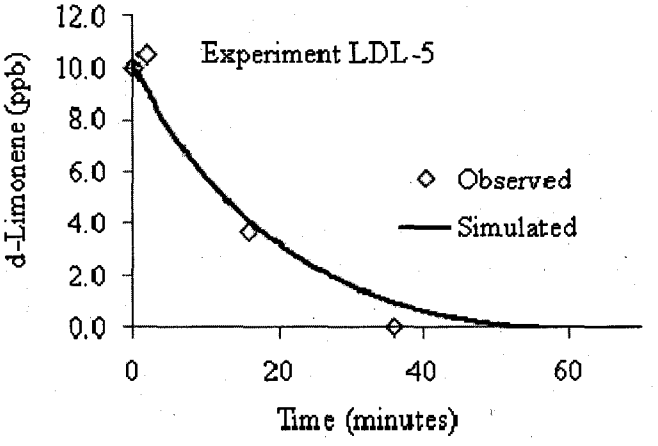

(a)

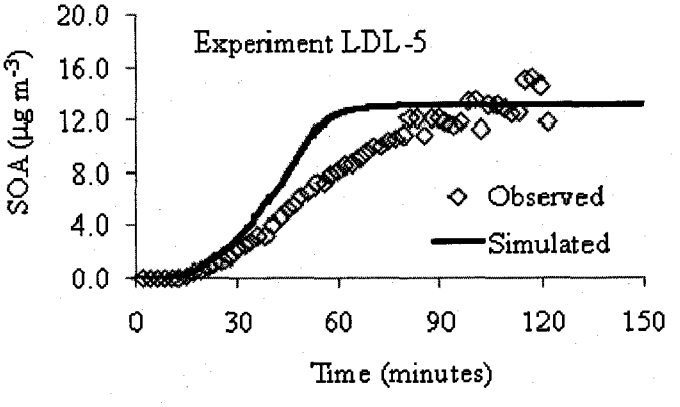

(b)

Figure 5.8A. Modeling results for d-limonene experiments: (a) simulated and observed d-limonene concentration profile; (b) simulated and observed SOA mass concentration evolution.

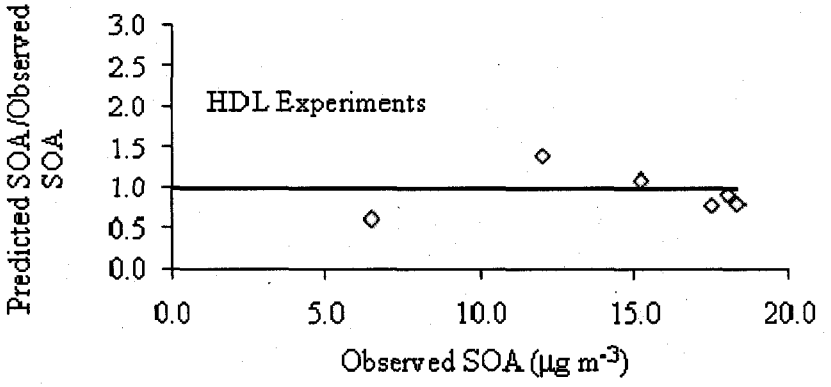

(c)

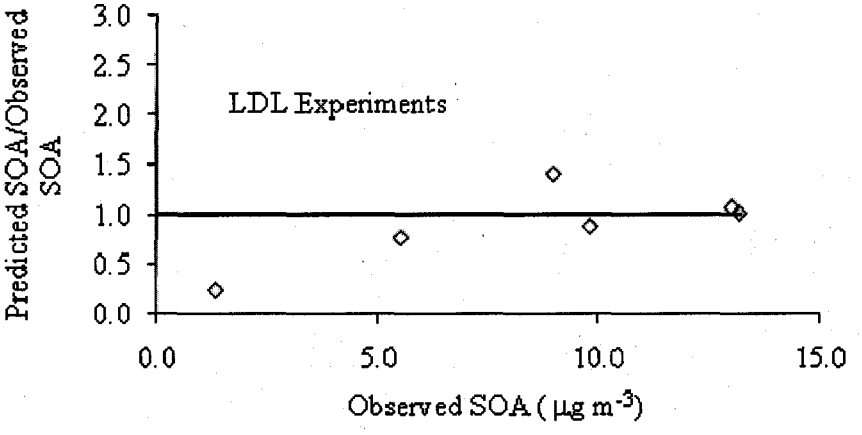

(d)

Figure 5.8B. Modeling results for d-limonene experiments: (c) simulated and observed final SOA concentrations for all HDL experiments; (d) simulated and observed final SOA concentrations for all LDL experiments.

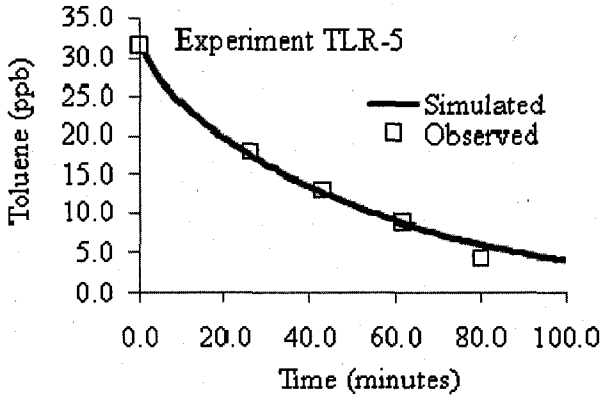

(a)

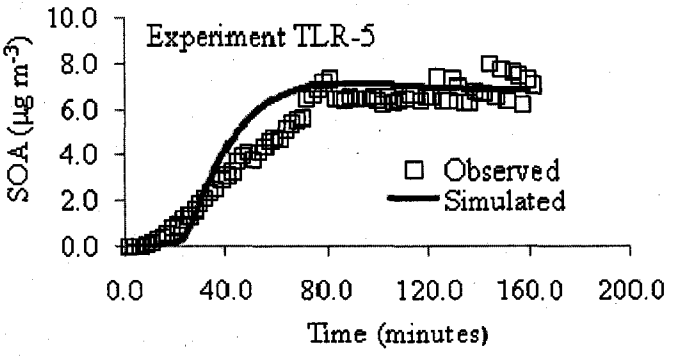

(b)

Figure 5.9A. Modeling results for toluene experiments: (a) simulated and observed final toluene concentration profile; (b) simulated and observed final SOA mass concentration evolution.

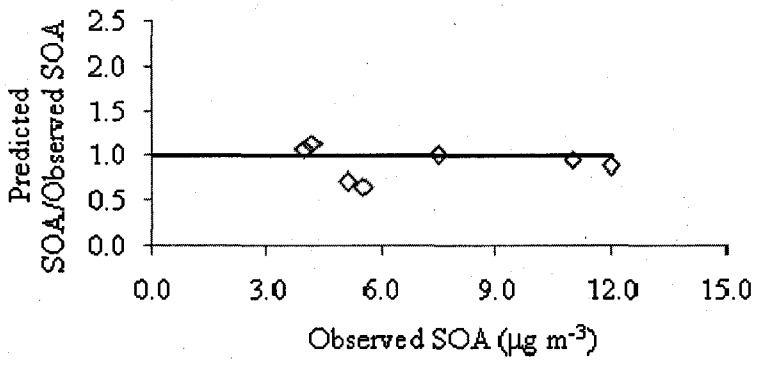

(c)

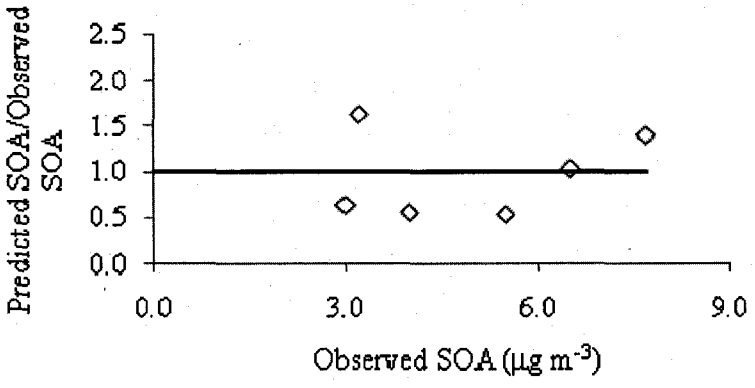

(d)

Figure 5.9B. Modeling results for toluene experiments: (c) simulated and observed SOA concentrations for all THR experiments; (d) simulated and observed SOA concentrations for all TLR experiments.

CHAPTER VI

CONCLUSIONS

Laboratory chamber simulation experiments indicate that the oxidation of α-pinene, β-pinene, d-limonene, toluene, and *m*-xylene by chlorine atom (Cl) generates significant amounts of secondary organic aerosol (SOA) [*Cai and Griffin*, 2006; *Cai et al.*, 2007]. α-Pinene and β-pinene exhibit similar SOA yields from the oxidation initiated by Cl. The d-limonene SOA yield from Cl-initiated oxidation, however, depends on the ratio between the initial mixing ratios of Cl precursor (molecular chlorine, Cl_2) and d-limonene in the chamber. If this ratio is larger than ~7.5, the double bonds and reactive intermediate products in d-limonene are likely oxidized completely, and SOA yields from Cl-initiated oxidation are higher than those of α-pinene and β-pinene. Conversely, if this ratio is smaller than ~7.5, SOA yields from Cl-initiated oxidation are smaller than those of α-pinene and β-pinene. Other researchers have noted a similar dependence of SOA yields on the oxidant level for both monoterpenes and aromatic SOA precursors [*Karlsson et al.*, 2001; *Huff Hartz et al.*, 2005]. It is argued, therefore, that multiple SOA yield curves are common for species with multiple unsaturated carbon-carbon bonds when the initial concentration ratio of hydrocarbon to oxidant changes. The SOA yields of α-pinene, β-pinene, and d-limonene when oxidized by Cl are generally comparable to those from photooxidation in the presence of nitrogen oxides. The measured toluene and *m*-xylene SOA yields are comparable to each other, but only toluene SOA yields depend

on the initial ratio of concentrations of Cl_2 to hydrocarbon. Therefore, two SOA yield curves are derived for toluene. Calculations based on measured yields indicate that in the marine boundary layer, coastal areas, or inland areas with industrial Cl sources, SOA formation from the Cl-initiated oxidation of the five compounds could be a significant source of SOA in the early morning when considering Cl mixing ratio and the rate constants for the reaction of these hydrocarbons with Cl.

For the aromatic precursors, an empirical model based on simultaneous mass and heat transfer is developed to simulate SOA mass growth. Two parameters are used in the model to describe quantitatively SOA growth dynamics. One is the characteristic time for aerosol mass growth, which is the time for aerosol concentration to reach one half of the final equilibrium SOA mass concentration. It is found to be highly correlated with the square root of the product of initial hydrocarbon and Cl_2 mixing ratios. Another model parameter is the characteristic time for diffusion obtained by model calibration, which is correlated linearly to the initial hydrocarbon mixing ratios. The developed empirical model can be used to constrain numerical modeling of SOA formation.

Analysis of the data from an Aerosol Mass Spectrometer (AMS) for the aromatic compounds indicates that chloride accounts for only a small fraction of the formed secondary aerosol (less than 2%). For *m*-xylene, spectral data and delta analysis show that large, likely aromatic, fragments dominate the SOA in early stages of experiments but are converted to more oxidized species as the experiments progress. Toluene does not display similar behavior.

The mechanisms for the reactions of α-pinene, β-pinene, d-limonene, and toluene with Cl have been developed within the framework of the Caltech Atmospheric

Chemistry Mechanism (CACM) [*Griffin et al.*, 2002]. The proposed mechanisms combined with an absorptive partitioning model [*Pankow*, 1994] are employed to simulate observed SOA formation in the chamber experiments described above. For the four compounds of interest, the measured precursor decay curves and SOA concentration evolution profiles are reproduced reasonably. The predicted dominant compositions in the aerosol phase are qualitatively consistent with other reported experimental observations.

The effects of surface tension on SOA formation are also examined in this dissertation [*Cai and Griffin*, 2005]. Simulation results in this study indicate that the Kelvin effect on SOA formation depends on both the semi-volatile species and the polarity of preexisting primary organic aerosol (POA). If the POA contains a large fraction of non-polar organic species, aerosol surface tension becomes very small, and the Kelvin effect is small and may be negligible. If the POA is dominated by polar organic compounds, the Kelvin effect on SOA formation is significant when the POA initial diameter is smaller than approximately 100 nm. The Kelvin effect is larger (i.e., smaller Kelvin factors) for semi-volatile organic compounds (SVOCs) with larger molecular weights. Because SVOCs with larger molecular weights usually have smaller vapor pressures, the Kelvin effect is greater for those SVOCs that are more likely to partition to the aerosol phase. The theoretical simulations presented here suggest that future modeling of ambient or indoor SOA formation may need to consider the Kelvin effect due to particle diameters often being less than 200 nm. In laboratory cases, where initial aerosol seed size is centered around approximately 100 nm, the Kelvin effect on derived partitioning coefficients may also need to be considered.

Cl-initiated oxidation may enhance significantly ozone (O_3) formation in coastal areas and industrialized areas. It is estimated that Cl-hydrocarbon reactions in the South Coast Air Basin of California (SoCAB) cause increases of up to 10 ppb in O_3 mixing ratios in coastal locations [*Knipping and Dabdub*, 2003]. Chlorine emissions in southeast Texas have the potential to enhance one-hour-averaged ozone mixing ratios by 70 ppb in localized areas during morning hours [*Chang and Allen*, 2005]. The SVOCs generated from Cl-hydrocarbon reactions may result in significant increases in regional SOA concentrations. The regional scale enhancement of SOA formation by Cl-VOC reactions should be further examined via three-dimensional air quality modeling. The CACM model updated with the reaction mechanisms developed in this dissertation can be implemented into a three-dimensional air quality model to simulate regional enhancement of SOA formation. When polluted air is transported to the marine boundary layer, Cl concentration is expected to increase due to the reaction between sea salt and NO_y [*Finlayson-Pitts*, 2003; *von Glasow and Crutzen*, 2003]. A global general circulation transport and chemistry model can be used to investigate the interaction between polluted continental air masses and the marine boundary layer and how this interaction affects the formation of clouds.

Further experiments should be performed to investigate the effects of environmental factors such as NO_x level and humidity on the SOA yields measured in this study. Characterization of the species in SOA formed from Cl-initiated oxidation of the typical monoterpenes (α-pinene, β-pinene, d-limonene), and aromatics (toluene and *m*-xylene) will be helpful to better evaluate the developed SOA formation mechanisms. Benzen and isoprene recently have been identified as important precursors for SOA

formation [*Claeys et al.*, 2004; *Kroll et al.*, 2005; *Martin-Reviejo and Wirtz*, 2005]. Laboratory chamber experiments need to be conducted to measure their SOA yields. Dimethyl Sulfide (DMS) is an important compound related to the formation of Cloud Condensation Nuclei (CCN) in the marine boundary layer [*Fitzgerald*, 1991]. The effect of SOA formation from the Cl-initiated oxidation of DMS on the formation of CCN should also be explored. In addition, further experimental work is needed to investigate conditions that favor non-equilibrium absorptive partitioning in SOA formation.

APPENDIX

Lumping Schemes for d-Limonene Oxidation Mechanism

Lumping-scheme 1: TLP0 = LP16 + LP17 + LP18

Lumping-scheme 2: TLP1 = (LP1+LP2+LP3+LP4+LP5) + (LP13+LP14+LP15) + (TZP1 + TZP2 + TZP3 + TZP4 + TZP5 + TZP6 + TZP7 + TZP8 +TZP9 + TZP10 + TZP11 + TZP12)

Lumping scheme 3: TLP2 = LP6 + (LP7+LP8+LP10+LP11+LP12)+ (LP24+LP23) +(LP9P1 + LP9P2 + LP9P3)

For lumping-scheme 1:

The reaction rate constant for the reactions with Cl atom is assumed to be 2.5E-10 (cm^3 $molecule^{-1}$ s^{-1}) [*Thevenet et al.*, 2000]. Due to the existence of multiple reactive sites in these compounds, the reaction pathways are complex. To simplify these reactions, one assumed generic product is used to replace all the products for the reactions. The partitioning properties of this generic product are determined by fitting the observed aerosol formation data.

For lumping-scheme 2:

Cl atoms may attack the double bond, -OH group, and -OOH group, or abstract H atoms in these molecules. However, we assume in this scheme that Cl atom only adds to the exocyclic double bond. The rate constant for these reactions is estimated as 3.1E-10 (cm^3 $molecule^{-1}$ s^{-1}) based on the branching ratio of the exocyclic and endocyclic pathways and the rate constant for the endocyclic pathway. When the gas-phase reaction simulation is complete, the mixing ratios of all their corresponding nonreactive products are calculated using the initial ratio of their concentrations before they are lumped. Only the "unlumped" product mixing ratios are used in the partitioning simulation.

For lumping-scheme 3:

Similar to Scheme 2, we assume that Cl atom adds to the endocyclic double bond. The rate constant for these reactions is estimated as 4.6E-10 (cm^3 $molecule^{-1}$ s^{-1}) [*Finlayson-Pitts et al.*, 1999] by analogy to the reaction of α-pinene with Cl atom.

The implementation flow chart for the lumping-schemes:

The implementation flow chart for above lumping-schemes is shown in Figure A1. Inthis chart, M is the total number of the lumped compounds. $R_1(-R_i)$ and $R_2(-R_i)$ a lumped reactant and product surrogate respectively. R_1-R_i and R_2-R_i represent the *i*th lumpedreactant and product compound respectively. MW_i is the molecular weight for the *i*th lumped product. $P^0_{L,i}$ denotes the molecular weight for the *i*th lumped product. Square brackets are mixing ratios. AP is a number used for partitioning simulation.

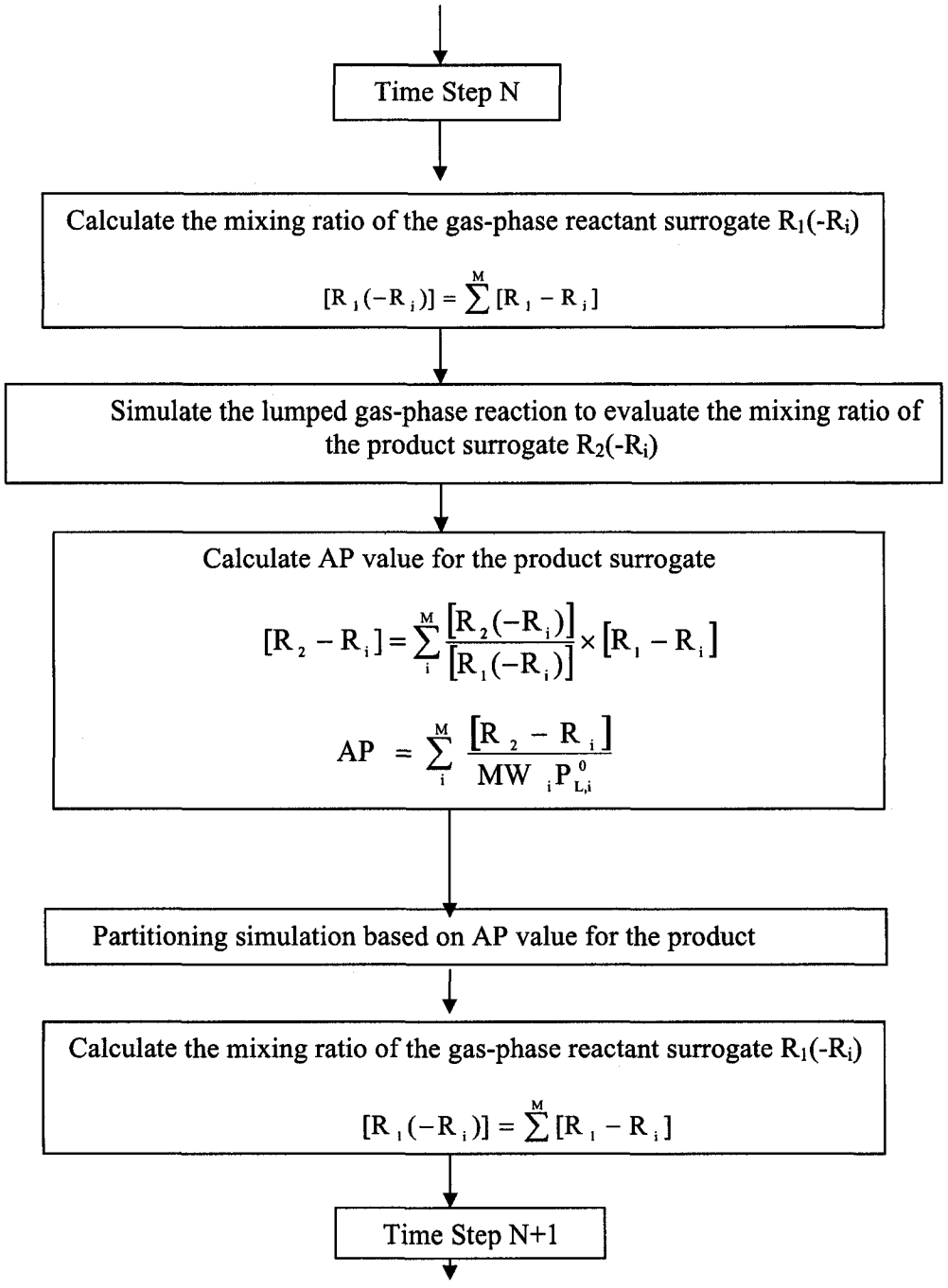

Figure A1. The implementation flow chart for the lumping scheme in the mechanism for the reaction of d-limonene with Cl.

REFERENCES

Alfarra, M.R., D. Paulsen, M. Gysel, A.A. Garforth, J. Dommen, A. S. H. Prevot, D. R. Worsnop, U. Baltensperger, and H. Coe (2006), A mass spectrometric study of secondary organic aerosols formed from the photooxidation of anthropogenic and biogenic precursors in a reaction chamber, *Atmos. Chem. Phys.*, *6*, 5279-5293.

Allan, J.D., J.L. Jimenez, H. Coe, K. N. Bower, P.I. Williams, and D.R. Worsnop (2003), Quantitative sampling using an Aerodyne Aerosol Mass Spectrometer: Part 1: Techniques of data interpretation and error analysis, *J. Geophys. Res.,108*, D34090, doi: 10.1029/2002JD002358.

Andersson-Skold, Y., and D. Simpson (2001), Secondary organic aerosol formation in northern Europe: A model study, *J. Geophys. Res.*, *106*, 7357-7374.

Andreae, M.O., and P.J. Crutzen (1997), Atmospheric aerosol: Biogeochemical sources and role in atmospheric chemistry, *Science, 276*, 1052-1058.

Anttila, T., and V.M. Kerminen (2003), Condensational growth of atmospheric nuclei by organic vapours, *J. Aerosol Sci.*, *34*, 41-61.

Ariya, P.A., B.T. Jobson, R. Sander, H. Niki, and G.W. Harris (1998), Measurements of C_2-C_7 hydrocarbons during the polar sunrise experiment 1994: Further evidence for halogen chemistry in the troposphere, *J. Geophys. Res.,103*, 13,169-13,180.

Ariya, P.A., H. Niki, G.W. Harris, K.G. Anlauf, and D.E.J. Worthy (1999), Polar sunrise experiment 1995: Hydrocarbon measurements and tropospheric Cl and Br-atom chemistry, *Atmos. Environ., 33,* 931-938.

Aranda, A., E. Martinez, Y. Diaz de Mera, A. Rodriguez, D. Rodriguez and J.Cuartero (2003), Low-pressure study of the reactions of Cl atoms with acrylic acid and allyl alcohol, *Atmos. Environ.*, *37*, 4361-4369.

Artaxo, P., W. Maenhaut, H. Storms, and R. Vangrieken (1990), Aerosol characteristics and sources for the Amazon basin during the wet season, *J. Geophys. Res.*, *95*, 16971-16985.

Artaxo, P., H. Storms, F. Bruynseels, R. Vangrieken, and W. Maenhaut (1988), Composition and sources of aerosols from the Amazon Basin, *J. Geophys. Res., 93,* 1605-1615.

Aschmann, S.M., R. Atkinson, and J. Arey (2002), Products of reaction of OH radicals with α-pinene, *J. Geophys. Res., 107,* D14, 4191, 10.1029/2001JD001098.

Atkinson, R. (1994), Gas-phase tropospheric chemistry of organic compounds, *J. Phys. Chem Ref. Data, Monograph 2.*

Atkinson, R. (1997), Gas-phase tropospheric chemistry of volatile organic compounds: 1. Alkanes and alkenes, *J. Phys. Chem. Ref. Data, 26,* 215-290.

Atkinson, R. (2007), Rate constants for the atmospheric reactions of alkoxy radicals: An updated estimation method, *Atmos. Environ., 41,* 8468-8485.

Bahreini, R., M.D. Keywood, N.L. Ng, V. Varutbangkul, S. Gao, R.C. Flagan, J.H. Seinfeld, D.R. Worsnop, and J.L. Jimenez (2005), Measurements of secondary organic aerosol from oxidation of cycloalkenes, terpenes, and *m*-xylene using an Aerodyne aerosol mass spectrometer, *Environ. Sci. Technol.,39,* 5674–5688.

Barthelmie, R.J., and S.C. Pryor (1999), A model mechanism to describe oxidation of monoterpenes leading to secondary organic aerosol: 1.α-pinene and β-pinene, *J. of Geophys. Res. 104,* 23,657-23,699.

Bedjanian, Y., G. Laverdet, and G. Le Bras (1998), Low-pressure study of the reaction of Cl atoms with isoprene, *J. Phys. Chem. A, 102,* 953-959.

Bell, M., and H. Ellis (2004), Sensitivity analysis of tropospheric ozone to modified biogenic emissions for the mid-Atlantic region, *Atmos. Environ., 38,* 1879-1889.

Bierbach, A., I. Barnes, and K.H. Becker (1996), Rate coefficients for the gas-phase reaction reactions of bromine radicals with a series of alkenes, dienes, and aromatic hydrocarbons at 298K, *Int. J. Chem. Kinet., 28,* 565-577.

Brauers, T., U. Aschmutat, U. Brandenburger, H.-P. Dorn, M. Hausmann, M. Hessling, A. Hofzumahaus, F. Holland, C. Plass-Dulmer, and D.H. Ehhalt (1996), Intercomparison of tropospheric OH radical measurements by multiple-folded long-path laser absorption and laser induced fluorescence, *Geophys. Res. Lett., 23,* 2545-2548.

Blando, J.D., and B.J. Turpin (2000), Secondary organic aerosol formation in cloud and fog droplets: a literature evaluation of plausibility, *Atmos. Environ.*, *34*, 1623-1632.

Burden, R.L., and H.D. Faires (1989), *Numerical Analysis, 4th edition*, PWS-Kent, Boston,MA.

Cai, X., and R.J. Griffin (2003), Modeling the formation of secondary organic aerosol in coastal areas: role of the sea-salt aerosol organic layer, *J. Geophys. Res.*, *108*, 4440, doi: 10.1029/2002JD003053.

Cai, X., and R.J. Griffin (2006), Secondary aerosol formation from the oxidation of biogenic hydrocarbons by chlorine atoms, *J. Geophys. Res.*, *111*, D14206, doi:1029/2005JD006857.

Cai, X., and R.J. Griffin (2005), Theoretical modeling of the size-dependent influence of surface tension on the absorptive partitioning of semi-volatile organic compounds, *J. Atmos. Chem.*, *50*, 139-158.

Cai, X., L.D. Ziemba, and R.J. Griffin (2007), Secondary aerosol formation from the oxidation of anthropogenic hydrocarbons by chlorine atoms, *Environ. Sci. and Technol, submitted.*

Chang, S., and D.T. Allen (2005), Atmospheric chlorine chemistry in Southeast Texas: Impacts on ozone formation and control, *Environ. Sci. Technol.*, *40*, 251-262.

Calvert, J.G., R. Atkinson, K.H. Becker, R.M. Kamens, J.H. Seinfeld, T.J. Wallington, and G. Yarwood (2001), The atmospheric oxidation of aromatic hydrocarbons, *Oxford University Press,* New York.

Canosa-Mas, C.E., R. Hilary, M.D. Hutton-Squire, D.J.S. King, C.T. Katherine, and R.P. Wayne (1999), Laboratory kinetic studies of the reaction of chlorine atoms with species of biogenic origin: d-carene, isoprene, methacrolein, and methyl vinyl ketone, *J. Atmos. Chem.*, *34*, 163-170.

Capouet, M., J. Peeters, B. Noziere, and J.F. Muller (2004), α–Pinene oxidation by OH: simulations of laboratory experiments, *Atmos. Chem. Phys.*, *4,* 2285-2311.

Carter, W.P.L., D.R. Cocker III, D.R. Fitz, I.M. Malkina, K. Bumiller, C.G. Sauer, J.T. Pisano, C. Bufalino, and C. Song (2005), A new environmental chamber for evaluation of gas-phase chemical mechanisms and secondary aerosol formation, *Atmos. Environ.*, *39*, 7768-7788.

Chameides, W.L., R.W. Lindsay, J. Richardson, and C.S. Kiang (1988), The role of biogenic hydrocarbons in urban photochemical smog: Atlanta as a case study, *Science, 241*, 1473-1475.

Chang, S., and D.T. Allen (2005), Atmospheric chlorine chemistry in Southeast Texas: Impacts on ozone formation and control, *Environ. Sci. Technol., 40*, 251-262.

Charlson, R.J., S.E. Schwartz, J.M. Hales, R.D. Cess, J.A. Coakley, J.E. Hansen, and D.J. Hofmann (1992), Climate forcing by anthropogenic aerosols, *Science, 255,* 423-430.

Charlson, R.J., J.H. Seinfeld, A. Nenes, M. Kulmala, A. Laaksonen, and M.C. Facchini (2001), Reshaping the theory of cloud formation, *Science, 292*, 2025-2026.

Chen, J., and R.J. Griffin (2005), Modeling secondary organic aerosol formation for α-pinene, β-pinene, and d-limonene, *Atmos. Envrion., 39*, 7731-7744.

Chung, S.H., and J.H. Seinfeld (2002), Global distribution and climate forcing of carbonaceous aerosols, *J. Geophys. Res., 107,* D194407, doi:10.1029/2001JD001397.

Claeys, M., et al. (2004a), Formation of secondary organic aerosols through photooxidation of isoprene, *Science, 303*, 1173-1176.

Claeys, M., W. Wang, A.C. Ion, I. Kourtchev, A. Gelencser, and W. Maenhaut (2004b), Formation of secondary organic aerosols from isoprene and its gas-phase oxidation products through reaction with hydrogen peroxide, *Atmos. Environ., 38*, 4093-4098.

Cocker III, D.R., S.L. Clegg, R.C. Flagan, and J.H. Seinfeld (2001a), The effect of water on gas-particle partitioning of secondary organic aerosol, Part I: α-pinene/ozone system, *Atmos. Environ., 35*, 6049-6072.

Cocker III, D.R., B.T. Mader, M. Kalberer, R.C. Flagan, and J.H. Seinfeld (2001b), The effect of water on gas-particle partitioning of secondary organic aerosol, Part II: *m*-xylene and 1,3,5-trimethylbenzene photooxidation systems, *Atmos. Environ., 35,* 6073-6085.

Colville, C.J., and R.J. Griffin (2004a), The roles of individual oxidants in secondary organic aerosol formation from Δ^3-carene: 1. Gas-phase chemical mechanism, *Atmos. Environ., 38*, 4001-4012.

Colville, C.J., and R. J. Griffin (2004b), The roles of individual oxidants in secondary Organic aerosol formation from Δ^3-carene: 2. SOA formation and oxidant contribution. *Atmos. Environ., 38,* 4013-4023.

Davis, M.E, C. Tapscott, and P.S. Stevens (2005), Measurements of the kinetics of the OH-initiated oxidation of β-pinene: Radical propagation in the OH + β-pinene + O_2 + NO reaction system, *Int. J. Chem. Kinet., 37*, 522-531.

de Gouw, J., *et al.* (2005), Budget of organic carbon in a polluted atmosphere: Results from the New England Air Quality Study in 2002, *J. Geophys. Res., 110*, D16305, doi: 10.1029/2004JD005623.

Dechapanya, W., M. Russell, and D.T. Allen (2004), Estimates of anthropogenic secondary organic aerosol formation in Houston, Texas, *Aerosol Sci. Technol., 38*, 156-166.

Didyk, B.M., B.R.T. Simoneit, L.A. Pezoa, M.L. Riveros, and A.A. Flores (2000), Urban aerosol particles of Santiago, Chile: Organic content and molecular characterization, *Atmos. Environ., 34*, 1167-1179.

Dockery, D.W., C.A. Pope, X.P. Xu, J.D. Spengler, J.H. Ware, M.E. Fay, B.G. Ferris, and F.E. Speizer (1993), An association between air-pollution and mortality in six United-States cities, *New England Journal of Medicine, 329*, 1753-1759.

Drewnick, F., J.J. Schwab, J.T. Jayne, M. Canagaratna, D.R. Worsnop, K.L. Demerjian (2004), Measurements of ambient aerosol composition during PTMACS-NY 2001 using an aerosol mass spectrometer. Part I: Mass concentrations, *Aerosol Sci. Technol., 38,* 92-103.

Dubtsov, S.N., G.G. Dultseva, E.N. Dultsev, and G.I. Skubnevskaya (2007), Investigation of aerosol formation during bezaldehyde photolysis, *J. Phys. Chem. B, 110*, 645-649.

Duce, R.A., V.A. Mohen, P.R. Zimmerman, D. Grosjean, W. Cautreels, R. Chatfield, R. Jaenicke, J.A. Ogren, E.D. Pellizzari, and G.T. Wallace (1983), Organic material in the global troposphere, *Rev. Geophys., 21*, 921-952.

Ervens, B., G. Feingold, G.J. Frost, S.L. Clegg, and S.M. Kreidenweis (2004a), A modeling study of aqueous production of dicarboxylic acids: 1.Chemical pathways and speciated organic mass production, *J. Geophys. Res., 105*, D15205, doi: 10.1029/2003JD004387.

Ervens, B., G. Feingold, G.J. Frost, S.L. Clegg, and S.M. Kreidenweis (2004b), A modeling study of aqueous production of dicarboxylic acids: 2. Implications for cloud microphysics, *J. Geophys. Res., 109*, D15206, doi: 10.1029/2004JD004575.

Facchini, M.C., S. Decesari, M. Mircea, S. Fuzzi, and G. Loglio (2000), Surface tension of atmospheric wet aerosol and cloud/fog droplets in relation to their organic carbon content and chemical composition, *Atmos. Environ. 34*, 4853-4857.

Facchini, M.C., M. Mircea, S. Fuzzi, and R.J. Charlson (1999), Cloud albedo enhancement by surface active organic solvents in growing droplets, *Nature, 401*, 257-259.

Fantechi, G., N.R. Jensen, O. Saastad, J. Hjorth, and J. Peeters (1998), Reactions of Cl atoms with selected VOCs: Kinetics, products and mechanisms, *J. Atmos. Chem., 31*, 247-267.

Fehsenfeld, F., et al. (1992), Emissions of volatile organic compounds from vegetation and the implications for atmospheric chemistry, Glob. Biogeochem. Cycles, *6*, 389-430.

Finlayson-Pitts, B.J. (2003), The tropospheric chemistry of sea salt: A molecular-level view of the chemistry of NaCl and Na Br, *Chem. Rev., 103*, 4801-4822.

Finlayson-Pitts, B.J., C.J. Keoshian, B. Buehler, and A.A. Ezell (1999), Kinetics of reaction of chlorine atoms with some biogenic organics, *Intl. J. Chem. Kinet., 31*, 491-499.

Finlayson-Pitts, B.J. (1993), Chlorine atoms as a potential tropospheric oxidant in the marine boundary layer, *Res. Chem. Interm., 19*, 235-249.

Finlayson-Pitts, B.J, and J.N. Pitts (2000), Chemistry of the upper and lower atmosphere, *Academic Press,* Burlington, MA

Fitzgerald, J.W. (1991), Marine aerosols-A Review, *Atmos. Environ., 25*, 533-549.

Forstner, H.J.L., R.C. Flagan, and J.H. Seinfeld (1997), Secondary organic aerosol from photooxidation of aromatic hydrocarbons: Molecular composition, *Environ. Sci. Technol., 31*,1345-1358.

Fredenslund, A., J. Gmehling, M.L. Michelsen, P. Rasmussen, and J.M. Prausnitz (1977), Computerized design of multicomponent distillation-columns using the UNIFAC group contribution method for calculation of activity coefficients, *Ind. Eng. Chem. Process Design Develop., 16*, 450-462.

Ganske, J.A., H.N. Berko, and B.J. Finlayson-Pitts (1992), Absorption cross-sections for gaseous $ClNO_2$ and Cl_2 at 219 K — Potential organic oxidant source in the marine troposphere, *J. Geophys. Res., 97*, 7651-7656.

Gao, S., M. Keywood, N. Ng, J. Surratt, V. Varutbangkul, R. Bahreini, R.C. Flagan, and J.H. Seinfeld (2004), Low-molecular weight and oligomeric components in secondary organic aerosol from the ozonolysis of cycloalkenes and α-pinene, *J. Phys. Chem.*, *108*, 10147-10164.

Geller, M.D., S. Kim, C. Misra, C. Sioutas, B.A. Olson, and V.A. Marple (2002), A methodology for measuring size-dependent chemical composition of ultrafine particles, *Aerosol Sci. Technol., 36*, 748-762.

Geyer, A., et al. (2003), Direct observation of daytime NO_3: Implication for urban boundary layer chemistry, *J. Geophys. Res., 109*, D124368, doi:10.1029/2002JD002967.

Gmehling, J., J. Li, and M. Shiller (1993), A modified UNIFAC model: 2. Present parameter matrix and results for different thermodynamic properties, *Ind. Eng. Chem. Res., 32*, 178-193.

Griffin, R.J., D.R. Cocker III, D. Dabdub, and J.H. Seinfeld (1999a), Estimate of global atmospheric organic aerosol from oxidation of biogenic hydrocarbons, *Geophys. Res. Lett.*, *26*, 2721-2724.

Griffin, R.J., D.R. Cocker III, R.C. Flagan, and J.H. Seinfeld (1999b), Organic aerosol formation from the oxidation of biogenic hydrocarbons, *J. Geophys. Res., 104*, 3555-3567.

Griffin, R.J., D.R. Cocker III, and J.H. Seinfeld (1999b), Incremental aerosol reactivity: Application to aromatic and biogenic hydrocarbons, *Environ. Sci. Technol., 33*, 2403-2408.

Griffin, R.J., D. Dabdub, M.J. Kleeman, M.P. Fraser, G.R. Cass, and J.H. Seinfeld (2002a), Secondary organic aerosol: III. Urban/regional scale model of size and composition resolved aerosols, *J. Geophys. Res., 107*, 4334, doi: 10.1029/2001JD000544.

Griffin, R.J., D. Dabdub, and J.H. Seinfeld (2002b), Secondary organic aerosol, 1. Atmospheric chemical mechanism for production of molecular constituents, *J. Geophys. Res.*, *107*, 4332, doi: 10.1029/2001JD000541.

Griffin, R.J., K. Nguyen, D. Dabdub and J.H. Seinfeld (2003), A combined hydrophobic-hydrophilic module for predicting secondary organic aerosol formation, *J. Atmos. Chem.*, *44*, 171-190.

Griffin, R.J., D. Dabdub, and J.H. Seinfeld (2005), Development and initial evaluation of a dynamic species-resolved model for gas-phase chemistry and size-resolved gas/particle partitioning associated with secondary organic aerosol formation, *J. Geophys. Res., 110*, D05304, doi:10.1029/2004JD005219.

Guenther, A., et al. (1995), A global model of natural volatile organic compound emissions, *J. Geophys. Res.,* 100, 8873-8892.

Hakola, H., J. Arey, S.M. Aschmann, and R. Atkinson (1994), Product formation from the gas-phase reactions of OH radicals and O_3 with a series of monoterpenes, *J. Atmos. Chem., 18*, 75-102.

Hallquist, M., I. Wängberg, E. Ljungstrom, I. Barnes, and K.H. Becker (1999), Aerosol and product yields from NO_3 radical-initiated oxidation of selected monoterpenes, *Environ. Sci. Technol., 33*, 553-559.

Heald, C.L., D.J. Jacob, R.J. Park, L.M. Russell, B.J. Huebert, J.H. Seinfeld, H. Liao, and R.J. Weber (2005), A large organic aerosol source in the free troposphere missing from current models, *Geophys. Res. Lett., 32*, L18809, doi: 10.1029/2005GL023831.

Held, A., A. Nowak, W. Birmili, A. Wiedensohler, R. Forket, and O.Klemm (2004), Observations of particle formation and growth in a mountainous forest region in central Europe, *J. Geophys. Res., 109*, D23204, doi:10.1029/2004JD005346.

Hitzenberger, R., A. Berner, A. Kasper-Giebl, M. Loflund, and H. Puxbaum (2002), Surface tension of Rax cloud water and its relation to the concentration of organic material, *J. Geophys. Res., 107*, 4752, doi:10.1029/2002JD002506.

Hoffmann, T., J.R. Odum, F. Bowman, D. Collins, D. Klockow, R.C. Flagan, and J.H. Seinfeld (1997), Formation of organic aerosols from the oxidation of biogenic hydrocarbons, *J. Atmos. Chem., 26*, 189-222.

Huff Hartz, K.E., A.A. Presto, R. Pathak, J.E. Tischuk, B.J. Marquis, S.N. Pandis, and N.M. Donahue (2005), Temperature dependence of the yield and kinetics of secondary organic aerosol formation during the limonene ozonolysis reaction, paper presented at the 24th Annual AAAR Conference, Austin, TX, October 17-21.

Hurley, M.D., O. Sokolov, T.J. Wallington, H. Takekawa, M. Karasawa, B. Klotz, I. Barnes, and K.H. Becker (2001), Organic aerosol formation during the atmospheric degradation of toluene, *Environ. Sci. Technol., 35*, 1358-1366.

Jaoui, M., E. Corse, T.E. Kleindienst, J.H. Offenberg, M. Lewandowski, and E.O. Edney (2006), Analysis of secondary organic aerosol compounds from the photooxidation of d-limonene in the presence of NO_x and their detection in ambient PM2.5, *Environ. Sci. Technol., 40*, 3819-3828.

Jenkin, M.E. (2004), Modeling the formation and composition of secondary organic aerosol from alpha- and beta-pinene ozonlysis using MCM v3, *Atmos. Chem. Phys., 4*, 1741-1757.

Jenkin, M.E., S.M. Saunders, and M.J. Pilling (1997), The tropospheric degradation of volatile organic compounds: A protocol for mechanism development, *Atmos. Environ., 31*, 81-104.

Jet Propulsion Laboratory (1997), Chemical kinetics and photochemical data for use in stratospheric modeling, *JPL Publication 97-4.*

Johnson, D., S.R. Utembe, and M.E. Jenkin (2006), Simulating the detailed chemical compositions of secondary organic aerosol formed on a regional scale during the TORCH 2003 campaign in the southern UK, *Atmos. Chem. Phys., 6*, 419-431.

Kaiser, E.W., and T.J. Wallington (1996), Pressure dependence of the reaction $Cl+C_3H_6$, *J. Phys. Chem., 100*, 9788-9793.

Kalberer, M., J. Yu, D.R. Cocker III, R.C. Flagan, and J.H. Seinfeld (2000), Aerosol formation in the cyclohexene-ozone system, *Environ. Sci. Technol., 34*, 4894-4901.

Kamens, R.M., M. Jang, C. Chien, and K. Leach (1999), Aerosol formation from the reaction of alpha-pinene and ozone using a gas-phase kinetic-aerosol partitioning theory, *Environ. Sci. Technol., 33*, 1430-1438.

Kanakidou, M., et al. (2005), Organic aerosol and global climate modeling: a review, *Atmos. Chem. Phys., 5*, 1053-1123.

Kanakidou, M., K. Tsigaridis, F.J. Dentener, and P.J. Crutzen (2000), Human-activity-enhanced formation of organic aerosols by biogenic hydrocarbon oxidation, *J. Geophys. Res., 105*, 9243-9254.

Karlsson, R.S., J.J. Szente, J.C. Ball, and M.M. Maricq (2001), Homogeneous aerosol formation by the chlorine atom initiated oxidation of toluene, *J. Phys. Chem. A, 105,* 82-96.

Kavouras, I.G., and E.G. Stephanou (2002), Direct evidence of atmospheric secondary organic aerosol formation in forest atmosphere through heteromolecular nucleation, *Environ. Sci. Technol., 36*, 5083-5091.

Keene, W.C., D.J. Jacob, and S.M. Fan (1996), Reactive chlorine: A potential sink for dimethyl sulphide and hydrocarbons in the marine boundary layer, *Atmos. Environ., 30*, R1-R3.

Keywood, M.D., V. Varutbangkul, R. Bahreini, R.C. Flagan, and J.H. Seinfeld (2004), Secondary organic aerosol formation from the ozonolysis of cycloalkenes and related compounds, *Environ. Sci. Technol., 38*, 4157-4164.

Kieser, B.N., J.W. Bottenheim, T. Sideris, and H. Niki (1993), Spring 1989 observation of lower tropospheric chemistry in the Canadian Arctic, *Atmos. Environ. Part A-General Topics, 27*, 2979-2988.

Knipping, E.M., and D. Dabdub (2003), Impact of chlorine emissions from sea-salt aerosol on coastal urban ozone, *Environ. Sci. Technol., 37*, 275-284.

Knipping, E.M., M.J. Lakin, K.L. Foster, P. Jungwirth, D.J. Tobias, R.B. Gerber, D. Dabdub, and B.J. Finlayson-Pitts (2000), Experiments and simulations of ion-enhanced interfacial chemistry on aqueous NaCl aerosols, *Science, 288*, 301-306.

Kroll, J.H., N.L. Ng, S.M. Murphy, R.C. Flagan, and J.H. Seinfeld (2005), Secondary organic aerosol formation from isoprene photooxidation under high-NO_x conditions, *Geophys. Res. Lett., 32*, L18808, doi: 10.1029/2005GL093637.

Iinuma, Y., O. Boge, T. Gnauk, and H. Herrmann (2004), Aerosol chamber study of α-pinene/O_3 reaction: influence of particle acidity on aerosol yields and products, *Atmos. Environ., 38*, 761-773.

Jang, M., N.M. Czoschke, S. Lee, and R.M. Kamens (2002), Heterogeneous atmospheric aerosol production by acid-catalyzed particle-phase reactions, *Science, 298*, 814-817.

Jang, M., N.M. Czoschke, and A.L. Northcross (2005), Semiempirical model for organic aerosol growth by acid catalyzed heterogeneous reactions of organic carbonyls, *Environ. Sci. Technol., 39*, 164-174.

Jayne, J.T., D.C. Leard, X. Zhang, P. Davidovits, K.A. Smith, C.E. Kolb, and D.R. Worsnop (2000), Development of an aerosol mass spectrometer for size and composition analysis of submicron particles, *Aerosol. Sci. Technol., 33*, 49-70.

Jenkin, M.E. (2004), Modeling the formation and composition of secondary organic aerosol from alpha- and beta-pinene ozonlysis using MCM v3, *Atmos. Chem. Phys., 4*, 1741-1757.

Jobson, B.T., H. Niki, Y. Yokouchi, J. Bottenheim, F. Hopper, and R. Leaitch (1994), Measurement of C_2-C_6 hydrocarbons during the polar sunrise 1992 experiment: Evidence for Cl atom and Br atom chemistry, *J. Geophys. Res., 99*, 25,355-25,368.

Johnson, D., P. Cassanelli, and R.A. Cox (2004), Isomerization of simple alkoxyl radicals: New temperature-dependent rate data and structure activity relationship, *J. Phys. Chem. A., 108*, 519-523.

Johnson, D., M.E. Jenkin, K. Wirtz, and M. Martin-Reviejo (2005), Simulating the formation of secondary organic aerosol from the photooxidation of aromatic hydrocarbons, *Environ. Chem., 2*, 35-48.

Johnson, D., S.R. Utembe, M.E. Jenkin, R.G. Derwent, G.D. Hayman, M.R. Alfarra, H. Coe, and G. McFiggans (2006), Simulating regional scale secondary organic aerosol formation during the TORCH 2003 campaign in the southern UK., *Atmos. Chem. Phys., 6*, 403-4018.

Kalberer, M., *et al.* (2004), Identification of polymers as major components of atmospheric organic aerosols, *Science, 303,* 1659-1662.

Kamens, R.M., M. Jang, C. Chien, and K. Leach (1999), Aerosol formation from the reaction of alpha-pinene and ozone using a gas-phase kinetic-aerosol partitioning theory, *Environ. Sci. Technol., 33*, 1430-1438.

Kamens, R.M., and M. Jaoui (2001), Modeling aerosol formation from α-pinene plus NO_x in the presence of natural sunlight using gas-phase kinetics and gas-particle partitioning theory, *Environ. Sci. Technol., 35*, 1394-1405.

Kanakidou, M., *et al.* (2005), Organic aerosol and global climate modeling: a review, *Atmos. Chem. Phys.*, 5, 1053-1123.

Karlsson, R.S., J.J. Szente, J.C. Ball, and M.M. Maricq (2001), Homogeneous aerosol formation by the chlorine atom initiated oxidation of toluene, *J. Phys. Chem. A, 105,* 82-96.

Kavouras, I.G., and E.G. Stephanou (2002), Direct evidence of atmospheric secondary organic aerosol formation in forest atmosphere through heteromolecular nucleation, *Environ. Sci. Technol., 36*, 5083-5091.

Keene, W.C., D.J. Jacob, and S.M. Fan (1996), Reactive chlorine: A potential sink for dimethyl sulphide and hydrocarbons in the marine boundary layer, *Atmos. Environ., 30*, R1-R3.

Kerminen, V.M. (1999), Roles of SO_2 and secondary organics in the growth of nanometer particles in the lower atmosphere, *J. Aerosol Sci., 30*, 1069-1078.

Kleeman, M.J., J.J. Schauer, and G.R. Cass (2000), Size and composition distribution of fine particulate matter emitted from motor vehicles, *Environ. Sci. Technol., 34*, 1132-1142.

Kieser, B.N., J.W. Bottenheim, T. Sideris, and H. Niki (1993), Spring 1989 observation of lower tropospheric chemistry in the Canadian Arctic, *Atmos. Environ. Part A-General Topics, 27*, 2979-2988.

Knipping, E.M., and D. Dabdub (2003), Impact of chlorine emissions from sea-salt aerosol on coastal urban ozone, *Environ. Sci. Technol., 37*, 275-284.

Knipping, E.M., M.J. Lakin, K.L. Foster, P. Jungwirth, D.J. Tobias, R.B. Gerber, D. Dabdub, and B.J. Finlayson-Pitts (2000), Experiments and simulations of ion-enhanced interfacial chemistry on aqueous NaCl aerosols, *Science, 288*, 301-306.

Köhler, H. (1936), The nucleus in the growth of hygroscopic droplets, *Trans. Far. Soc. 32*, 1152-1161.

Lack, D.A., X.X. Tie, N.D. Bofinger, A.N. Wiegand, and S. Madronich (2004), Seasonal variability of secondary organic aerosol: A global modeling study, *J. Geophys. Res., 109*, D03203, doi10.1029/2003JD003418.

Larsen, B.L., P. Rasmussen, and A. Fredenslund (1987), A modified UNIFAC group-contribution model for prediction of phase-equilibria and heats of mixing, *Ind. Eng. Chem. Res., 26*, 2274-2286.

Larsen, B.R., D.D. Bella, M. Glassius, R. Winterhalter, N.R. Jensen, and J. Hjorth (2001), Gas-phase OH oxidation of monoterpenes: gaseous and particulate products, *J. Atmos. Chem., 38*, 231-276.

Lary, D.J. (2005), Halogens and the chemistry of the free troposphere, *Atmos. Chem. Phys., 5*, 227-237.

Leaitch, W.R., J.W. Bottenheim, T.A. Biesenthal, S.M. Li, P.S.K. Liu, K. Asalian, H. Dryfhout-Clark, F. Hopper, and F. Brechtel (1999), A case study of gas-particle conversion in an eastern Canadian forest, *J. Geophys. Res.*, *104*, 8095-8111.

Lewis, A.C., N. Carslaw, P.J. Marriott, R.M. Kinghorn, P. Morrison, A.L. Lee, K.D. Bartle, and M.J. Pilling (2000), A large pool of ozone-forming carbon compounds in urban atmospheres, *Nature*, *405*, 778-781.

Lim, H.J., A.G. Carlton, and B.J. Turpin (2005), Isoprene forms secondary organic aerosol through cloud processing: Model simulations, *Environ. Sci. Technol., 39,* 4441-4446.

Lim, Y.B., and P.J. Ziemann (2005), Products and mechanism of secondary organic aerosol formation from reactions of n-alkanes with OH radical in the presence of NO_x, *Environ. Sci. Technol 39* (23), 9229-9236

Liousse, C., C. Michel, B. Bessagnet, H. Cachier, and R. Rosset (2005), 0-D Modeling of carbonaceous aerosols over greater Paris focusing on the organic particle formation, *J. Atmos. Chem., 51,* 207-221.

Lippmann, M., K. Ito, A. Nadas, and R. Burnett (2000), Association of particulate matter components with daily mortality and morbidity in urban populations, Research Report 95, Health Effects Institute, Cambridge, M.A.

Lunden, M., D. Black, M. McKay, K. Revzan, A. Goldstein, and N. Brown (2006), Characteristics of fine particle growth events observed above a forested ecosystem in the Sierra Nevada Mountains in California, *Aerosol Sci. Technol.*, *40*, 373-388.

Lupis, C.H.P. (1983), *Chemical Thermodynamics of Materials*, Elsevier Science Publishing Co., Inc., Amsterdam.

Maricq, M.M., J.J. Szente, and E.W. Kaiser (1994), Reaction of chlorine atoms with methylperoxy and ethylperoxy radicals, *J. Phys. Chem.*, *98*, 2083-2089.

Marti, J.J., R.J. Weber, P.H. McMurry, F. Eisele, D. Tanner, and A. Jefferson (1997), New particle formation at a remote continental site: Assessing the contributions of SO_2 and organic precursors, *J. Geophys. Res.*, *102*, 6331-6339.

Martin-Reviejo, M., and K. Wirtz (2005), Is benzene a precursor for secondary organic aerosol?, *Environ. Sci. Technol., 39*, 1045-1054.

Martinez, E., B. Cabanas, A. Aranda, P. Martin, and S. Salgado (1999), Absolute rate coefficient for the gas-phase reaction of NO_3 radical with a series of monoterpenes at T = 298 to 433 K, *J. Atmos. Chem., 33*, 265-282.

Matsunaga, S.N., C. Wiedinmyer, A.B. Guenther, J.J. Orlando, T. Karl, D.W. Toohey, J.P. Greenberg, and Y. Kajii (2005), Isoprene oxidation products are a significant atmospheric aerosol component, *Atmos. Chem. Phys. Discuss., 5*, 11,143-11,156.

Mazurek, M., M.C. Mason-Jones, H.D. Mason-Jones, L.G. Salmon, G.R. Cass, K.A. Hallock, and M. Leach (1997), Visibility-reducing organic aerosols in the vicinity of Grand Canyon National Park: Properties observed by high resolution gas chromatography, *J. Geophys. Res., 102,* 3779-3793.

McKeen, S.A., E.Y. Hsie, and S.C. Liu (1991), A study of the dependence of rural ozone on ozone precursors in the eastern United States, *J. Geophys. Res., 96*, 15,377-15,394.

McLafferty, F.W., and F. Turecek (1993), Interpretation of Mass Spectra, University Science Books, Sausolito, CA.

Morrison, R.T. , and R.N. Boyd (1987), *Organic Chemistry*, Allyn and Bacon, Needham Heights, MA.

Murphy, D.M., D.S. Thomson, and T.M.J. Mahoney (1998), *In situ* measurement of organic, meteoritic material, mercury, and other elements in aerosols at 5 to 19 kilometers, *Science, 282,* 1664-1669.

Mylonas, D.T., D.T. Allen, S.H. Ehrman, and S.E. Pratsinis (1991), The sources and size distributions of organonitrates in Los Angeles aerosol, *Atmos. Environ., 25A*, 2855-2861.

Myrdal, P.B., and S.H. Yalkowsky (1997), Estimating pure component vapor pressures of complex organic molecules, *Ind. Eng. Chem. Res., 36*, 2494-2499.

Nenes, A., R.J. Charlson, M.C. Facchini, M. Kulmala, A. Laaksonen, and J.H. Seinfeld (2002), Can chemical effects on cloud droplet number rival the first indirect effect?, *Geophys. Res. Lett., 29*, 1848, doi: 10.1029/2002GL015295.

Nelson, L., O. Rattigan, R. Neavyn, H. Sidebottom, J. Treacy, and O.J. Nielsen (1990), Absolute and relative rate constants for the reactions of hydroxyl radicals and chlorine atoms with a series of aliphatic alchohol and ethers at 298K, *Int. J. Chem. Kinet., 22*,1111-1126.

Niki, H., P.D. Maker, C.M. Savage, and L.P. Breitenbach (1981), An FTIR study of the isomerization and O_2 reaction of n-butoxy radicals. *J. Phys. Chem.*, *85*, 2698-2700.

Ng, N.L., J.H. Kroll, A.W.H. Chan, P.S. Chhabra, R.C. Flagan, and J.H. Seinfeld (2007), Secondary organic aerosol formation from *m*-xylene, toluene, and benzene, *Atmos. Chem. Phys.*, *7*, 3909-3922.

Notario, A., A.Mellouki, and G. Le Bras (1999), Rate constants for the gas-phase reactions of chlorine atoms with a series of ketones, *Int. J. Chem. Kinet.*, *32*, 62-66.

Noziere, B., I. Barnes, and K.H. Becker (1999), Product study and mechanisms of the reactions of a-pinene and of pinonaldehyde with OH radicals, *J. Geophys. Res.*, *104*, 23, 645-23,656.

Odum, J.R., T. Hoffmann, F. Bowman, D. Collins, R.C. Flagan, and J.H. Seinfeld (1996), Gas/particle partitioning and secondary organic aerosol yields, *Environ. Sci. Technol., 30*, 2580-2585.

Odum, J.R., T.P.W. Jungkamp, R.J. Griffin, R.C. Flagan, and J.H. Seinfeld (1997a), The atmospheric aerosol-formation potential of whole gasoline vapor, *Science, 276*, 96-99.

Odum, J.R., T.P.W. Jungkamp, R.J. Griffin, H.J.L. Forstner, R.C. Flagan, and J.H. Seinfeld (1997b), Aromatics, reformulated gasoline, and atmospheric organic aerosol formation, *Environ. Sci. Technol., 31*, 1890-1897.

Olariu, R.I., K.H. Becker, and B. Klotz (2000), Rate coefficients for the gas phase reaction of OH radicals with selected dihydroxybenzenes and benzoquinones, *Int. J. Chem. Kinet.*, *32*, 696-702.

Olivier, J.G.J., J.P.J. Bloos, J.J.M. Berdowski, A.J.H. Visschedijk, and A.F. Bouwman (1999), A 1990 global emission inventory of anthropogenic sources of carbon monoxide on 1° x 1° developed in the framework of EDGAR/GEIA, *Chemosphere, 1*, 1-17.

Pandis, S.N., R.A. Harley, G.R. Cass, and J.H. Seinfeld (1992), Secondary organic aerosol formation and transport, *Atmos. Environ., 13*, 2269-2282.

Pandis, S.N., A.S. Wexler, and J.H. Seinfeld (1993), Secondary organic aerosol formation and transport. 2. Predicting the ambient secondary organic aerosol size distribution, *Atmos. Environ., 27A*, 2403-2416.

Pankow, J.F. (1994), An absorption model of gas/particle partitioning of organic compounds in the atmosphere, *Atmos. Environ., 28*, 185-188.

Pankow, J.F. (1994b), An absorption model of the gas/particle partitioning involved in the formation of secondary organic aerosol, *Atmos. Environ., 28*, 189-193.

Pankow, J.F., J.H. Seinfeld, W.E. Asher, and G.B. Erdakos (2001), Modeling the formation of secondary organic aerosol. 1. Application of theoretical principles to measurements obtained in the α-pinene, β-pinene, sabinene, Δ^3-carene, and cyclohexene/ozone systems, *Environ. Sci.Technol., 35*, 1164-1172.

Pickle, T., D.T. Allen, and S.E. Pratsinis (1990), The sources and size distributions of aliphatic and carbonyl carbon in Los Angeles aerosol, *Atmos. Environ., 24*, 2221-2228.

Presto, A.A., K.E.H. Hartz, and N.M. Donahue (2005), Secondary organic aerosol production from terpene ozonolysis. 2. Effect of NO_x concentration, *Environ. Sci. Technol., 39*, 7046-7054.

Poling, B.E., J.M. Prausnitz, and J.P. O'Connell (2000), *The Properties of Gases and Liquids*, McGraw-Hill, New York.

Pope, C.A., R.T. Burnett, M.J. Thun, E.E. Calle, D. Krewski, K. Ito, and G.D. Thurston (2002), Lung cancer, cardio-pulmonary mortality, and long-term exposure to fine particulate air pollution, *J. Amer. Med. Assoc., 287*, 1132–1141.

Putaud, J.P., *et al.* (2004), A European aerosol phenomenology: physical and chemical characteristics of particulate matter at kerbside, urban, rural and background sites in Europe, European Commission, Report # EUR 20411 EN, http:ccu.ej.jrc.it/ccu.

Pszenny, A.A.P., W.C. Keene, D.J. Jacob, S. Fan, J.R. Maben, M.P. Zetwo, M. Springer-Young, and J.N. Galloway (1993), Evidence of inorganic chlorine gases other than hydrogen chloride in marine surface air, *Geophys. Res. Lett, 20*, 699-702.

Pszenny, A.A.P., E.V. Fisher, R.S. Russo, B.C. Sive and R.K. Varner (2007), Estimates of Cl atom concentrations and hydrocarbon kinetic reactivity in surface air at Appleedore island, Maine (USA), during International Consortium for Atmospheric Research on Transport and Transformation/Chemistry of Halogens at the Isles of Shoals, *J. Geophys. Res., 112*, D10S13, doi:10.1029/2006JD007725.

Pszenny, A.A.P., E.V. Fisher, R.S. Russo, B.C. Sive, and R.K. Varner (2007), Estimates of Cl atom concentrations and hydrocarbon kinetic reactivity in surface air at

Appledore Island, Maine (USA), during International Consortium for Atmospheric Research on Transport and Transformation Chemistry of Halogens at the Isles of Shoals, *J. Geophys. Res.*, *112*, D10S13, doi:10.1029/2006JD007725.

Pun, B.K., R.J. Griffin, C. Seigneur, and J.H. Seinfeld (2002), Secondary organic aerosol 2. Thermodynamic model for gas/particle partitioning of molecular constituents, *J. Geophys. Res.*, *107*, 4333-4341, doi:10.1029/2001JD000542.

Pun, B.K., S.-Y. Wu, C. Seigneur, J.H. Seinfeld, R.J. Griffin, and S.N. Pandis (2003), Uncertainties in modeling secondary organic aerosols: Three-dimensional modeling studies in Nashville, TN, *Environ. Sci. Technol.*, *37*, 3647-3661.

Putaud, J.P., *et al.* (2004), A European aerosol phenomenology: physical and chemical characteristics of particulate matter at kerbside, urban, rural and background sites in Europe, European Commission, Report # EUR 20411 EN, http:ccu.ej.jrc.it/ccu.

Ramirez-Ramirez, V.M., and I. Nebot-Gil (2005), Theoretical study of the OH addition to the endocyclic and exocyclic double bonds of the [sic] d-limonene, *Chem. Phys. Lett, 409*, 23-28.

Rechsteiner, C.E. (1990), Boiling point, in W.J. Lyman, W.F. Reehl and D.H. Rosenblatt (eds.), *Handbook of Chemical Property Estimation Methods*: *Environmental Behavior of Organic Compounds*, 12-1-12-55.

Roberts, G.C., M.O. Andreae, J. Zhou, and P. Artaxo (2001), Cloud condensation nuclei in the Amazon Basin: 'marine' conditions over a continent?, *Geophys. Res. Lett.*, *28*, 2807-2810.

Robinson, A.L., N.M. Donahue, M.K. Shrivastava, E.A. Weitkamp, A.M. Sage, A.P. Grieshop, T.E. Lane, J.R. Pierce, and S.N. Pandis (2007), Rethinking organic aerosols: Semivolatile emissions and photochemical aging, *Science*, *315*, 1259-1262.

Rogge, W.F., M.A. Mazurek, L.M. Hildemann, G.R. Cass, and B.R.T. Simoneit (1993), Quantification of urban organic aerosols at a molecular level: Identification, abundance, and seasonal variation, *Atmos. Environ.* , *27A*, 1309-1330.

Roselle, S.J., T.E. Pierce, and K.L. Schere (1991), The sensitivity of regional ozone modeling to biogenic hydrocarbons, *J. Geophys. Res.*, *96*, 7371-7394.

Rossi, M.J. (2003), Heterogeneous reactions on salts, *Chem. Rev.*, *103*, 4823-4882.

Russell, L.M., A.A. Mensah, E.V. Fisher, B.C. Sive, R.K. Varner, W.C. Keene, J. Stutz, and A.A.P. Pszenny (2007), Nanoparticle growth following photochemical α- and β-pinene oxidation at Appledore Island during International Consortium for Research on Transport and Transformation/Chemistry of Halogens at the Isles of Shoals 2004, *J. Geophys. Res.*, *112*, D10S21, doi: 10.1029/2006JD007736.

Saathoff, H., C. Linke, K.-H. Naumann, E. Weingartner, and U. Schurath (2005), Aerosol yields from the ozonolysis of α-pinene and limonene, paper presented at the European Aerosol Conference, Ghent, Belgium, August 28-September 2.

Saxena, P., and L.M. Hildemann (1996), Water-soluble organics in atmospheric particles: A critical review of the literature and application of thermodynamics to identify candidate compounds, *J. Atmos. Chem., 24*, 57-10.

Schauer, J.J., W.F. Rogge, L.M. Hildemann, M.A. Mazurek, and G.R. Cass (1996), Source apportionment of airborne particulate matter using organic compounds as tracers, *Atmos. Environ., 30,* 3837-3855.

Schell, B., I.J. Ackermann, H. Hass, F.S. Binkowski, and A. Ebel (1995), Modeling the formation of secondary organic aerosol within a comprehensive air quality model system, *J. Geophys. Res.*, *106*, *28*, 275-28,293.

Schwarzenbach, R.P., P.M. Gschwend, and D.M. Imboden (1993), *Environmental Organic Chemistry*, John Wiley, Hoboken, NJ.

Seinfeld, J.H., G.B. Erdakos, W.E. Asher, and J.F. Pankow (2001), Modeling the formation of secondary organic aerosol (SOA). 2. The predicted effects of relative humidity on aerosol formation in the α-pinene, β-pinene, sabinene, Δ^3-carene, and cyclohexene/ozone systems, *Environ. Sci. Technol.*, *35*, 1806-1817.

Seinfeld, J.H., and J.F. Pankow (2003), Organic atmospheric particulate material, *Annu. Rev. Phys. Chem., 54*, 121-140.

Seinfeld, J.H., T.E. Kleindienst, E.O. Edney, and J.B. Cohen (2003), Aerosol growth in a steady-state, continuous-flow chamber: application to studies of secondary aerosol formation, *Aerosol Sci. Technol., 37*, 728-734.

Seinfeld, J.H., and S.N. Pandis (1998), *Atmospheric Chemistry and Physics, From Air Pollution to Climate Change*, John Wiley, Hoboken, NJ.

Sheehan, P.E., and F.M. Bowman (2001), Estimated effects of temperature on secondary organic aerosol concentrations, *Environ. Sci. Technol.*, *35*, 2129-2135.

Singh, H.B., and J.F. Kasting (1988), Chlorine-hydrocarbon photochemistry in the marine troposphere and lower stratosphere, *J. Atmos. Chem., 7*, 261-285.

Song, C., K. Na, and D.R. Cocker III (2005), Impact of the hydrocarbon to NO_x ratio on secondary organic aerosol formation, *Environ. Sci. Technol., 39*, 3143-3149.

Spicer, C.W., E.G. Chapman, B.J. Finlayson-Pitts, R.A. Plastridge, J.M. Hubbe, J.D. Fast, and C.M. Berkowitz (1998), Unexpectedly high concentrations of molecular chlorine in coastal air, *Nature, 394*, 353-356.

Stanier, C.O., and S.N. Pandis (2005), Atmospheric secondary organic aerosol yields: Model parameter estimation from smog chamber results, *J. Geophys. Res.*, submitted

Stumm, W., and J.J. Morgan (1996), *Aquatic Chemistry*: *Chemical Equilibria and Rates in Natural Waters,* Wiley-Interscience, Hoboken, NJ.

Suarez, J.T., C. Torresmarchal, and P. Rasmussen (1989), Prediction of surface tensions of nonelectrolyte solutions, *Chem. Eng. Sci., 44* , 782-786.

Takekawa, H., H. Minoura, and S. Yamazaki (2003), Temperature dependence of secondary organic aerosol formation by photo-oxidation of hydrocarbons, *Atmos. Environ., 37*, 3413-3424.

Takegawa, N., T. Miyakawa, Y. Kondo, J.L. Jimenez, Q. Zhang, D.R. Worsnop, and M. Fukuda (2006), Seasonal and diurnal variation of submicron organic aerosol in Tokyo observed using the Aerodyne aerosol mass spectrometer, *J. Geophys. Res., 111*, D11206, doi:10.1029/2005JD006515.

Talbot, R.W., M.O. Andreare, H. Berresheim, P. Artaxo, M. Garstang, R.C. Harriss, K.M. Beecher, and S.M. Li (1990), Aerosol chemistry during the wet season in central Amazonia-the influence of long-range transport, *J. Geophys. Res., 95*, 16,955-16,969.

Talbot, R.W., M.O. Andreae, T.W. Andreae, and R.C. Harriss (1988), Regional chemistry of the Amazon basin during the dry season, *J. Geophys. Res., 93*, 1499-1508.

Tanaka, P.L., *et al.* (2003), Direct evidence for chlorine-enhanced urban ozone formation in Houston, Texas, *Atmos. Environ., 37*, 1393-1400.

Tanaka, P.L., D.T. Allen, E. C. McDonald-Buller, S. Chang, Y. Kimura, C. B. Mullins, G.Yarwood, and J. D. Neece (2003b), Development of a chlorine mechanism for use

in the carbon bond IV chemistry model, *J. Geophys. Res.*, *108*, D44145, doi:10.1029/2002JD002432.

Takegawa, N., T. Miyakawa, Y. Kondo, J.L. Jimenez, Q. Zhang, D.R. Worsnop, and M. Fukuda (2006), Seasonal and diurnal variation of submicron organic aerosol in Tokyo observed using the Aerodyne aerosol mass spectrometer, *J. Geophys. Res.*, *111*, D11206, doi:10.1029/2005JD006515.

Thevenet, R., A. Mellouki, and G. L. Bras (2000), Kinetics of OH and Cl reactions with a series of aldehydes, *Int. J. Chem. Kinet.*, *32*, 676-685.

Tsigaridis, K., and M. Kanakidou (2003), Global modeling of secondary organic aerosol in the troposphere: a sensitivity analysis, *Atmos. Chem. Phys., 3,* 1849-1869.

Turpin, B.J., and J.J. Huntzicker (1995), Identification of secondary organic aerosol episodes and quantification of primary and secondary organic aerosol concentration during SCAQS, *Atmos. Environ., 29,* 3527-3544.

Twomey, S., A.K. Davidson, and K.J. Seton (1978), Results of five years of observations of cloud nucleus concentration at Robertson, New South Wales, *J. Atmos. Sci., 35*, 650-656.

VanReken, T.M., T.A. Rissman, G.C. Roberts, V. Varutbangkul, H. Jonsson, R.C. Flagan, and J.H. Seinfeld (2003), Toward aerosol/cloud condensation nuclei (CCN) closure during CRYSTAL-FACE, *J. Geophys. Res.*, *108*, 4633, doi:10.1029/2003JD003582.

Venkataraman, C., and S.K. Friedlander (1994), Size distribution of polycyclic aromatic-hydrocarbon and elemental carbon 2. Ambient measurements and effects of atmospheric processes, *Environ. Sci. Technol.*, *28*, 563-572.

Volkamer, R., J.L. Jimenez, F.S. Martini, K. Dzepina, Q. Zhang, D. Salcedo, L.T. Molina, D.R. Worsnop, and M.J. Molina (2006), Secondary organic aerosol formation from anthropogenic air pollution: Rapid and higer than expected, *Geophys. Res. Lett.*, *33*, L17811, doi: 10.1029/2006GL026899.

von Glasow, R., and P.J. Crutzen (2003), Tropospheric halogen chemistry, in Treatise on Geochemistry, edited by K.K. Turekian and H.D. Holland, pp.21-64, Yale University, Press, New Haven, Conn.

Wainman, T., J.F. Zhang, C.J. Weschler, and P.J. Lioy (2000), Ozone and limonene in indoor air: A source of submicron particle exposure, *Environ. Health Perspect. 108*, 1139-1145.

Walas, S.M.(1985), *Phase Equilibrium in Chemical Engineering,* Butterworth-Heineman, Woburn, MA.

Wang, L., J. Arey, and R. Atkinson (2005), Reactions of chlorine atoms with a series of aromatic hydrocarbons, *Environ. Sci. Technol., 39*, 5302-5310.

Warneck, P. (2003), In-cloud chemistry opens pathway to the formation of oxalic acid in the marine atmosphere, *Atmos. Environ., 37*, 2423-2427.

Wingenter, O.W., M.K. Kubo, N.J. Blake, T.W. Smith, Jr., D.R. Blake, and F.S. Rowland (1996), Hydrocarbon and halocarbon measurements as photochemical and dynamical indicators of atmospheric hydroxyl, atomic chlorine, and vertical mixing obtained during Lagrangian flights, *J. Geophys Res., 101*, 4331-4340

Wingenter, O.W., D.R. Blake, N.J Blake, B.C. Sive, F.S Rowland, E. Atlas, and F. Flocke (1999), Tropospheric hydroxyl and atomic chlorine concentrations, and mixing time scales, determined from hydrocarbon and halocarbon measurements made over the southern ocean, *J. Geophys. Res., 104*, 21819-21828.

Wingenter, O.W., C.S. Barkeley, N.J. Blake, D.R. Blake, and F.S. Rowland (2005), Atomic chlorine concentrations derived from ethane and hydroxyl measurements over the equatorial Pacific Ocean: Implications for dimethyl sulfide and bromine monoxide, *J. Geophys. Res., 110*, D20308, doi:10.1029/2005JD005875.

Yao, X.H., M. Fang, and C.K. Chan (2002), Size distributions and formation of dicarboxylic acids in atmospheric particles, *Atmos. Environ., 36*, 2099-2107.

Yu, J., D.R. Cocker III, R.J. Griffin, R.C. Flagan, and J.H. Seinfeld (1999a), Gas-phase ozone oxidation of monoterpenes: Gaseous and particulate products, *J. Atmos. Chem. 34*, 207-258.

Yu, J., R.J. Griffin, D.R. Cocker III, R.C. Flagan, J.H. Seinfeld, and P. Blanchard (1999b), Observation of gaseous and particulate products of monoterpene oxidation in forest atmospheres, *Geophys. Res. Lett., 26*, 1145-1148.

Zhang Q., et al. (2007), Ubiquity and dominance of oxygenated species in organic aerosols in anthropogenically influenced Northern Hemisphere mid-latitudes, *Geophys. Res. Lett., 34*, L13801, doi:10.1029/2007GL029979.